



# Fluid Flow and Petroleum and Mineral Resources in the Upper (<20-km) Continental Crust

LAWRENCE M. CATHLES, III<sup>†</sup>

*Snee Hall, Cornell University, Ithaca, New York 14850*

AND JENNIFER J. ADAMS

*Geology and Geophysics, University of Calgary, 2500 University Drive, NW, Calgary, Alberta Canada T2N 1N4*

## Abstract

Fluid flow in the upper continental crust is driven by energy from the sun through precipitation, sediment deposition, compaction, and petroleum generation, evaporative brine formation, as well as by heat from the Earth's interior. Flow over geologic time and commonly across large distances has produced a diverse suite of resources with physical or chemical characteristics that reflect climate, changes in atmospheric and oceanic chemistry, and tectonics. Review of manifestations of fluid flow and economic resources in North America shows that the juxtaposition of highly oxidized and highly reduced sediments, the generation of nonaqueous fluids, and the presence of nonaqueous fluids in the pore space is important to resource formation. Mississippi Valley-type (MVT) lead-zinc deposits and trace mineralization stretching across ~1,000 km are associated with basins that now are filled with underpressured gas (Arkoma, western Canada, Appalachian basins). Oxidized brines produced sedimentary rock-hosted stratiform deposits when they were driven through organic shales capping the midcontinent rift at several discrete times separated by ~10 m.y. Accumulations of nearly 100 wt percent uranium formed when oxidized brines encountered methane seeps in the Athabasca basin. Hydrocarbons leaking through hundreds of salt-margin faults support gas seeps and methane hydrate accumulations in the offshore Gulf of Mexico. Hydrocarbon dikes in Utah, sand flame structures in Delaware, mineral deposition followed by gangue and ore mineral corrosion in the midcontinent, lead-zinc veins in the anhydrite caps of salt domes in the Gulf of Mexico suggest pulses of fluid flow.

To quantitatively assess these phenomena, we review the basics of nonisothermal, multiphase fluid flow at under- and overpressured conditions. The maximum intrinsic permeability of clean sand is summarized; ways to estimate, measure, or infer intrinsic permeability are tabulated. It is shown that free convection in clean sands will fill pores with silica most rapidly at a 4-km depth in an overpressured basin and that filling will take ~25 m.y. We calculate the conditions under which generated petroleum will displace rather than percolate through basin pore waters and we show that the permeability of basin sediments is dynamically determined by the escape of fluids while sediments are actively accumulating or hydrocarbons generating. The calculations show that the observed suite of gas- and water-filled, over- and underpressured basins are the expected consequences of the likely range of basin organic content and sedimentation rates.

The quantitative review and parameter constraints provide a basis for assessing an extensive literature on MVT deposits in North America, the Kupferschiefer sedimentary-hosted rock stratiform deposits in Europe, and convectively formed sediment-hosted stratiform deposits. The Kupferschiefer deposits require expulsion of brines from nearly the entire Permian Zechstein basin to ore districts on its southern margin. The brief elevation of temperature during Permian MVT ore deposition in North America requires short pulses of rapid brine expulsion. Currently popular suggestions such as cross-basin gravity-driven flow or episodic expulsion from overpressured basins are not compatible with geologic and physical constraints. Viable mechanisms are difficult to identify. We suggest glacial meltwater loading of the gas-filled portions of basins as one possibility. Where the subsurface plumbing system is favorable, convective sediment-hosted stratiform deposits may accumulate in lithified sediments as the result of brine reduction. More commonly ore metals sulfides accumulate at or very near the sediment-water interface, and fault configuration is an important control.

Our review and analysis suggest that identifying the factors critical to or strongly enabling the formation of resources may be a good way to penetrate the combination-lock complexity of their formation. Of the many factors potentially involved in the formation of MVT and sedimentary rock-hosted stratiform deposits, for example, capped regional-scale permeable aquifers that contain oxidized sediments and brine seem most important. Modeling coupled hydrocarbon-mineral resource systems over the tens of millions of years required for their formation, and the thorough testing of these models against field data, are suggested as a strategy for identifying the critical relationships between resources and the operation and evolution of the Earth system.

## Introduction

FEW PROCESSES are as important to humans as fluid flow in the upper continental crust. It sustains rivers between rains, transports nutrients, affects volcanic eruptions, earthquakes,

and igneous intrusion, and chemically alters the crust. Here we consider the processes by which fluid-flow systems scavenge valuable material from a large volume of rock, transport the material, and deposit it in the much smaller, economically valuable volumes, called ore deposits. Part of our interest is practical. We would like to be able to explore better for such

<sup>†</sup> Corresponding author: e-mail, cathles@geology.geo.cornell.edu

economic deposits. Part is scientific. Resource accumulations provide a great deal of information about fluid-flow, chemical, and biological processes operating in the subsurface, both now and in the past.

In this paper, we consider fluid flow in the upper continental crust. Flow in the continental crust differs from that in the oceanic crust because it is driven by energy from the sun as well as the Earth's interior. Solar energy drives fluid flow in several ways. Winds move water vapor from the ocean to higher elevations over the continents where it precipitates, seeps into the subsurface, moves to rivers, and returns to the ocean. Rainfall also causes mechanical erosion and transports sediment to deltas and other low areas where these sediments accumulate, compact, and are warmed by heat escaping from the Earth's interior. The increase in temperature with burial drives organic and inorganic reactions, which commonly result in positive volume changes and/or generate fluid (e.g., CO<sub>2</sub>, petroleum, and water). Sediment compaction and these reactions drive fluids out of the sedimentary package, a second kind of largely sun-driven fluid flow. Finally, evaporation of surface water can leave residual brines that sink and accumulate in the crust, a third kind of sun-driven flow. Magmas produced by mantle processes also drive fluid circulation and positive volume, fluid-generating reactions (e.g., dehydration, decarbonation, etc.). These fluid movements may be superimposed on sun-driven movements and are commonly related to them through plate tectonic processes but are independent in the sense that turning off the sun-driven flows would not stop flow driven by the Earth's internal heat. Intrusion-driven convection was reviewed in the *Economic Geology 75<sup>th</sup> Anniversary Volume*. We focus here mainly on resources for which solar energy was a major formation factor.

The scale of fluid movement on continents can be extremely large (thousands of kilometers). Aqueous fluids in the upper ~3 km of the continental crust usually have pressures within a few percent of hydrostatic pressure, and we have good intuition for the factors controlling their movements. However, deeper pore waters (which are commonly more saline than seawater) can be highly over- or underpressured with respect to hydrostatic pressure, and other fluid phases (such as petroleum liquids and gases) generally are not hydrostatically pressured. Aqueous fluids under strongly nonhydrostatic pressures are commonly associated with nonaqueous fluids (e.g., petroleum, a term referring to nonaqueous hydrocarbon and nonhydrocarbon fluids). The flow of nonaqueous fluids can cause disproportionately large chemical changes, and the generation of these fluids can drive long-distance migration of pore waters.

A major challenge to understanding fluid flow in the upper crust and its chemical consequences is a proper appreciation for the diversity of flow systems, their spatial and temporal scales, and their broad geologic context. To develop perspective, we devote the first part of this paper to a description of fluid flow and ore deposits in North America, which are similar to deposits on other continents. This defines the context and range of phenomena that must be explained and provides entry references to a broad literature. We then develop physical-chemical principles and material property constraints (calculations in the Appendices) that can help us understand what is observed. Finally, we examine sedimentary rock-hosted

ore deposits that are particularly interesting, instructive, contentious, or scientifically problematic, and suggest areas for future research. With this approach, we hope to communicate the diversity of interactions over time and space that are involved in fluid flow and flow-induced chemical change in the upper continental crust, and stimulate interest, research, and ideas for exploration.

Before looking at North American resources, some general background comments are useful. Metal deposition commonly occurs where pore waters move from one lithology into another that has a strongly contrasting oxidation state. The subaerial exposure of continents has facilitated the juxtaposition of sediments of contrasting oxidation state since ~2.3 Ga, when the atmosphere became oxidized (e.g., red beds). As biological activity increased, highly reduced organic-rich black shales were preserved where organic matter was not consumed or oxidized. There is a natural tendency for red beds to be overlain by black shales and evaporites in some settings (Eugster, 1985). For example, in a continental or near-continental (shelf-slope) setting, rifting causes initial uplift, allowing for, especially in arid settings, the formation of oxidized sediments. Evaporation in such arid settings produces brines and may deposit evaporites. Density stratification of these brines causes euxenic (oxygen-starved) bottom-water conditions in shallow lakes or seas, which promote the burial of organic-rich muds. Later, when sediments load the highly deformable evaporite beds, salt diapirs may penetrate the stratigraphic column. Faults at diapir margins and at salt-floored slumps facilitate fluid movement through stratigraphic column.

Changes in the chemical composition of meteoric water and seawater over geologic time have affected metal transport and ore deposit formation. Secular variation in the O<sub>2</sub> content of the atmosphere is perhaps the most important factor driving these changes. As articulated recently by Holland (2003), major shifts in surface-water chemistry or in phenomena that could affect it, include the following:

1. The rise in atmospheric O<sub>2</sub> at ~2.3 Ga to a third of present levels, which mobilized Mo, Re, and U, and allowed the extensive development of red beds for the first time.

The continued rise of atmospheric O<sub>2</sub> during the Snowball Earth temperature cycles at the end of the Proterozoic, which allowed ocean sulfate to approach present concentrations and the modern sulfur cycle to be established. Newly evolved marine microorganisms that secreted silica and carbonate for ballast and could drag organic matter to the sea floor when they died may have initiated the Snowball Earth cycles. The burial of organic matter increased the O<sub>2</sub> levels in the atmosphere and increased the <sup>13</sup>C/<sup>12</sup>C ratio of carbonates in the oceans. The amount of O<sub>2</sub> that was released greatly exceeded the capacity of the atmosphere and oceans to absorb it. The result was that sulfide was converted to sulfate, and anhydrite and gypsum became significant components of the sedimentary column.

2. The (possible) decline of ocean salinity during the Proterozoic as evaporites accumulated in the continental crust (Knauth, 1998).

3. Phanerozoic changes in the Mg, Ca, and SO<sub>4</sub> concentrations by factors of 2 to 3 when the dispersal of supercontinents

raised sea levels and the area of carbonate shelves was increased or during periods of rapid sea-floor spreading when hydrothermal circulation at midocean ridges was particularly intense (Horita et al., 2002).

4. The increase of O<sub>2</sub> from 22 to ~35 vol percent of the atmosphere in the Permo-Carboniferous as vascular plants that were more effective at sequestering organic carbon became common. The largest coal deposits accumulated at this time. A marked increase in the <sup>13</sup>C/<sup>12</sup>C ratio of ocean water reflects the burial of isotopically light organic carbon. The high O<sub>2</sub> levels supported gigantism in insects with diffusional respiration, e.g., dragonflies with a 70-cm wingspan (Berner, 2001).

5. Changes of the world's ocean bottom waters from oxic to anoxic when continental configurations blocked north-south ocean circulation. Two-thirds of the world's hydrocarbon source rocks accumulated in the east-west elongate, equatorial Permo-Carboniferous Tethys ocean (Masters et al., 1991).

6. The Cenozoic expansion of deciduous trees whose leaf loss and decay increased the volume fraction of CO<sub>2</sub> in soil gas of the unsaturated zone and accelerated weathering (Bloom, 1998).

7. The dissemination of coccoliths in the Cretaceous and Cenozoic shifted carbonate deposition from the continental shelves to the deep oceans, where carbonate is less susceptible to dolomitization but is subject to steady destruction (and return to the atmosphere as CO<sub>2</sub>) in subduction zones (Bloom, 1998).

8. The widespread dissemination of grasses (erosion-resistant turf) in the Miocene (Bloom, 1998) that retarded erosion.

### Ore Deposits of North America

North American ore districts, mineral occurrences, and manifestations of fluid flow that are discussed as instructive examples in this section are shown in Figure 1. The locations are superimposed on a color depiction of depth to basement that indicates the thickness of sedimentary cover and helps to establish the geologic and geodynamic context of Phanerozoic ore deposition. The map follows the conventional approach of taking basement to be the Precambrian sedimentary, metamorphic, or igneous rocks under most of North America. In this context, huge piles of sediment, reaching thicknesses of 14 km in many areas, have accumulated on the North American continent. Note that the basement is defined as pre-Mesozoic south of the Ouachita and east of the Appalachian fronts and largely pre-Cretaceous west of the Rocky Mountain front.

Because of the way basement is defined, the sediment accumulations reflect the closing and opening phases of only the last Wilson cycle. During the closing phase, which occurred on the eastern and southern margins from the Cambrian to Pennsylvanian and on the western margin from the Devonian through the Laramide orogeny, the oceanic portions of the North American plate subducted beneath the approaching plates. Sediments and sedimentary rocks, island arcs, or continental fragments scraped off (obducted) onto the North American craton caused its lithosphere to be flexed down. The resulting depressions filled with sediments, forming foreland basins, including the Appalachian basin (7 km thick) on the eastern margin of the North American craton;

the Arkoma (10 km), Anadarko (6.5 km), and West Texas (7 km) basins at the southern margin; and the Western Canada Sedimentary Basin (5 km) in the west.

Plots of sediment accumulation with time are shown in Figure 2. The Appalachian and Ouachita foreland basins started to form in the Cambrian and culminated with rapid subsidence and sediment accumulation in the Late Carboniferous. Sediment accumulation was most rapid in the Ouachita foreland after ~325 Ma. Subsidence rates reached kilometers per million years. Periods of rapid subsidence and sediment accumulation occurred during the Taconic orogeny and the two phases of the Appalachian orogeny, Acadian and Alleghanian at ~475 and ~325 Ma, respectively. High sedimentation rates occurred in the Western Canada Sedimentary Basin during the Laramide orogeny in the Late Cretaceous from 90 to 60 Ma.

### Mississippi Valley-type deposits

The most striking ore deposit association in Figure 1 is that between MVT deposits and foreland basins of the Appalachian, Ouachita, and Rocky Mountain orogenies. Large deposits and significant occurrences (stars numbered 1–14, Fig. 1) are common, but trace Pb-Zn-(F)-(Ba) MVT mineralization is even more widely distributed (see Heyl and West, 1982; Coveney and Goebel, 1983). Most notable are the seven major MVT ore districts associated with the Arkoma basin and Ouachita accretionary prism (deposits 6–12, Fig. 1).

Research on MVT deposits over many years (Anderson and Macqueen, 1988) has led to the following observations or conclusions: (1) carbonates are always associated; (2) unconformities that produced karsts, brines, and fine-grained dolomite commonly appear to be related to mineralization; (3) hydrothermal dolomite is commonly produced by the venting brine; and (4) collapse and carbonate-removal features such as horizontal collapse fractures in some mines suggest that permeability enhancement was caused by dolomitization along the migration pathways (see review in Machel, 2004). In general, economic MVT deposits form where very permeable aquifers pinch out or are intersected by faults that forced basal brines to vent to the surface.

The flow of mineralizing solutions must have occurred on a large scale because cathodoluminescent bands in the hydrothermal dolomite can be correlated over distances of ~275 km south from the Viburnum Trend in Missouri (9, Fig. 1; see summary in Cathles, 1993). Hydrothermal dolomitization seems to have occurred in pulses because periods of dolomite dissolution are interspersed with luminescent bands of deposition. Similarly, precipitation of ore minerals seems to have occurred in pulses. Mine office specimens in the Viburnum Trend show galena cubes growing on the corroded surfaces of previous generations of galena cubes. Sverjensky (1981) documented at least eight pulses of mineralization interspersed with dissolution in the Buick mine. Nearby, in the Tri-State ore district of Kansas, Oklahoma, and Missouri, Hagni (1976) documented eight intervals of chalcopyrite and pyrite deposition, six intervals of sphalerite, and five intervals of galena and quartz deposition. In the Upper Mississippi MVT district, periods of corrosion between periods of deposition are evident within iron-rich bands in sphalerite, which correlate over distances of at least 23 km (10, Fig. 1, Fig. 3; McLimans et al.,

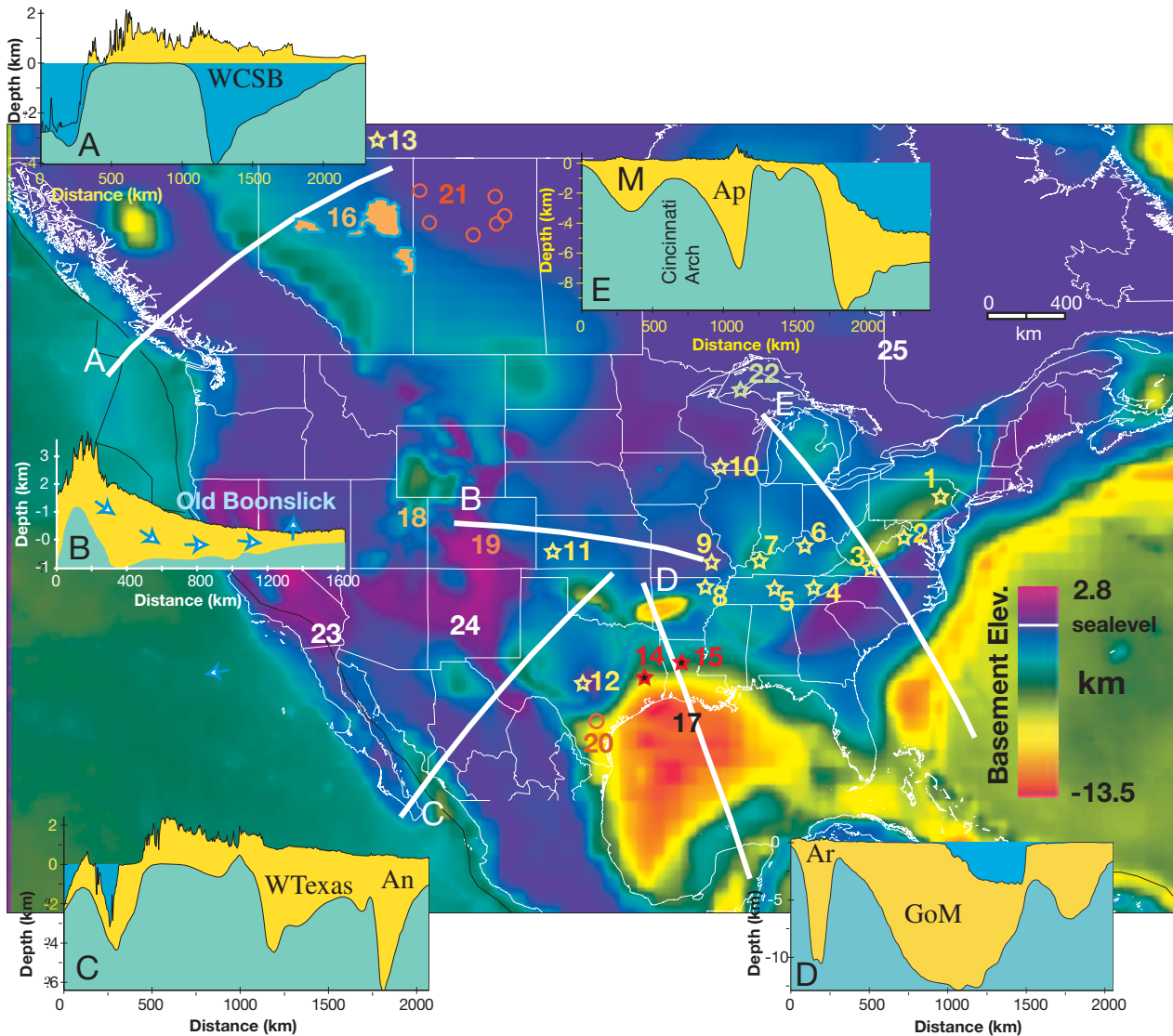


FIG. 1. Depth-to-basement map of North America (basement as conventionally defined, e.g., Bayley and Muehlberger, 1968) Precambrian over most of the craton but pre-Mesozoic in the east of the Appalachian and south of the Ouachita fronts and pre-Cretaceous west of the Rocky Mountain front except western California, where basement is the Franciscan Formation. Surface topography is from the U.S. Geological Survey gtopo30 data set and bathymetry from Smith and Sandwell (1997). The projection is equirectangular. East-west and north-south distances are the same everywhere but oblique distances are distorted. Full references (metadata) and electronic access to the data set is available at <http://atlas.geo.cornell.edu>.

Five cross sections show basement and surface topography elevation. Basins are identified in these sections (An = Anadarko basin, Ap = Appalachian basin, Ar = Arkoma basin, GoM = Gulf of Mexico basin, M = Michigan basin, WCSB = Western Canada Sedimentary Basin, WTexas = West Texas basin).

Ore deposits and other features discussed in the text are cited as follows: (15, Fig. 1). MVT-type ore deposits and occurrences are indicated by stars and numbered 1 to 15. Deposits 1 to 5 lie on or east of the Cincinnati Arch and are associated with Appalachian basin fluids (1 = Friedensville, 2 = Timberville, 3 = Austinville, 4 = East Tennessee, 5 = Central Tennessee; locations from Misra et al., 1996). Deposits 6 to 12 are associated with Ouachita accretionary prisms and Arkoma basin fluids (6 = Central Kentucky, 7 = southwestern Illinois-western Kentucky, 8 = northern Arkansas, 9 = Southeast Missouri including both the Viburnum Trend and Old Lead Belt, 10 = Upper Mississippi Valley, 11 = western Kansas, and 12 = Central Texas; locations from Heyl, 1967). The association of these deposits with these basins is discussed by Clendenin and Duane (1990), Leach and Rowan (1986), and Bradley and Leach (2003). In the Western Canada Sedimentary Basin, 13 = Pine Point, North West Territories. MVT occurrences 14 and 15 are subeconomic MVT mineralization in the anhydrite caps of the Gulf of Mexico basin salt domes. Locations 16 to 18 are hydrocarbon sites (16 = Athabasca tar sands and basin-center gas in Alberta, 17 = South Eugene Island Block 330 oil and gas reservoirs in the offshore Louisiana Gulf of Mexico, 18 = 100-km-long solidified hydrocarbon dikes in the Unita basin, Utah). Deposits 19 to 21 are uranium deposits (19 = roll-front and tabular deposits in Wyoming, 20 = roll-front deposits in the Texas margin of the Gulf of Mexico basin, and 21 = unconformity deposits in the Proterozoic Athabasca basin, Saskatchewan). Location 22 is the White Pine sedimentary rock-hosted stratiform base metal deposit, Michigan. Locations 23 to 25 are cases of intrusion-driven flow (23 = the Salton Sea geothermal system and the associated Imperial carbon dioxide system in southern California, 24 = a 50-km-diam hot sill 19 km beneath Socorro, New Mexico, 25 = volcanic basins in the Abitibi greenstone belt, Quebec, Canada).

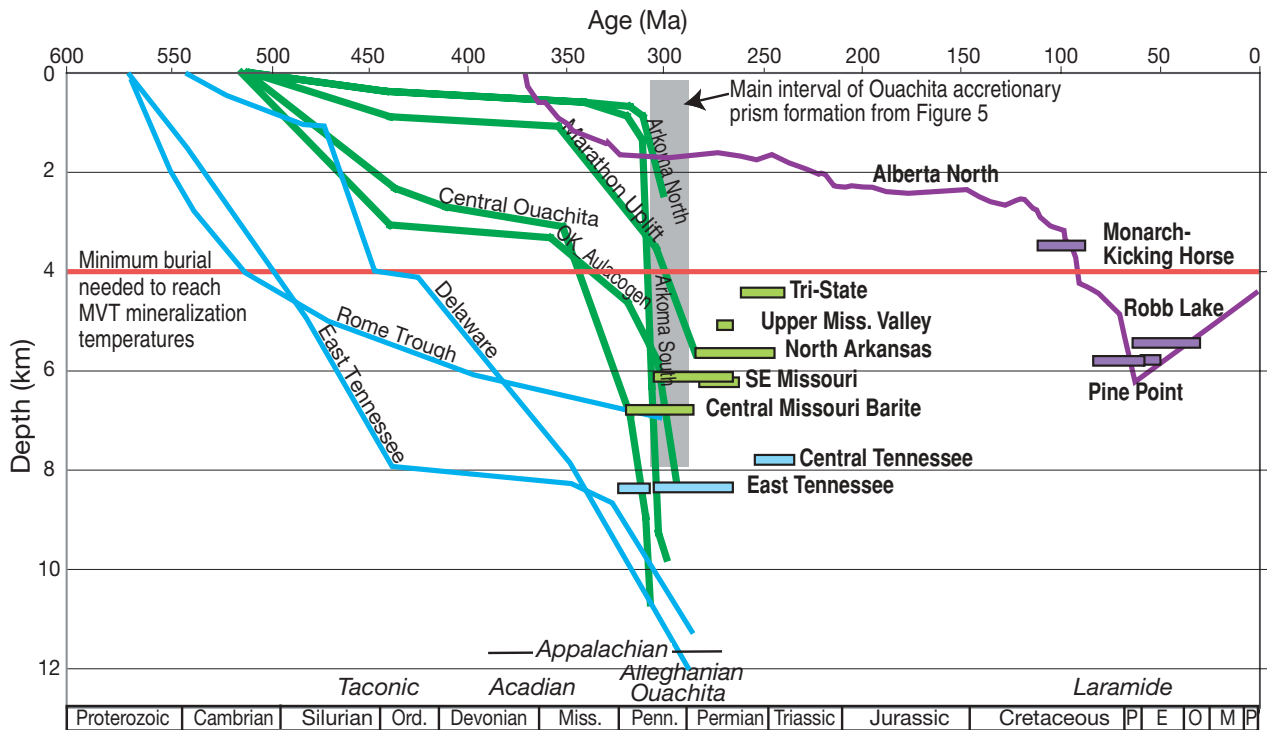


FIG. 2. Sediment accumulation (in present compacted state) for the Appalachian basin from Fisher (1975), basement subsidence curves for selected Ouachita basins from Arbenz (1989), and subsidence curve for the Western Canada Sedimentary Basin from Riediger et al. (2002). The red line at a 4-km depth signifies the minimum thickness of sedimentary strata needed to reach MVT mineralization temperatures. The subsidence and accumulation curves (at the localities indicated by labels) are linked to their associated MVT districts by color: Appalachian basin and deposits = turquoise; Ouachita, Arkoma basin, and deposits = green; and Western Canada Sedimentary Basin and deposits = purple. The MVT districts are plotted as bars that indicate the range in paleomagnetic estimates for the age of mineralization, summarized by Leach et al. (2001). The depth of the age bars of the deposits is selected to aid visual comparison to the accumulation and/or subsidence curves and has no other significance. Except for the Tri-State (in SW Missouri) and the Monarch Kicking Horse and Robb Lake deposits in the Western Canada Sedimentary Basin (purple), the deposits are all located in Figure 1.

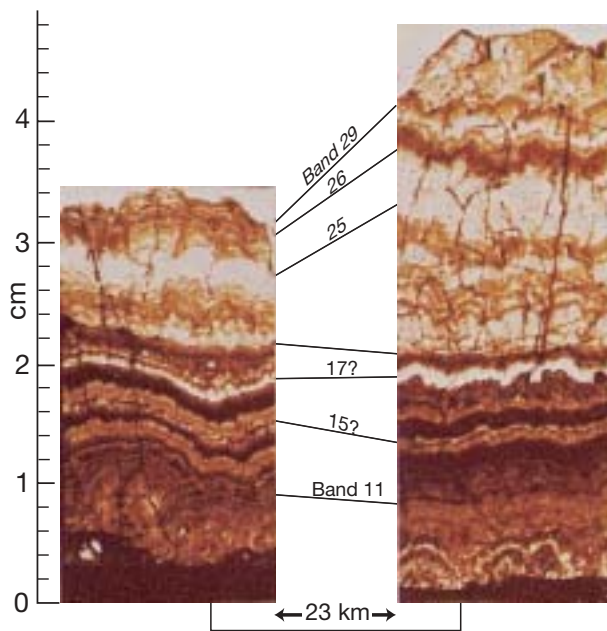


FIG. 3. Spherulite in open-space filling veins in the Upper Mississippi Valley MVT district (13, Fig. 1). Distinctive color banding caused by variable iron content in the spherulite correlates across tens of kilometers. After McLimans et al. (1980).

1980). The geology, the pattern of mineralization, and the coherence of the banding suggest that brines moved out of the foreland basins in pulses through deep (usually near base of basin) aquifers. When within a kilometer or so of the surface (Anderson and Macqueen, 1988), the brines vented through, and precipitated sulfides along, escape routes of all sizes, from minor fractures to major conduits, the latter forming accumulations of ore.

**MVT timing:** MVT deposits have traditionally been difficult to date because the radiometric isotopes in ore and gangue minerals were geochemically mobile. Recently, however, paleomagnetic and sophisticated radiogenic dating methods have been developed that circumvent or resolve these difficulties. The new paleomagnetic dates (Fig. 2) reveal a temporal relationship between the development of orogenies (Appalachian and Ouachita) and their foreland basins and associated MVT mineralization and hydrothermal dolomite alteration. Figure 2 shows that MVT deposits formed after their associated basins had accumulated substantial thicknesses of sediments and as much as 50 m.y. after sedimentation rates had become very high.

Paleomagnetic poles were reset by chemical changes over broad regions of North America, not just near the sites of ore deposition. Chemical resetting can be related to chemical changes caused by fluid movements or to diagenesis (e.g., the

conversion of smectite to illite or the maturation of organic matter of too low concentration to migrate). Near-MVT deposits resetting is clearly caused by the former effect, but regional resetting may be diagenetic; thus, caution in interpreting the regional patterns of magnetization is warranted. However, the current consensus is that pore-water movements from the Appalachian and Ouachita foreland basins reset magnetic pole positions over very broad regions (McCabe and Elmore, 1989).

The chemical resetting in siliciclastics and carbonates in the Appalachian basin occurred from 275 to 255 Ma, after tectonic folding in eastern Pennsylvania but before folding in western Pennsylvania (Stamatakos et al., 1996). Regional remagnetization occurred in the Western Canada Sedimentary Basin during the Laramide (Symons et al., 1999; Cioppa et al., 2003). Limestones in these areas may retain their diagenetic magnetization, whereas dolomites and areas of MVT mineralization are reset to much younger ages. The paleomagnetic ages of the hydrothermal dolomite tend to predate those in the mineralized areas by a few tens of million years (Symons and Stratakos, 2002). In southern Oklahoma, paleomagnetic data suggest multiple fluid-flow events over a ~60-m.y. period in the late Paleozoic (Elmore, 2001).

*Arkoma basin:* How was it that these foreland basins, particularly the Arkoma, were so very effective in expelling brines and forming MVT mineralization? Part of the answer is certainly the remarkable plumbing system of this region. The granites and rhyolites of the North American midcontinent basement had been eroded for ~1,000 m.y. when the

Cambrian seas transgressed. As a result, the transgression produced an unusually thick, and remarkably extensive, sandstone (Lamotte and Mount Simon Formation), over which thick carbonates were deposited (Fig. 4; Collinson et al., 1988). When the seas regressed in the early Ordovician, extensive karst developed, and the next transgression laid down the extensive St. Peter Sandstone. In the Late Ordovician at ~438 Ma, this permeable sequence was capped by the black, Appalachian-sourced, impermeable Maquoketa Shale (Collinson et al., 1988). This package of sedimentary rocks extends from east of the Llano uplift in Texas into Wisconsin, a huge area of the North American continent (see Fig. 4 for Cambrian portion of the stratigraphy), and was in place when the Ouachita accretionary prism formed (Fig. 5). One could not imagine a better capped set of aquifers to deliver brines to the interior of the continent from the Arkoma basin. Basinal and accretionary prism brines were discharged where the sandstones and carbonates approached the surface and/or were intersected by numerous or major faults. The MVT deposits are exactly where one would expect them to be from a large-scale fluid-flow point of view.

*Gulf of Mexico basin:* Foreland basins host the largest MVT deposits, but instructive cases on near-economic mineralization and remarkably common showings of sphalerite mineralization associated with salt domes exist in the currently active Gulf of Mexico basin (Tieh and Ledger, 1987).

This basin opened in the Jurassic, and evaporites, black shales, and carbonates (at its margins) were deposited. However, most of the sediments in the northern Gulf of Mexico

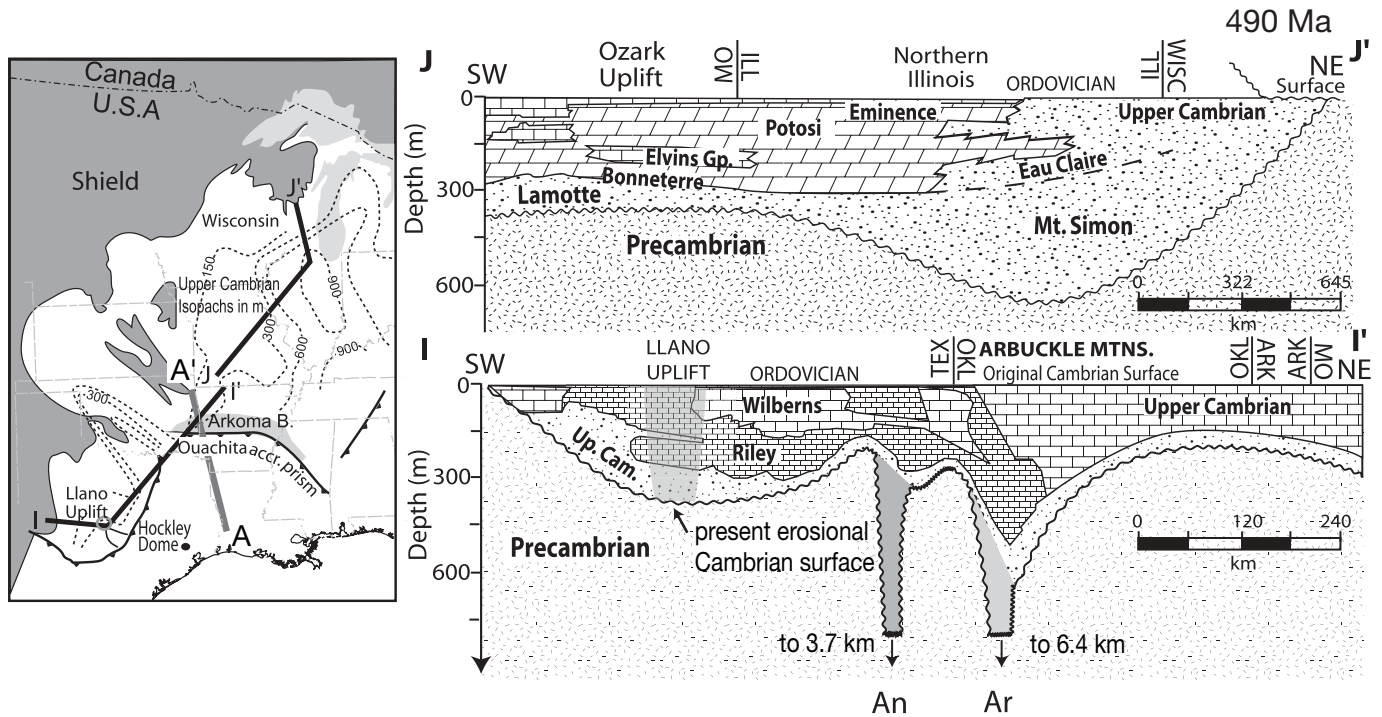


FIG. 4. Sections across the midcontinent at the end of the Cambrian from the Shell Atlas (Cook and Bally, 1975) show the extensive nature of the Cambrian Lamotte-Mount Simon sandstone and the overlying, subsequently karstified, Cambrian carbonates. The dashed contours in the insert indicate the thickness of the Upper Cambrian (Mt. Simon and younger) strata. Isopach maps of the Ordovician St. Peter Sandstone, and the ~438 Ma Maquoketa Shale, not shown in the section, can be found in figures 7, 21, and 22 in Collinson et al. (1988).

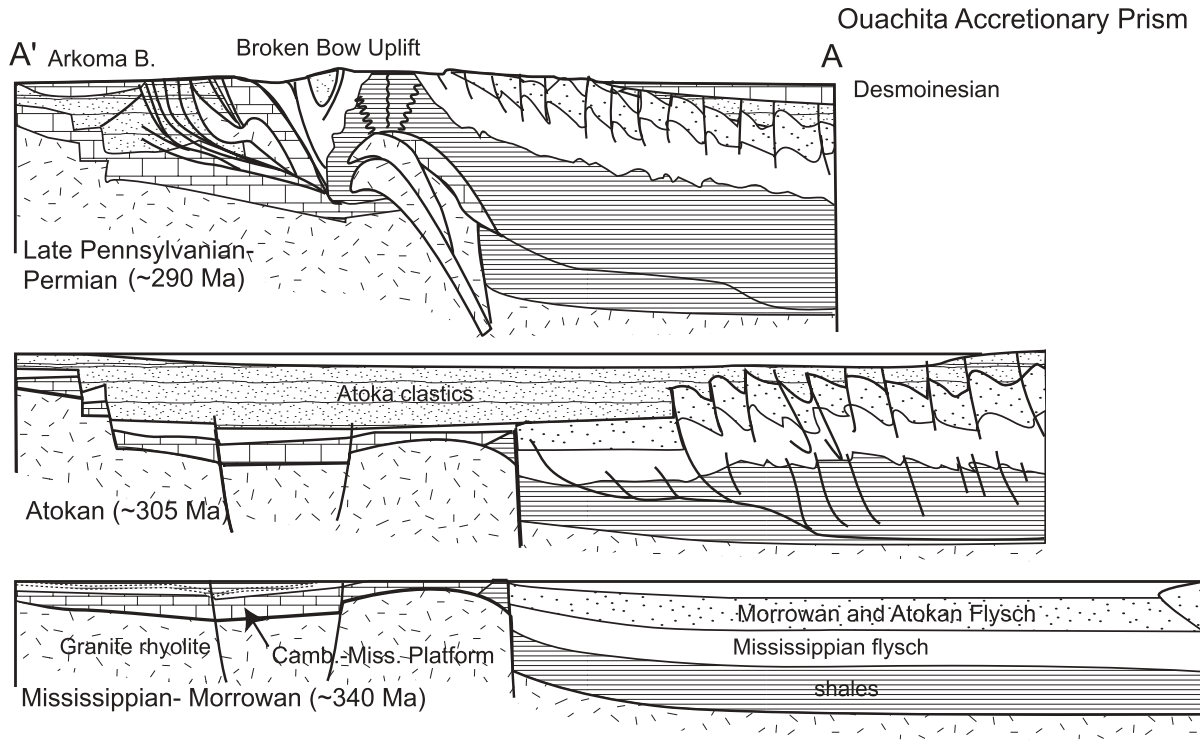
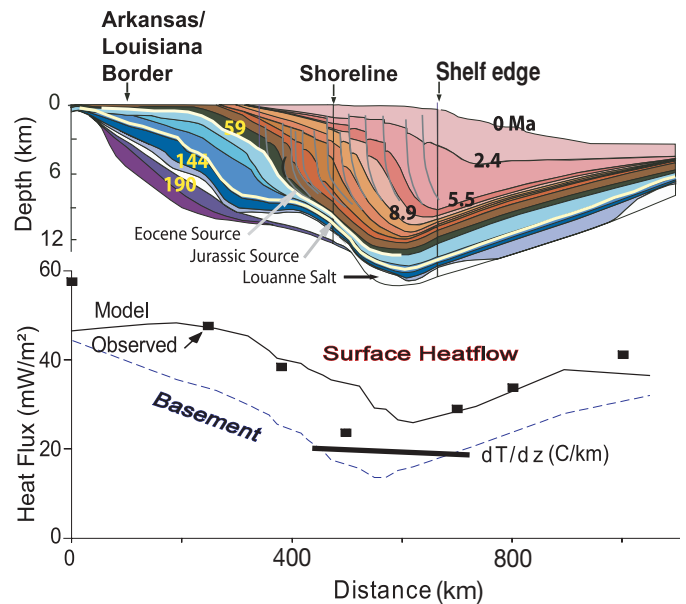


FIG. 5. Development of the Ouachita accretionary prism and the Arkoma basin (340–290 Ma), after Arbenz (1989). Section A-A' is located in Figure 4.

basin (Fig. 6) are clastics that were transported by the Mississippi River over the last ~60 m.y. after the Laramide uplift of the Rocky Mountains. As the Mississippi River drainage became progressively better organized, the rate of deposition accelerated. Present rates exceed 2 km/m.y., which are high enough to reduce heat flow at the shelf break by a factor of two (Fig. 6). In general, heat flow and thermal gradients return to steady state ~60 m.y. after high sedimentation ceases, e.g., in the northern part of the basin. Continued heating after the rate of sedimentation wanes means that hydrocarbon maturation may continue for tens of millions of years after maximum burial. If hydrocarbon generation is responsible for brine migration, this thermal reequilibration could explain the time lag between MVT mineralization and sedimentation curtailment shown in Figure 2.

As sediments in the Gulf of Mexico progressively loaded an extensive Jurassic salt layer (the ~1.5-km-thick Louanne salt; Fig. 6), the salt was remobilized upward through domes and ridges and produced salt sills. These sills were subsequently loaded and remobilized to form second-generation and perhaps even third-generation sills (McBride, 1998). The Sigsbee escarpment in the central Gulf of Mexico is one of these sills. Salt remobilization controls the pattern of faulting and

FIG. 6. North-south section through Louisiana from the Louisiana-Arkansas border to the Sigsbee Knolls in the Gulf of Mexico. Ages of selected horizons are indicated in Ma. Sedimentation rates of >2 km/m.y. near the current shelf break have a depressed surface heat flux to ~30 mW/m<sup>2</sup> and basement heat flux to <20 mW/m<sup>2</sup>, making the geothermal gradient (dT/dz) only 20°C/km here. Square symbols indicate measured surface heat flux, and lines are calculated heat fluxes. The heat flux that is initially reduced by rapid sedimentation recovers over periods of ~60 m.y. (e.g., heat flux in northern Louisiana and Arkansas is nearly double that in the high sedimentation areas in offshore Louisiana). The McKenzie stretching factor at 158 Ma is determined from the present sediment thickness and water depth. Radiogenic heat in sediments is 0.73 nW/kg. Crustal heat generation at top of basement is 3.2 mW/m<sup>3</sup> and it decreases exponentially by a factor of *e* every 7.5 km; thermal conductivity of shale is 1.5 W/m<sup>1</sup>K<sup>1</sup>. Details of calculation are given in Cathles and Losh (2002).



active sedimentation in much of the northern Gulf. Loading causes salt withdrawal and the formation of small, ~30-km-diameter minibasins that are ringed by salt domes and salt walls with faulted margins (Alexander and Flemings, 1995).

The rapid deposition of fine-grained sediments causes pore fluids to become highly overpressured relative to hydrostatic pressure. Pore pressures reach ~80 percent of the lithostatic load at depths of ~3 km under Louisiana and at much shallower depths (~500 m or less) near the shelf edge (Cathles, 2002). Hydrocarbons and aqueous fluids are expelled from source rocks in the deeper overpressured parts of the basin via faults at the margins of the salt domes and ridges. Eighty percent of the hundreds of offshore oil and methane seeps are localized at these faulted margins (Milkov and Sassen, 2001). Onshore, ground waters dissolve halite from the salt domes where they are exposed to hydrostatic (normally pressured) pore waters. The residual anhydrite accumulates and forms caps above the domes, while the resulting brines sink and pond where fluid pressure increases above hydrostatic pressure (a.k.a., the top of overpressure, Hanor, 1987).

Subeconomic MVT mineralization occurs as sulfide layers a few millimeters thick in the anhydrite caps. Two such locations (14–15) are shown in Figure 1. Horizontal galena veins enclosed in xenoblastic anhydrite in the cap of the Hockley dome (14, Fig. 1) contain euhedral crystals of anhydrite (Fig. 7). Ulrich et al. (1984) pointed out that because euhedral anhydrite is only available at the top of a salt dome where halite is being dissolved (anhydrite is deformed to a xenoblastic texture in the cap and brines cannot flow through salt), sulfide deposition must have occurred intermittently when pulses of overpressured metal-bearing brine flowed across the halite-

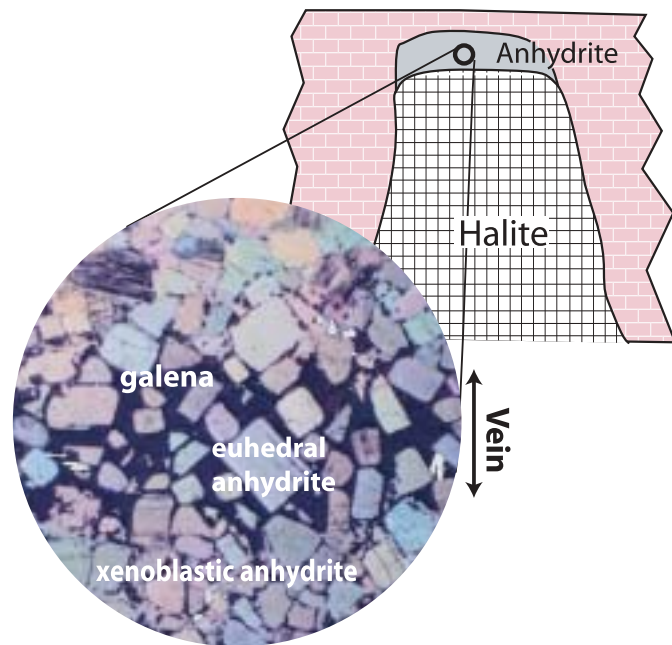


FIG. 7. Photomicrograph of a galena vein in the anhydrite cap of the Hockley salt dome (14, Fig. 1, also located in Fig. 4). Euhedral crystals of anhydrite that are preserved in this galena vein that is now above the salt-anhydrite interface require that the vein formed where waters are dissolving salt at the interface of the salt dome and its cap. Modified from Hallager et al. (1990).

anhydrite interface. Hallager et al. (1990) discussed mineralization in the anhydrite cap as an analogue for larger MVT deposits, pointing out that galena bands in salt domes occur within a few centimeters of pyrrhotite bands, and that the iron content of sphalerite bands in these deposits varies as it does in the Upper Mississippi Valley district. Paleomagnetic profiles across the mineralized parts of the Winnfield dome cap show that the period of caprock growth and mineralization exceeded 12 m.y., with mineralizing pulses occurring every ~300 yrs (Cathles et al., 1990).

#### *Cascadia margin accretionary prism dewatering*

Fluids are being expelled today by tectonic compaction and thermal dehydration from the Cascadia accretionary prism. The prism is increasing in thickness at rates of 10 to 20 km/m.y. On the sea floor above the accretionary wedge, mud volcanoes and diapirs, and even serpentine diapirs, suggest discharge of overpressured fluids. At the toe of the accretionary wedge, the fluids vent through faults during periods of deformation and fracturing at rates sufficiently high to increase near-surface heat flow. The discharging fluids have chloride concentrations less than seawater, indicating a 30 to 50 percent dilution by nonsaline water released by diagenetic crystallization of smectite to illite and quartz to opal. The discharge of this low-salinity diagenetic water is thought to have been episodic and recent because otherwise chloride diffusion from the ocean would have restored the chlorinity of the pore waters to that of seawater. The strongly cleaved interior of the subduction zone extending to depths of 45 km seems to be the source of the low-salinity fluids.

Maturation of ~0.4 wt percent total organic carbon in the sediments produces a steady methane flux through the faults. Methane hydrates accumulate in faults and in sediment pores to depths where temperature exceeds the stability limit of hydrate. This is indicated by seismic reflections from gas that is trapped beneath the hydrate-filled pores. Bottom-simulating seismic reflections over extensive areas of the continental shelves suggest widespread plugging of sediment pores with hydrate.

This discussion is largely drawn from an excellent summary of accretionary prism dewatering by Moore and Vrolijk (1992).

#### *Fluid phase, pressure, and salinity in foreland basins*

A number of additional observations are critical to understand fluid flow in foreland basins of North America. First, some of these basins have retained anomalous pressures (both near-lithostatic and significantly subhydrostatic pressures) for protracted periods of geologic time. Second, pores in the deep, central portions of many of them are filled entirely with underpressured gas.

A pressure profile through the Anadarko basin (Fig. 8; Al-Shaieb et al., 1994) shows a normal hydrostatic pressure gradient (10.5 MPa/km) for an 80,000-mg/L brine to a depth of ~3 km, whereupon overpressures relative to hydrostatic develop. The top of overpressure cuts across stratigraphic contacts, whereas, except for a few minor pockets of deeper overpressure, the bottom of overpressure is at the base of the Woodford Shale. The overpressured interior of the basin is divided into so-called pressure compartments in which the



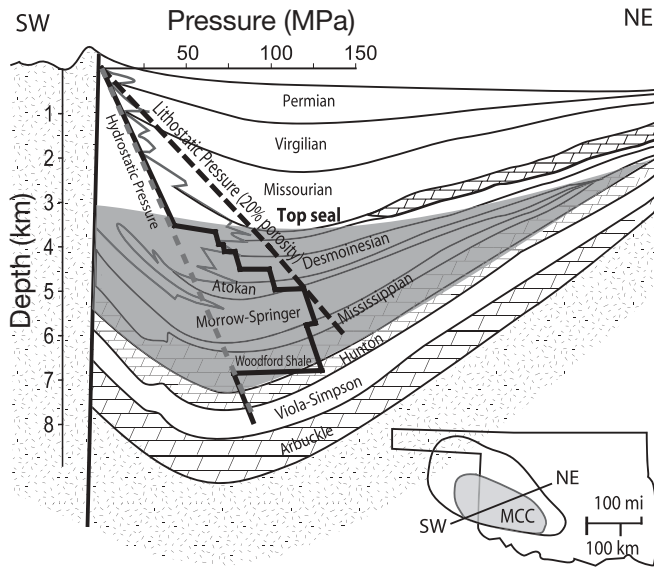


FIG. 8. Cross section through the central portion of the Anadarko basin with a superimposed pressure profile and dashed lines that indicate hydrostatic and lithostatic fluid-pressure gradients. The overpressured portion of the Anadarko basin is referred to by Al Shaieb et al. (1994) as a Mega (pressure) Compartment Complex (MCC) and is shaded in the section and plan. Steps in the pressure profile depict pressure compartmentation. Pressures approach lithostatic at some depths. Fluid pressures return to normal hydrostatic in the basal carbonates. A composite from Al-Shaieb et al. (1994).

pressure is variably elevated with respect to hydrostatic pressure, but the pressure gradient within each compartment is hydrostatic pressure (10.2 MPa/km). The seals that separate the compartments are represented in Figure 8 by sharp increases or decreases in fluid pressure with depth. In combination, the hydrostatic gradient and seals mean that the fluids can move around freely within any compartment and could vent rapidly if the seals surrounding the compartment were to rupture. Pressure compartmentation is common in basins (see Hunt, 1990; Ortoleva, 1994; Surdam, 1997; Law and Spencer, 1998), and anomalous pressures commonly last for hundreds of millions of years. High fluid overpressures in the Anadarko mega (pressure) compartment complex have been preserved for ~250 m.y. after curtailment of sedimentation and minor denudation (Al-Shaieb et al., 1994). Sand flame structures in the Delaware Water Gap area of the Appalachian basin suggest similar formerly overpressured conditions in this area. As shown in Figure 9, sand flames penetrate into the adjacent shale, which has developed slaty cleavage. This penetration suggests hydraulic fracturing followed by flow that is rapid enough to entrain and carry sand into the shale and points to the possibility that slaty cleavage is caused by rapid fluid release (Maxwell, 1962).

The pressure situation in the Arkoma basin that lies just east of the Anadarko basin is very different; the fluids there are underpressured (Davis, 1984; Houseknecht and McGilvery, 1990; Meckel et al., 1992; Popov et al., 2001). Below a water-saturated zone, the sediments are gas saturated; water saturation (the fraction of the pore space filled with liquid water) is at irreducible levels, i.e., levels so low that no further water can be extracted. Pressures increase

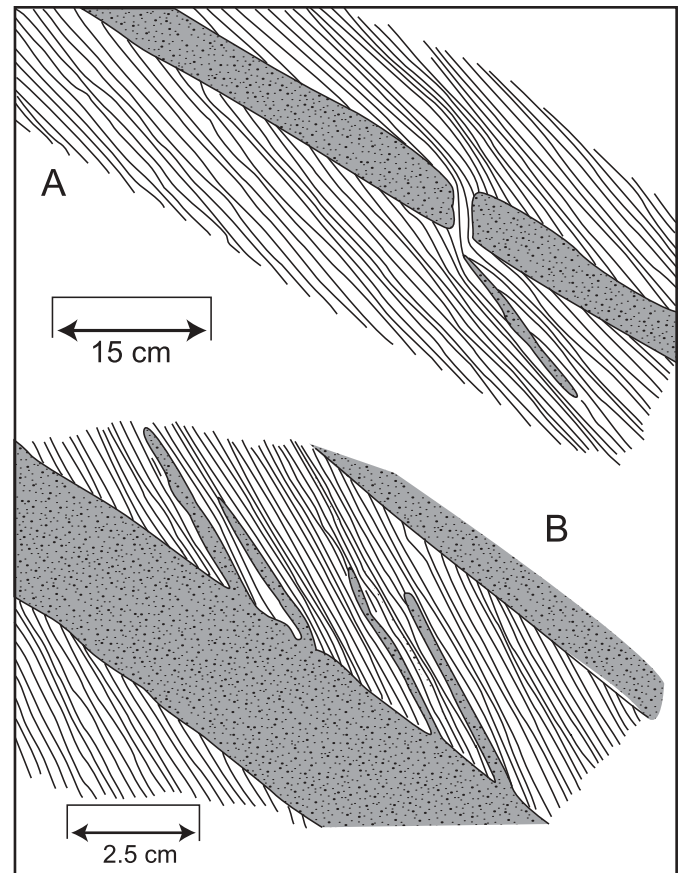


FIG. 9. Dewatering of shale is inferred from the relationships of the sand lenses (dark gray stippled pattern) and shale with slaty cleavage (wavy ruled pattern). The top diagram shows that the shale has dewatered downward, displacing the sand into the slate below. Sketches and suggested interpretation are from Maxwell (1962).

with depth along a gas-static (~1 MPa/km) rather than the hydrostatic (~10 MPa/km) path. In general, underpressured conditions are probably more common in basins than overpressured conditions (see Law, 2002). Huge volumes of sediment with permeability  $<10^{-16}$  m<sup>2</sup> (0.1 md) and pores saturated with methane gas commonly occupy the central parts of basins. This has become known as basin-center gas (Law, 2002). For instance, the Appalachian basin (Fig. 10) contains underpressured (with respect to hydrostatic) basin-center gas extending from New York to Tennessee (Law, 2002; Ryder and Zagorski, 2003). Over 76,500 gas wells have been drilled into this basin. A significant part of the production is from Devonian strata with underpressured gas and microarcy permeability that must be hydraulically fractured to produce the gas (de Witt, 1986).

#### Hydrocarbon fluids

*The Western Canada Sedimentary Basin:* The Western Canada Sedimentary Basin (16, Fig. 1) provides one of the world's most spectacular examples of hydrocarbon migration, hydrocarbon-induced pore water expulsion, and basin-center gas (Masters, 1984). This foreland basin resulted from shortening and eastward overthrusting that began in the mid-Jurassic

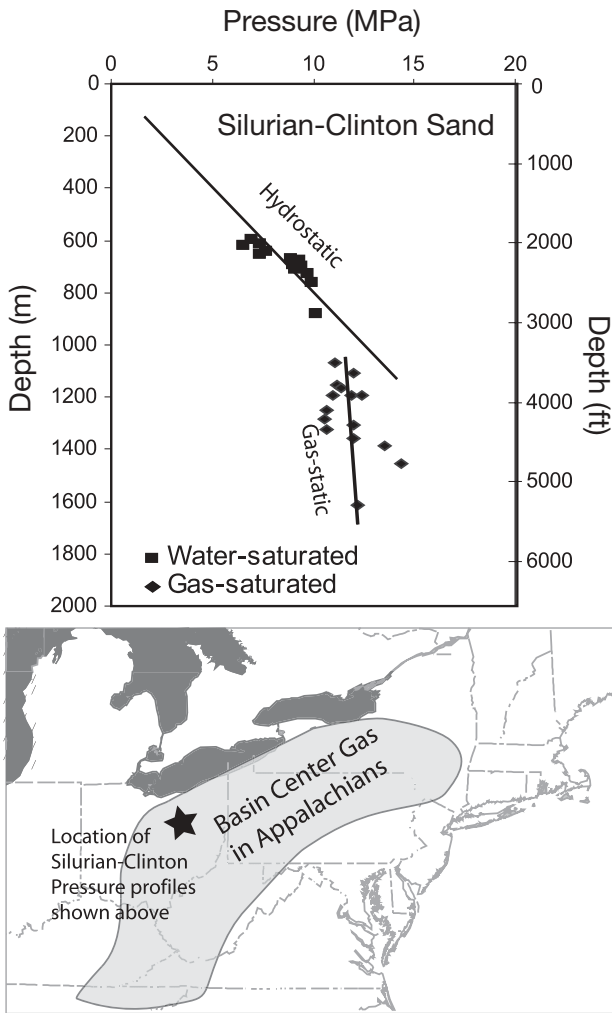


FIG. 10. The distribution of underpressured basin-center gas in the Appalachian basin (after Law, 2002) is shown in the plan map. In the gray area, deeper basin sediments are gas saturated and underpressured. A pressure-depth plot in the Clinton sand of central Ohio (located by star) shows the underpressuring of the gas-saturated zone. Pressure-depth plot is from Davis (1984).

and culminated in the Laramide orogeny with the formation of the Rocky Mountains (Price, 1986). Maximum burial was reached in the Paleocene (~60 Ma), roughly coincident with the onset of peak hydrocarbon generation (Allan and Creaney, 1991). Oils migrated more than 200 km to the east along sub-Cretaceous unconformities that were capped by an effective seal (the 15-m-thick Joli Fou clay shale and overlying Colorado Group shales). The Athabasca-Sweetgrass anticline, a drape structure created by dissolution of Devonian salt by ground-water incursion from the east (Fig. 11), trapped  $400 \times 10^9 \text{ m}^3$  of oil, which was subsequently biodegraded to the  $200 \times 10^9 \text{ m}^3$  of bitumen that is now present (Deroo et al., 1977; Creaney and Allan, 1990; Allan and Creaney, 1991; Gussow, 1995). The migration pathways host an additional  $50 \times 10^9 \text{ m}^3$  of bitumen. The bitumen present today represents an original oil volume of  $500 \times 10^9 \text{ m}^3$  ( $3,000 \times 10^9$  barrels of oil). This is equal to the total conventional oil resources of the world (710 billion barrels produced and consumed plus 2,300

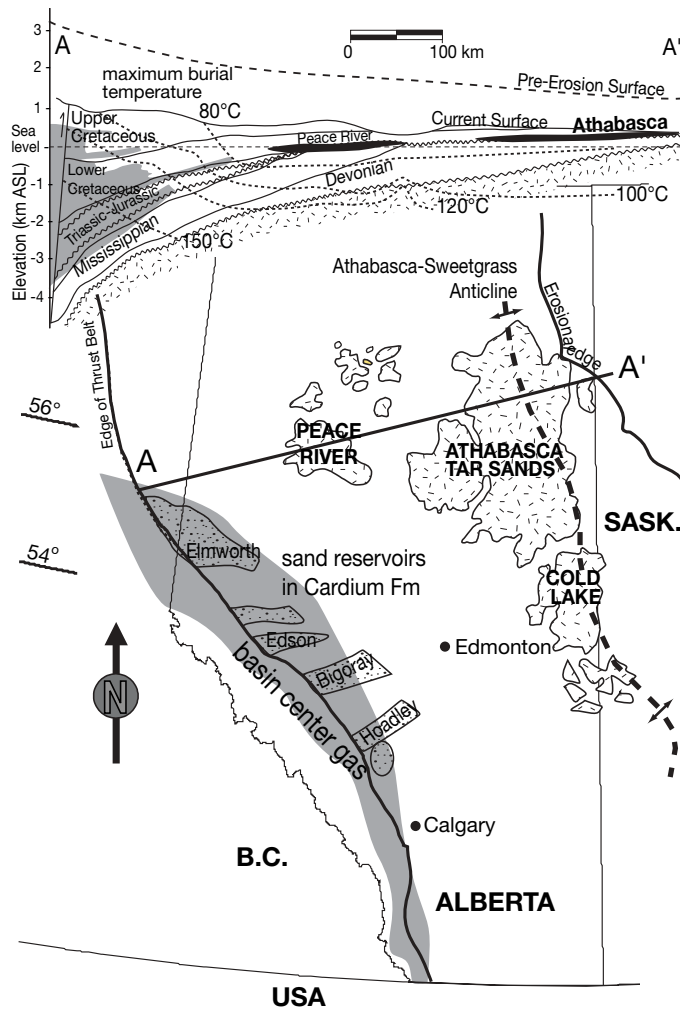


FIG. 11. Distribution of tar sands (Peace River, Athabasca, and Cold Lake) and underpressured, basin-center gas (gray shade) in the Western Canada Sedimentary Basin. Tar sands are sands whose pores are filled with bitumen and heavy oil, which we include here under the term bitumen. Stippled areas along the western thrust belt are sands in the Cardium Formation from which underpressured gas is currently produced. Modified from Masters (1984), Willett et al. (1997), and chapters in Mossop and Shetsen (1994).

billion barrels remaining to be produced or likely to be discovered; U. S. Geological Survey, 2000).

But the oil is only part of the story. An equally staggering volume of gas ( $\sim 270 \times 10^{12} \text{ m}^3$ ), almost equal to the total extractable world gas endowment of  $300 \times 10^{12} \text{ m}^3$  (Masters et al., 1991) was also generated in this area. Much of this gas may have escaped through erosional breaches in the Athabasca-Sweetgrass anticline that had been filled with biodegraded oil. However, as indicated by shading in Figure 11, a great deal remains in the central parts of the Western Canada Sedimentary Basin as basin-center gas. Basin-center gas was first discovered and documented in this locality by Masters (1984) and coworkers. It is not possible to drill a well that does not encounter gas in the shaded areas of Figure 11 (Masters, 1984). The exploration challenge is only to find zones that are permeable enough for commercial production. In the Cadomin Formation, such zones are the northwest-southeast-oriented reworked delta beach and bar sands

and/or conglomerates indicated by stippling in Figure 11 (Masters, 1984; Krause et al., 1994). One of these sand horizons hosts the Elmworth field which contains  $\sim 0.5 \times 10^{12}$  m<sup>3</sup> of recoverable gas.

The basin-center gas zone (Fig. 11) contains 4,800 km<sup>3</sup> of sand with an average porosity of 6.7 percent and gas saturation of 60 percent (Masters, 1984). Assuming a similar volume of gas is contained in the siltstones and coal fractures, gas occupies 380 km<sup>3</sup> of pore space in this area and must have displaced an equal volume of brine—a volume of water equal to that discharged by the Mississippi River in 8.4 months. If the brine contained 100 ppm Pb + Zn,  $\sim 38$  million tons (Mt) of metal would have been transported in the gas-displaced brines. This is far more than the  $\sim 9$  Mt of metal contained in the Pine Point MVT deposits (13, Fig. 1) associated with the Western Canada Sedimentary Basin (Table 1).

*Gulf of Mexico basin:* The currently active Gulf of Mexico basin provides additional insights. Unlike the Western Canada Sedimentary Basin with its long-distance lateral petroleum migration and highly efficient trap, the northern Gulf is a massively leaky flow-through petroleum system. Here hydrocarbons migrate mostly vertically and are expelled to the sea floor from overpressured parts of the basin almost as soon as they leave their thin (<100-m-thick) Jurassic and Eocene source strata (Fig. 6). More than  $100 \times 10^9$  m<sup>3</sup> oil and gas equivalent have been expelled into the oceans in the last  $\sim 15$  m.y. from a relatively small 125-  $\times$  200-km area offshore of Louisiana (Cathles and Losh, 2002). The venting is manifested in the hundreds of natural offshore seeps and also by methane hydrate accumulations in the fault plumbing systems of many of the vents (Roberts and Carney, 1997; Paull and Dillon, 2001; Chen and Cathles, 2003). Sea-floor vents in the Gulf tend to start as mud volcanoes with rapid fluid discharge, develop into localized gas vents with associated hydrate accumulations and biologic communities, and finally

form carbonate caps and hardgrounds as rates of gas venting drop below the levels required to sustain biological activity (Roberts and Carney, 1997).

The filling of hydrocarbon reservoirs in the Gulf appears to have been episodic. In the dozen or so stacked sand reservoirs of the South Eugene Island Block 330 field, located about 160 km off the Louisiana coast (17, Fig. 1), brine salinity varies from 30,000 to 200,000 mg/L, and, although all the oils are from the same general source, the oils range from colorless, low-density oils to very dark, higher density oils. The reservoirs seem to have filled at different times with slightly different oils, and the brines that were introduced into the reservoir sands with the hydrocarbons must also have moved along different pathways to account for their variable salinity (Losh et al., 2002).

Rapid, episodic expulsion of hydrocarbons is indicated by a number of observations from other localities. For example, meter-wide asphaltene veins in a 100-km-long portion of the Uinta basin (18, Fig. 1) are frozen examples of rapid, episodic hydrocarbon expulsion from shale. The asphaltene dikes have a minicolumnar (“pencilate”) jointing at their margins and enclose blocks of Bridger sandstone (Fig. 12). A fluid at temperatures above 70°C but solid at room temperature, the asphalt must have been expelled rapidly from the underlying Green River shale and rapidly cooled to entrain and suspend the sandstone blocks (Eldridge, 1901).

The Gulf of Mexico also provides good examples of the interaction of reduced fluids with oxidized sediments. When hydrocarbons come into contact with sulfate minerals such as anhydrite, the sulfate is reduced. At shallow depths where temperature is less than 80°C, microorganisms catalyze the biogenic sulfate reduction reaction (Head et al., 2003). At greater depths and temperatures, the reaction proceeds without bacterial assistance and is known as thermochemical sulfate reduction (Orr, 1977; Machel, 1987, 1989; Cross et al.,

TABLE 1. Metal Resources (mined plus reserves; in millions of metric tons) of Metric Tons of Metal for MVT Districts Discussed in the Text

Area	Deposit	Pb + Zn (Mt)	Pb/Pb + Zn	Total Pb + Zn (Mt)
Southeast Missouri Pb-Zn	Annapolis	0.02	1.00	51.8
	Central Missouri	0.03	0.79	
	Higdon	0.21	0.77	
	Indian Creek	0.37	1.00	
	Old Lead Belt	7.80	0.99	
	Mine Lamotte-Fredericktown	0.52	1.00	
	Potosi-Palmer-Valle mines	0.21	0.77	
	Viburnum Trend	42.60	0.93	
	Upper Mississippi Valley Zn-Pb	Upper Mississippi Valley	5.5	
Central Kentucky Zn	Fountain Run	1.81	0.00	1.8
Appalachian Zn	Friedensville	1.20	0.00	9.4
	Copper Ridge	0.37	0.00	
	Central Tennessee	1.68	0.00	
	Embreeville	0.18	0.09	
	Mascot-Jefferson City	2.54	0.00	
	Sweetwater	0.15	0.00	
	Austinville-Ivanhoe	1.50	0.02	
Western Canada basin Zn-Pb	Pine Point	9		9

Notes: Data are from Excel spreadsheet in U.S. Geological Survey Open-File Report 98-206 (Long et al., 1998); Upper Mississippi Valley district data are from Barnes et al. (1981); Pine Point resources are from Kyle (1980)

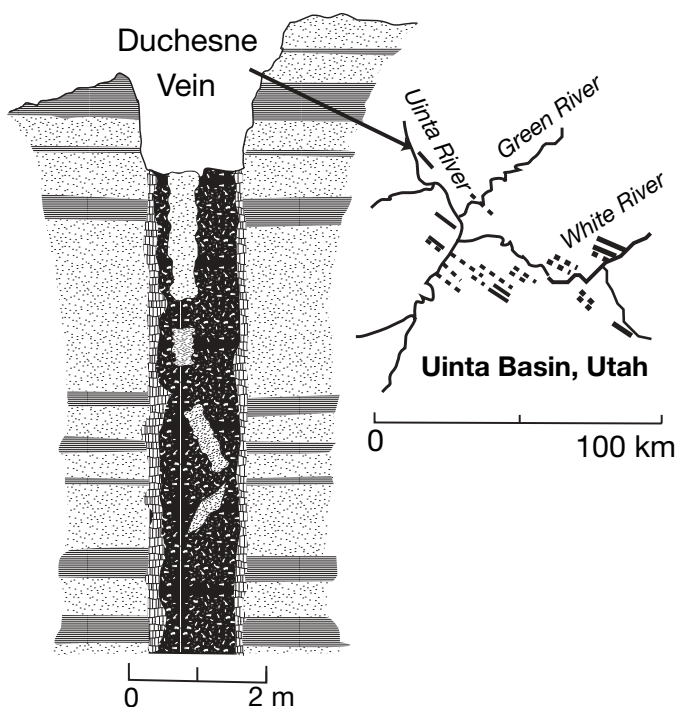


FIG. 12. Solid asphaltene dike (Duchesne vein) in the Uinta basin of Utah with pencillate chill margin and floating blocks of Bridger sandstone. Dikes of this kind extend laterally over ~100 km in Utah, as indicated by heavy solid and dashed lines in the plan view map. After Eldridge (1901).

2004). The  $H_2S$  produced by thermochemical sulfate reduction lowers the commercial value of oil and promotes sulfide mineral precipitation. Native sulfur deposits, which in the past have been of commercial interest, form in the biogenic sulfate reduction environment.

#### Long-distance hydrologic flow

The flow of meteoric water through the subsurface that occurs as part of the hydrologic cycle is far more commonplace and obvious to human observation than the movements of pore waters and hydrocarbons discussed above. For example, topography-driven subsurface flow sustains rivers between intermittent rains. Most ground-water movements are shallow and confined to a single drainage basin (e.g., App. 1, Table A1.14), but some topography-driven meteoric flow penetrates deep into the subsurface and travels over long distances. An excellent example is the 1,600-km transit of meteoric water from the Rocky Mountains to saline springs in Missouri. Ground waters with low  $^{18}O/^{16}O$  and  $^2H/^1H$  ratios recharge aquifers in the Rockies, dissolve salt in Kansas, and upwell and discharge in springs with 3 wt percent salinity like Old Boonslick in Missouri (sec. B, Fig. 1; Banner et al., 1989; Cathles et al., 1993). The upwelling of the Rocky Mountain waters occurs where these waters meet fresh waters migrating westward from the Ozark plateau (eastern end of sec. B, Fig. 1). The eastward-moving Rocky Mountain waters may increase the surface temperature gradient slightly in Kansas and Oklahoma to  $\sim 40^\circ C/km$  where the Interior Plains aquifer approaches the surface (see references and discussion in

Cathles, 1993), but salty springs in Missouri are cold and no associated base metal deposition has been noted.

Another instructive example of long-distance topography-driven flow occurs in eastern Australia. Rain falling on the Great Dividing Range on the east coast of Australia moves 1,200 km westward through two artesian aquifers at an average velocity of  $\sim 0.5$  to 1 m/yr in sedimentary horizons with 20 percent porosity (Bentley et al., 1986; Cathles et al., 1990). The waters require  $\sim 1$  to 2 m.y. to make their transit. As they do so, they accumulate He and Ar at the rate at which these gases are produced by radioactive decay in the entire underlying crust (Torgersen and Clarke, 1985). It appears that radiogenic He produced in the crust is normally vented to the atmosphere almost as fast as it is generated (Torgersen, 1989). However, in the Great Artesian basin, the flow of aquifer waters is sufficiently rapid that the gases are intercepted (i.e., the aquifer waters never become saturated with these noble gases). The passage of the radiogenic gases through the crust to the atmosphere (or to the Great Artesian basin aquifers) has puzzled isotope geologists (Ballentine and Burnard, 2002, p. 516) but is probably a good example of invasion percolation, which we discuss in the "Physical and Chemical Principles" section below.

#### Uranium mineralization

The flow of oxidized meteoric waters can strip uranium as  $U^{6+}$  from sedimentary rocks and precipitate it where the waters are reduced. Roll-front uranium deposits have formed over the last 140 m.y. from the Cretaceous to present in uplifted arkosic and tuffaceous fluvial sandstones in Wyoming (19, Fig. 1). Oxidized meteoric waters dissolve uranium from the tuffaceous material after they oxidize the pyrite and/or organic material in the sandstone aquifers. Uranium is deposited in crescent-shaped redox fronts on the upstream side of the as-yet-unoxidized sandstones. The redox fronts move through the sandstone at the rate at which the pyrite and organic material are oxidized by oxygen dissolved in the ground water (see App. 1, Table A1.9) and uranium accumulates as the front advances (Reynolds and Goldhaber, 1983; Adams, 1991; Plant et al., 1999).

There are a number of variants on this basic theme. Tabular epigenetic humate sandstone deposits (Adams, 1991) form where humate-bearing water has been expelled from surrounding strata. Some uranium is complexed with the humate and precipitates with it; some is later scavenged from oxidized ground waters that contact, and are reduced by, the humate. Another variant is represented by the epigenetic sulfide-sandstone uranium deposits (Adams, 1991) on the margin of the Gulf of Mexico in Texas (20, Fig. 1). Here, reductants are first introduced to the sandstone by fluids expelled from overpressured zones in the Gulf of Mexico basin. Oxidized meteoric water flowing south toward the Gulf causes uranium to be deposited at a moving redox front. Subsequent expulsion of reduced fluids from the overpressured parts of the basin may shift the redox fronts and uranium mineralization back to the north. The redox fronts and uranium mineralization occur at the interfaces between meteoric water invasion and overpressured water expulsion and both move back and forth, depending on the relative strength of the two flow systems (Goldhaber et al., 1978; Reynolds and Goldhaber, 1978).

Extremely high grade uranium (10–50 wt % elementary uranium) deposits were produced in the Athabasca basin of Canada (21, Fig. 1). The preferred model for these deposits involves the flow of oxidized uraniferous brines along an unconformity at the base of the basin, which is filled with Middle Proterozoic red-bed sandstone. When these brines encountered reduced strata or methane seeping out of basement fractures, uraninite was precipitated (Hoeve et al., 1980; Marmont, 1988; Plant et al., 1999).

#### *Sediment-hosted stratiform copper deposits*

The White Pine copper deposit, located on the southeastern margin of the 1.1 Ga Midcontinent rift (22, Fig. 1), is a typical expulsive sedimentary rock-hosted stratiform copper deposit (Brown, 1992), as detailed below. Here and later we distinguish deposits where metal was introduced in sedimentary rock (indurated sediments) from deposits where metals were introduced onto unconsolidated sediments. The former we refer to as sedimentary rock-hosted stratiform deposits, and the latter we refer to as sediment-hosted stratiform deposits. The midcontinent Proterozoic rift was filled with up to ~15 km of basaltic lavas and 10 km of overlying sediments, including the ~2-km-thick red (oxidized) Copper Harbor Conglomerate. Between 40 and 300 m of gray-green (reduced) marine siltstones and shales of the Nonesuch Formation were deposited on top of the Copper Harbor Formation. Where the Nonesuch Formation thins over the Porcupine Mountains volcanic structure, ~100°C brines were able to escape through this formation, mineralizing a band at the redox front ~5 m thick (White, 1971). Below this redox front, the Nonesuch Formation has been oxidized; above, it has not. From bottom to top in the mineralized band of copper sulfides, mainly chalcocite gives way to Cu-Fe sulfides (bornite and then chalcopyrite). This classic zoning indicates that the flow of the oxidized and mineralizing brine was vertical. Sand dikes and other fluid-escape structures that were mineralized preferentially (Mauk et al., 1992) suggest overpressured conditions in the Nonesuch Formation during mineralization.

A second period of mineralization, this time mainly native copper rather than chalcocite, occurred at least 10 m.y. after the first period of mineralization (Bornhorst, 1995; Swenson and Person, 2000). This mineralization was associated with reverse faulting that occurred during a slight closing of the rift at ~1060 Ma. The famous native copper deposits 100 km northeast of the White Pine deposit were produced at this time. Scattered occurrences of native copper occur between the two mined areas (Mauk et al., 1992). Mineralization seems to have occurred in this area whenever and wherever brines were expelled from the basin. The original copper source for these deposits is presumably the underlying basalt.

#### *Intrusion-related deposits and fluids*

Fluid flow that is important for crustal alteration and ore deposits is also driven by heat introduced into the crust by igneous intrusions. The geothermal energy extracted from sandstone reservoirs in the Salton Sea geothermal system (23, Fig. 1), for example, derives heat from basaltic intrusions at an actively spreading segment of the East Pacific Rise. As summarized by McKibben and Hardie (1997), this northern part of the Gulf of California has been filled with oxidized

Colorado River sediments. Delta switching between the Salton basin and the Gulf of California periodically produced saline lakes with evaporites similar to those of the present-day Salton Sea. Lacustrine brines sank, dissolved subsurface salts, and ponded at depth. Today, and intermittently over the last ~100,000 yrs, these brines have been heated by the magmatism in the Salton Sea rift (Fig. 13), causing the top of the brine layer to rise toward the surface. The slowly convecting brines are well mixed and their oxidation state is controlled by the pyrite-hematite-magnetite buffer. The hot, sloping brine interface, coincident with the 250°C isotherm, heats the overlying lower salinity (~4 wt % salinity) waters, also causing them to convect (Fig. 13). The Salton Sea geothermal power facility is located on this brine “ridge” (at ~ 500-m depth) where the hypersaline and less saline convective systems meet.

The hypersaline brines are rich in ore metals (>700 ppm Zn, >100 ppm Pb, 2.4 ppm Cu, 0.1 ppm Ag), and 17 Mt Fe, 5 Mt Zn, and 1 Mt Pb are dissolved in the large volume of hot brine in this area. Had the brines vented into a reduced environment, such as the H<sub>2</sub>S-rich bottom water of an anoxic lake, an exhalative, sedimentary rock-hosted stratiform base metal deposit similar to Mount Isa, Australia, would have been produced (a deposit that contains 10, 5, and 6 Mt of Fe, Zn, and Pb, respectively). By contrast, if the brines had vented into an oxic lake, such as the present-day Salton Sea, a stratiform Fe-Mn oxide deposit would likely have resulted. McKibben and Hardie (1997) concluded that the hypersaline brines at the Salton Sea have not produced significant mineralization because they have not discharged.

On the shores of the Salton Sea adjacent to the Salton Sea geothermal system, the 150- to 210-m-deep sandstone reservoirs of the Imperial carbon dioxide field are filled with  $18.4 \times 10^6$  m<sup>3</sup> of CO<sub>2</sub>. The gas, a byproduct of geothermal circulation, was exploited for dry ice from 1934 to 1954 (Muffler and White, 1968). Numerical modeling of steam flooding, a process whereby oil recovery is enhanced by the injection of steam, shows that CO<sub>2</sub> will be copiously produced from most strata where ~300°C waters are injected into the shallow subsurface. The hot waters react with siliciclastics to produce clays (hydrated aluminosilicates) by incorporating OH<sup>-</sup> from

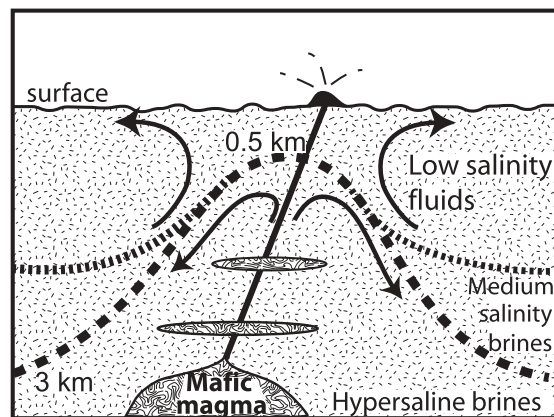


FIG. 13. Schematic section showing the bulge of hot Salton Sea brine below a convecting layer of lower salinity water. Arrows indicate fluid-flow direction. From McKibben and Hardie (1997).

water. This leaves  $H^+$  to react with carbonates and produce  $CO_2$ . Over  $2.8 \times 10^6 \text{ m}^3$  of  $CO_2$  was produced when steam was injected at Beuna Vista Hills, California, for example (Cathles et al., 1990).

$CO_2$  is produced by this same process in sedimentary basins without any intrusion if burial is sufficient for sediment temperatures to reach  $\sim 320^\circ\text{C}$ . For a normal geothermal gradient of  $20^\circ\text{C}/\text{km}$ , the partial pressures of water vapor and  $CO_2$  at  $320^\circ\text{C}$  exceed hydrostatic pore fluid pressures at a depth of  $\sim 7 \text{ km}$ , and a separate  $CO_2$ -rich vapor phase is formed, which migrates vertically by buoyancy. The vapor will react with aluminosilicates containing Ca, Mg, and Fe along its path, but if it reactively consumes these minerals by titration it can fill shallow reservoirs with  $CO_2$ . This has happened in the South China Sea (Cathles and Schoell, 1998) and is one of the risks of exploring for natural gas in this area. The Gulf of Mexico basin is generally not deep enough to produce  $CO_2$  but it did so in the Late Cretaceous ( $\sim 100 \text{ Ma}$ ) in Mississippi when the Jackson dome intruded and drove decarbonation reactions (Studlick et al., 1990). The discovery well, drilled by Chevron in the early 1960s, penetrated a  $CO_2$  reservoir in the Pisgah anticline. Gas vented from the well, decompressed adiabatically, and froze the surrounding vegetation. The well was sold to a chicken processor who used it to freeze his chickens (Alden Carpenter, pers. commun., 1985).

Similar processes may occur in the Abitibi greenstone belt, which can be considered a volcanic-filled basin. For example, seawater convection associated with the formation of volcanic-hosted massive sulfide (VHMS) deposits will produce hydrated minerals. When buried sufficiently these minerals will recrystallize and dewater, releasing a  $CO_2$ -rich, low-salinity fluid, which, because of its low salinity, can efficiently transport gold as bisulfide complexes (Cathles, 1987). These fluids will logically vent through basin border faults, potentially forming lode gold deposits. The flat mineralized veins in the Dome mine indicate that gold-mineralizing metamorphic fluids, which vented through these faults, were overpressured. Our point is not that the lode deposits necessarily formed in this way but that preparation by earlier processes, in this case hydrothermal convection, can be important for later mineralization.

Substantial  $CO_2$  and  $SO_2$  are also expelled from basaltic intrusions (Gerlach et al., 1996; Wallace, 2003) and can have an important impact on the oxidation state of crustal melts and the porphyry ore deposits that derive from them (Candella and Holland, 1986; Hattori, 1996; Hattori and Keith, 2001). This is of considerable potential importance to fluid flow and alteration in the upper crust, but we do not discuss it further in this paper. For details on convection around intrusions, see Cathles (1981, 1983).

### Physical and Chemical Principles

The previous section shows that the range of resource types and observations related to fluid flow is diverse and broad in time and space. To understand the interrelated processes and flow phenomena discussed above it helps to describe and analyze them mathematically in basic physical and chemical terms. Many texts derive the equations that describe subsurface fluid flow. An excellent recent text that addresses ore deposits is *Groundwater in Geologic Processes* by Ingebritsen and Sanford (1998). We will not repeat these derivations but

rather will present only what is necessary to understand the flow phenomena we have just reviewed, with some details elaborated upon in the appendices. The approach we take follows, extends, and updates that of England et al. (1987).

#### *Porous media fluid flow*

The basic theory of porous media fluid flow is straightforward. Pore fluids move in linear response to the forces imposed upon them. The movement is described by the flux of the fluid,  $\vec{V}_\alpha$ , where  $\alpha$  is the fluid phase (e.g., oil, liquid water, or gas) through a homogeneous, isotropic porous medium:

$$\vec{V}_\alpha = \frac{k k_r^\alpha}{\mu_\alpha} \vec{F}_\alpha. \quad (1)$$

In this equation,  $\vec{V}_\alpha$  is the flux of fluid phase  $\alpha$  in  $\text{m}^3 \text{m}^{-2} \text{s}^{-1}$ ,  $\vec{F}_\alpha$  is the force acting upon the fluid phase in  $\text{N}/\text{m}^3$ ,  $\mu_\alpha$  is its viscosity in  $\text{Pa}\cdot\text{s}$ ,  $k$  is the intrinsic permeability of the porous medium through which it flows in  $\text{m}^2$ , and  $k_r^\alpha$  is a dimensionless parameter called relative permeability whose values range between 0 to 1. The relative permeability accounts for the reduction in intrinsic permeability to one fluid phase caused by the presence of another. The arrow over the top of a symbol indicates a vector, which is a parameter that has both direction and magnitude. Symbols without a superscript arrow are scalar quantities that have only a magnitude. For example,  $\vec{V}_\alpha$  points in the direction of the fluid motion and has a magnitude equal to the velocity that the  $\alpha$  phase would have if it occupied the entire space (e.g., no rock or other fluid phase is present). Because it occupies only its fraction of the pore space, the average velocity of the  $\alpha$  phase is  $\vec{V}_\alpha / \phi S_\alpha$ , where  $S_\alpha$  is the volume fraction of the pore space it occupies at the point in question ( $\alpha$  phase saturation) and  $\phi$  is the rock or sediment porosity.

The forces that act on a subsurface fluid phase are typically pressure gradients and gravity:

$$\vec{F}_\alpha = -\vec{\nabla} p_\alpha + \rho_\alpha \vec{g}. \quad (2)$$

This equation holds for any fluid. The gradient operator,  $\vec{\nabla}$ , determines the direction of greatest increase in  $\alpha$  phase pressure,  $p_\alpha$  in Pa. The density of the fluid is  $\rho_\alpha$  in  $\text{kg}/\text{m}^3$ , and  $\vec{g}$  is the gravitational acceleration in  $\text{m}/\text{s}^2$  (which points vertically downward in a coordinate system with its vertical axis positive upward).

Petroleum is a general term that includes liquid oil, hydrocarbon gas (a vapor), and nonhydrocarbon fluids such as  $CO_2$  (typically a vapor phase). If petroleum and liquid, possibly saline water, occupy the same pore space, the difference in pressure between the phase that does not wet the solid (usually petroleum) and the phase that does wet the solid (usually water) is the capillary pressure,  $p_c$ . If the nonwetting phase fills pores as small as some radius  $r$ , but not smaller, the pressure in the nonwetting phase will be greater than that in the wetting phase by an amount  $2\gamma/r$ :

$$p_c = p_{\text{pet}} - p_w = 2 \frac{\gamma}{r}, \quad (3)$$

where  $\gamma$  is the interfacial surface tension between water and petroleum in  $\text{Pa}\cdot\text{m}$ .

Equation (3) explains how liquid water rises in a capillary tube and how trees draw water from their roots up to their leaves. The principles are illustrated in Figure 14 in which a fine capillary tube (equivalent to a rootlet), initially filled with air, has been dipped into a water-saturated sand. The water is attracted strongly to the inner walls of the capillary tube. A meniscus forms, and capillary forces pull the water into and up the tube with a tensional force around the rim of the meniscus equal to  $2\pi r\gamma \cos \theta$ , where  $\theta$  is the contact angle. The tensional force divided by the area of the capillary tube gives the capillary pressure,  $p_c = \frac{2\pi r\gamma \cos \theta}{\pi r^2} = 2\gamma \cos \theta / r$ .

The contact angle is small, so  $\cos \theta$  can almost always be taken to be 1 without loss of accuracy. We have assumed that this is the case in equation (3). Water rises in the capillary tube until the capillary pressure is balanced by the weight of the water, e.g.,  $p_c = \rho_w g h$ , where  $h$  is the height of the capillary interface above the water surface in the cup. Note that, because the air pressure is zero, the water pressure just below the air-water interface in the capillary tube,  $p_{w2}$ , is negative. The water molecules are thus in tension, and water is drawn (sucked) into the capillary, literally as a string of molecules.

The capillary tube can be used to inject air into the sand but only if the air pressure at its upper end is large enough to cancel the capillary suction forces, i.e., only if the air pressure exceeds  $p_c$ . This air entry (or water displacement) pressure must be exceeded for air to exit the capillary tube and move into the sand.

If we substitute equation (3) into equation (2) with  $\alpha$  equal to petroleum ( $pet$ ), we see:

$$\vec{F}_{pet} = -\vec{\nabla} p_w + \rho_{pet} \vec{g} - 2\gamma \nabla \frac{1}{r}. \quad (4a)$$

Substituting for  $\vec{\nabla} p_w$  using equation (2) with  $\alpha$  equal to water ( $w$ ) gives:

$$\vec{F}_{pet} = \vec{F}_w - (\rho_w - \rho_{pet}) \vec{g} - 2\gamma \nabla \frac{1}{r}. \quad (4b)$$

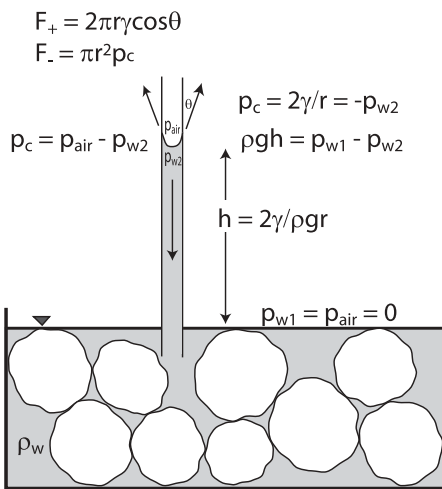


FIG. 14. Rise,  $h$ , of water in a capillary tube emplaced in sand with pores coarser than the tube diameter. Interfacial tension draws water up the capillary to a height where the weight of the water above the water table equals the capillary pressure. An air pressure,  $p_{air}$ , in the capillary greater than  $p_c$  is required to inject air into the sand through the capillary tube.

Equation (4b) shows that the force driving the petroleum phase is the same as that driving the water phase with two additions: a buoyancy term causes the lighter petroleum to move vertically through the pore space, and a capillary term pushes the nonwetting petroleum phase toward the larger pores. If there is lateral flow, buoyancy will cause lateral phase separation. The capillary expulsion of the nonwetting phase from the fine pores is the key to understanding relative permeability ( $k_r^\alpha$  in eq. 1) and is the key to understanding whether pore water will be invaded (i.e., penetrated by fingers of petroleum with negligible volume) or displaced (i.e., replaced and expelled) when petroleum is generated in a basin.

Equations (1), (2), and (4) completely describe multiphase fluid flow in the subsurface. If we were to numerically simulate multiphase fluid flow, we would need to add equations for conservation of mass and impose fluid continuity. Because our purpose here is simply to understand the basics of the flow, the above equations will suffice. We now need only be concerned with the magnitudes and characteristics of the parameters that control the flow described and some dimensionless combinations of these parameters that characterize the kinds of flow expected under various circumstances.

#### Relative permeability and invasion percolation

As discussed above and as illustrated in Figure 14, a nonwetting phase such as air or methane gas can enter a sediment saturated with water or brine if it is forced in with a pressure that exceeds the capillary entry pressure of the largest pore on the bounding surface; i.e.,  $(p_{gas} - p_w) > \frac{2\gamma}{r_{max}}$ , where  $r_{max}$  is the radius of the largest pore exposed to the gas. At this pressure, the gas can also pass through any of the connected pore throats that have a radius this large or larger. As the gas pressure is further increased, air penetrates smaller pore throats (at the edge and in the interior of the sample), a larger fraction of the pore space is filled with gas, and water is expelled from the sediment. Eventually, a point is reached at which even large increases in gas pressure result in only a very small increase in the fraction of the total pore space that is occupied by gas (i.e., gas saturation). At this point the wetting phase (water) is at its irreducible saturation,  $S_{iw}$ .

If, after gas has been forced into the sediment, its pressure is reduced, water will be pulled into the sample by capillary forces and gas expelled. This imbibed water will reduce the gas saturation. However, the imbibed water will not cause all the gas to be expelled. Some irreducible amount of the gas (nonwetting phase),  $S_{in}$ , will be left; Bear (1972) and Muskat (1937) discuss this further. The important point is that, during both expulsion and imbibition, the distribution of water and gas in the pore space is controlled by capillary forces. Capillarity pushes the nonwetting phase into the larger pores and throats, allowing the smaller pores and throats to be occupied by the wetting phase. Only if the pressure of the nonwetting phase is high can it occupy the smaller pores and throats of the sediment.

The relative permeability of the porous medium to wetting and nonwetting phases depends on the volume fraction of those phases in the pore space (Fig. 15). The relative permeability of a phase is closest to one when the phase occupies as

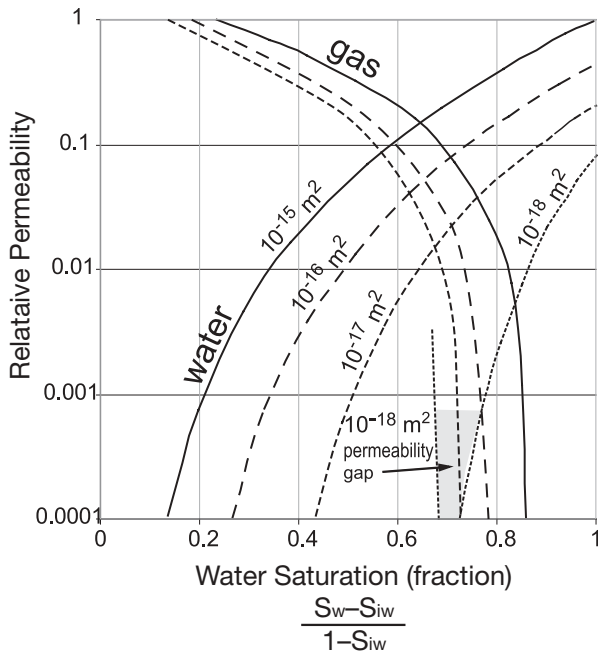


FIG. 15. Plot of relative permeability of both water and gas as a function of the water-saturation fraction for sediment of moderate to low permeability. Relative permeability is indicated for water and gas fluid phases by line style for sediments of different intrinsic permeability. For example, the solid line for water labeled “ $10^{-15} \text{ m}^2$ ” indicates the relative permeability of a sediment with  $10^{-15} \text{ m}^2$  permeability to water at various water saturations, while the other solid line labeled “gas” indicates the relative permeability to gas in the same sediment. Water-saturation fraction is the saturation relative to the saturation limits of each phase. Note that sediments of low permeability ( $<0.001 \text{ md}$ ) are impermeable to both phases over a range of water saturations near a water saturation fraction of 0.7 (shaded and labeled as permeability gap). Modified from Byrnes (2003).

much of the pore space as it can and is zero when the other phase occupies as much of the pore space as it can. The curves shift as the permeability of the porous medium decreases. For low permeability media, there is a range of water saturations near  $S_w = 0.7$ , within which the relative permeability of both phases is near zero. In this saturation interval (marked permeability gap in Fig. 15), both phases are immobile.

For any relatively homogeneous stratum, capillary effects can be incorporated into the relative permeability parameter  $k_r^a$  in equation (1), and the capillary terms in equation (4) can be dropped. Capillary forces only need to be considered explicitly at the boundaries between strata of rather strongly contrasting grain size. The capillary effect on flow can be especially strong in grain size-layered sediments, which is the rule rather than the exception in the subsurface. Laboratory experiments show that the capillary blockage of the flow of all fluid phases in grain size-layered media sediments can preserve over- or underpressures for geologic time periods (Shosa and Cathles, 2001). The blockage can be simply understood in terms of nonwetting phase entry pressure into each fine layer. Bubbles of the nonwetting phase act like stoppers, preventing the wetting phase from entering the pores of a finer grained layer.

For hydrocarbon migration, the stage when the nonwetting phase first invades and starts to percolate through the water-saturated pore space is of greatest importance. The style of very slow initial gas entry described above, wherein the nonwetting phase seeks the path of easiest entry, naturally produces a dendritic pattern (Fig. 16) of invasion that occupies very little of the pore space and has scale-invariant (fractal) and other interesting properties (Wilkinson, 1986; Lenormand et al., 1988; Carruthers and Ringrose, 1998; Carruthers, 2003). The dendritic, invasion-percolation pattern occurs when the rate of nonwetting phase invasion is small compared to its rate of migration. When the nonwetting phase invasion rate is fast compared to the rate at which it can migrate, the nonwetting fluid will displace the pore water like a piston. Further discussion can be found in Lenormand et al. (1988), Tokunaga et al. (2000), and Luo et al. (2004).

### Permeability

Permeability controls the rate at which single- or multi-phase fluids can flow through the connected pore space of a porous medium. We distinguish intrinsic permeability, which is a property of the medium at standard temperature and pressure, from dynamic permeability, which we define as the permeability that the lithology might have under nonstandard conditions, for example at high temperatures or pore pressures greater than hydrostatic. Intrinsic permeability is most reliably measured in the laboratory because it can be dynamically perturbed in the natural environment.

*Intrinsic permeability:* Permeability is measured in square meters and is controlled by the area of the smallest pore throats along a flow path connecting the largest pore throats. Sand permeability has been studied extensively for many years because it controls economic recovery of water and petroleum. Nelson (1994) provides a comprehensive review of laboratory measurements of sand permeability and, in a second paper (Nelson, 2000), the relationship between permeability and porosity and its evolution during compaction and

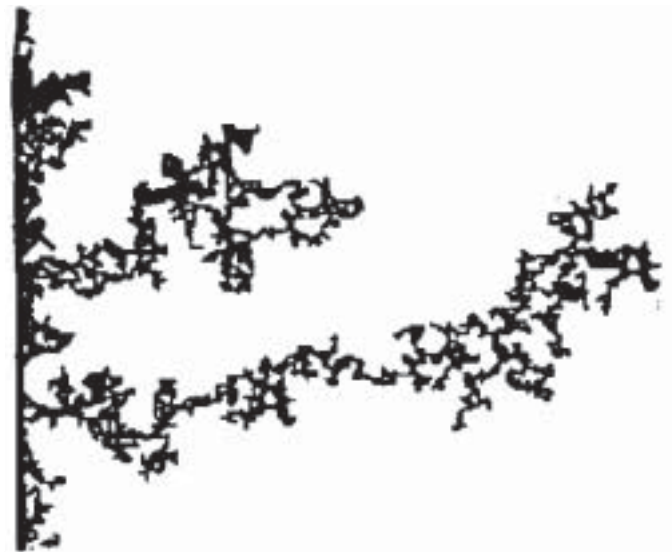


FIG. 16. Dendritic network of a nonwetting fluid percolating into a water-saturated porous medium. After Lenormand et al. (1988).



diagenesis is considered. The most permeable sandstones, quartz arenites, are composed of quartz. As the proportion of feldspar or rock fragments increases, sandstone permeability decreases. Permeability decreases and the range of permeability increases with compaction and diagenesis. Because pore throats are especially affected by compaction, porosity has been found to be a more useful master variable for describing permeability than grain size (Nelson, 2000).

In any particular formation or depositional facies, there is usually a rather linear relationship between porosity and the logarithm of permeability (Fig. 17, based on data from 26 formations). The left (coarse quartz arenite) boundary of the sandstone band in Figure 17 can be considered a practical upper bound for intrinsic permeability of clean (no clay) sandstones in nature. Fine-grained arkose or litharenite sandstones can be considered a lower bound for clean sandstones. The high-permeability end of this band (unconsolidated, well-sorted coarse sand with 100- to 1,000-D permeability) is constrained by careful laboratory measurements (Beard and Weyl, 1973). The low-permeability end of the band is compacted sandstone, with a permeability similar to that of compacted shale.

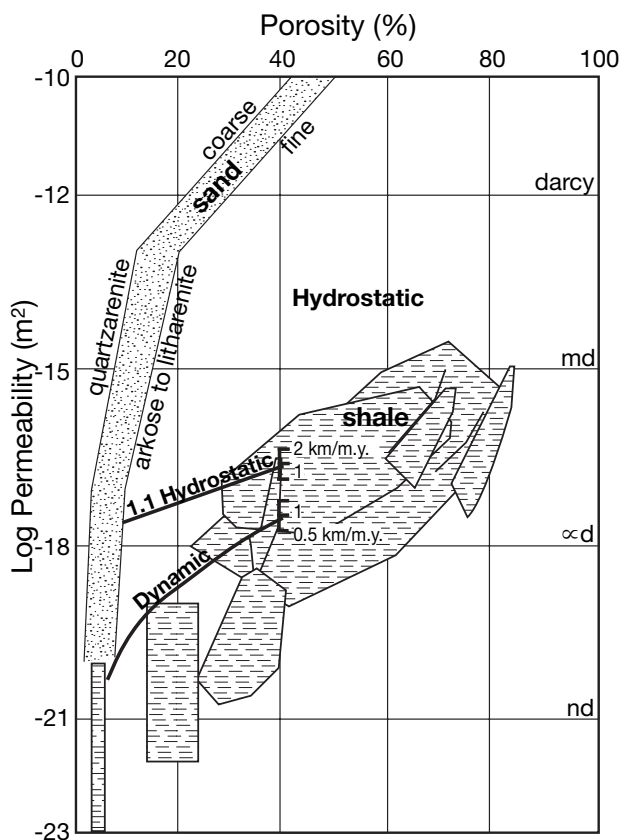


FIG. 17. Logarithm of permeability plotted against porosity for sandstones (Nelson, 1994; Nelson, 2000) and shales (Neuzil, 1994). Coarse quartz arenites are the most permeable lithology. The curve labeled “Dynamic” represents the minimum permeability that shales with different porosities (depths of burial) can have when the sedimentation rate is 1 km/m.y. The ticks at the right end of the curve indicate how the curve will shift if the sedimentation rate is 0.5 or 2 km/m.y. The curve marked “1.1 Hydrostatic” represents the permeability that basin sediments must have for pore pressures to exceed hydrostatic by only 10 percent at sedimentation rates between 0.5 to 2 km/m.y.

Laboratory measurements of shale permeability are more difficult because shales have such a low permeability that the effects of water chemistry must be considered. Neuzil (1994) has compiled reliable laboratory measurements (Fig. 17). Compared to sandstone, the logarithm of shale permeability shows a less concave and broader linear relationship with the logarithm of porosity. Highly porous, just-deposited mud of  $10^{-15}$  m<sup>2</sup> (millidarcy) permeability compact to shales of  $10^{-21}$  m<sup>2</sup> (nanodarcy) permeability. Sand and clay that are mixed on the pore scale have the lowest permeability when the clay completely fills the sandstone pores (Revil and Cathles, 1999). This is because the sand grains have zero permeability while the shale they replace has only a very low permeability. Thus, the presence of sand reduces the permeability of the mixture below that of pure shale. The lower bound on the shale permeability band (Fig. 17) may provide a reasonable estimate of this minimum permeability mixture.

The permeability of granular, nonvuggy carbonates depends on porosity in a fashion similar to sandstones (Nelson, 1994). Vuggy or karstified carbonates can be extremely permeable and require special treatment, however. Dolomites may or may not have a greater permeability than limestones. As reviewed by Machel (2004), enhancement of porosity and permeability during dolomitization occurs by mole-per-mole replacement, calcite and/or dolomite dissolution, fluid mixing, and thermochemical sulfate reduction, whereas, dolomite and calcium sulfate cementation and other processes fill porosity and reduce permeability. In general, dolostones found at depths greater than 2,000 m are more porous and permeable than limestones and dolomitic limestones. Processes vary from place to place, and porosity and permeability development must be investigated on a case-by-case basis. Igneous rocks show a permeability dichotomy similar to siliciclastic rocks. Basalts can be as permeable as sandstones and unfractured granite intrusions as impermeable as shale (Freeze and Cherry, 1979).

Overpressuring, clay coatings (Nelson, 1994), and oil staining (Bloch et al., 2002) can inhibit compaction and preserve permeability. The development of secondary porosity can increase permeability and can be used to infer cumulative fluid transport (Franca et al., 2003). Recent models show that permeability is related to the square of pore throat size multiplied by porosity. Electrical conductivity (Revil and Cathles, 1999) and capillary pressure measurements (Nelson, 1994) can probe this relationship and measure effective pore throat size. Nelson (2000) give an excellent review of models developed over the last 50 yrs and their motivation and uses.

*Dynamic permeability:* Intrinsic permeability is only a starting point because pressure and temperature can greatly change the permeability of natural materials. We know, for example, that igneous rocks become progressively more impermeable as they are heated above  $\sim 350^{\circ}\text{C}$  because models of midocean hydrothermal vents discharge waters far hotter than observed unless such a permeability decline is incorporated into the models (Cathles, 1983). The decline in permeability is probably caused by the pressure-dissolution of the grains that prop fractures open. On the other hand, thermal contraction at the margins of intrusions can fracture a rock and greatly increase its permeability (Lister, 1974). Temperature controls on permeability have been incorporated into

numerical models by altering permeability relative to the intrinsic value as a function of temperature. These models vent hydrothermal fluids across the sea floor at the same temperature range as black smokers and have other features similar to those observed in volcanogenic massive sulfide districts and ocean hydrothermal systems (Germanovich and Lowell, 1992; Cathles, 1997; see also Fournier, 1999; Carr and Cathles, in press).

Fluid pressure is another variable that can greatly change permeability. A familiar example is hydraulic fracturing, where fluids are injected into a well at pressures high enough to fracture the formation. A strong permeability increase, whether by dilation or the creation of fractures, occurs whenever pore-fluid pressures approach about 0.85 times lithostatic pressure. For example, an increase in permeability, from  $5 \times 10^{-18}$  to  $10^{-12} \text{ m}^2$ , has been measured in the decollement of the Barbados accretionary prism as pore pressure increases from hydrostatic to lithostatic (Fisher et al., 1996; Screaton et al., 1997).

Permeability in active sedimentary basins is controlled dynamically when pore pressures reach levels capable of hydraulically fracturing the sedimentary rocks. The permeability is dynamically adjusted so that pore fluids escape at the rate at which they are expelled by compaction, thermal expansion, and positive volume chemical reactions such as petroleum maturation. This dynamic permeability can be calculated assuming the hydraulic fracture pressure is a specified fraction of lithostatic, such as 0.85 (Apps. 2–4). The permeability required for the pore fluids to escape if fluid pressures exceed hydrostatic by 10 percent can also be calculated. Both of these curves are plotted in Figure 17 for sedimentation rates between 0.5 and 2 km/m.y. The “Dynamic” curve (Fig. 17) is the minimum permeability that the sediments in a basin can have at a specified sedimentation rate. If the sediments were less permeable, pressure would increase above the hydraulic fracture pressure of 0.85 times lithostatic pressure. If the sediments were more permeable, the basin would be less overpressured. The range in sediment permeability over which a basin becomes lithostatically pressured lies mostly between the “Dynamic” and “1.1 Hydrostatic” curves. This is not a very large range of permeability compared to the range in intrinsic permeability of sediments and sedimentary rock.

These permeability curves allow for determination of the conditions under which the petroleum that is generated in a basin will percolate through or displace the pore waters in the basin (App. 5). Consider the case where the petroleum (liquid oil and hydrocarbon gas plus nonhydrocarbon liquids) is generated at a ~6-km depth from a modestly organic-rich source stratum that is 100 m thick and contains 2 wt percent reactive kerogen. Suppose also that the kerogen matures over a 30°C temperature interval with a 100 percent net volume increase, and that the petroleum migration is driven by buoyancy and, if the basin is overpressured, also by the excess hydrostatic pressure gradient as indicated by equations (1) and (4b). Under these circumstances, Figure 18 shows that the petroleum migration rate will exceed the generation rate by a factor of five or more. Because the migration rate exceeds the generation rate, the petroleum will percolate through the overlying strata. However, if the source interval were a kilometer or more thick, the petroleum generation rate would be

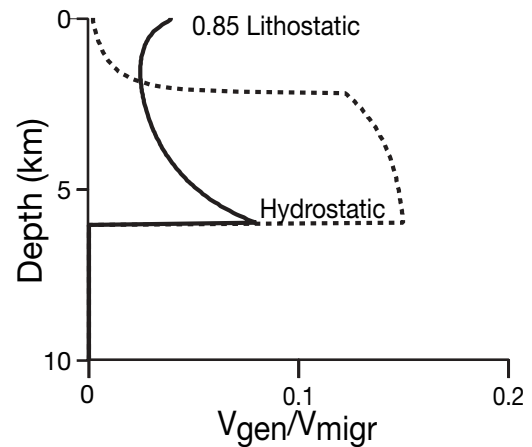


FIG. 18. The ratio of the rate of petroleum generation to the rate of petroleum migration plotted as a function of depth for basin pore pressures of 1.1 hydrostatic and 0.85 lithostatic in a basin overpressured from the surface. Hydrocarbons are generated from a 100-m-thick layer with 2 wt percent reactive kerogen at a 6-km depth. The sedimentation rate is 2 km/m.y. and the geothermal gradient is 20°C/km. A 100 percent volume increase occurs as kerogen is converted to gas over a 30°C temperature interval. Under these circumstances petroleum generation is less than the rate at which the gas will migrate, and gas will percolate through the overlying sediments by invasion percolation. However, as discussed in the text, if the organic source strata were thicker, the rate of petroleum generation would be greater than its migration rate, and the overlying pore fluids would be displaced by the generated gas.

15 times large (App. 3, eqs. A3.6, A3.7). The petroleum generation rate would then exceed its migration rate in both over- and hydrostatically pressured basins, and the generated petroleum would displace pore waters from overlying strata. The basin would fill with petroleum and, in mature basins, this petroleum would be petroleum gas. Increasing the sedimentation rate in hydrostatically pressured basins will encourage pore water displacement but will not do so in overpressured basins because both the rate of maturation and dynamic permeability depend on the sedimentation rate.

The important conclusion to be drawn from this discussion is that, under common geologic conditions, petroleum migration can occur by either invasion percolation or displacement. If the intrinsic permeability of the basin sediments is less than  $\sim 10^{-18} \text{ m}^2$ , the petroleum will displace or percolate through the pore waters at near-lithostatic pressures. If the sediment permeability is greater than  $\sim 10^{-17} \text{ m}^2$  the petroleum will displace or percolate through the pore waters at hydrostatic pressures.

If gas displaces the pore waters under hydrostatic conditions, pressures below the water-gas interface at the top of the gas-filled zone will increase with depth along a gas-static curve. If hydrostatic pore waters contact the base of the gas-filled interval, as in gas reservoirs, since gas weighs less than water, the gas will transmit the pressure at the base of the column to the top, and gas pressures at the top will be greater than hydrostatic pressure at that depth. If hydrostatic pressures are not applied at the base of the gas zone (or at its sides), because water contact is prevented by capillary sealing or low rock permeability, the gas-filled volume will be hydrostatic at its top where it contacts hydrostatically

pressured waters and progressively underpressured at greater depths (Fig. 10). Experiments by Davis (1984) illustrate this phenomenon.

We can thus expect to have under- or overpressured gas in the centers of basins. Where source beds are not kerogen rich or thick, we can expect to find water-saturated petroleum basins that are hydrostatically pressured or overpressured with respect to hydrostatic, depending on the permeability of the sedimentary rock. When source beds are richer in kerogen or thicker such that petroleum displaces pore waters, this displacement should occur over a time interval of petroleum generation (several to ten million years).

Finally, an important point is that uplift and erosion will not cause overpressured gas accumulations to become underpressured, as one might intuitively expect and is commonly assumed in the literature. In fact erosion will cause underpressured (basin-center) gas to become overpressured. This is because the high compressibility of the trapped gas causes it to depressurize only a little as the lithostatic load and the hydrostatic reference pressure are reduced by erosion. Considering all effects (cooling, etc.), unloading a basin by erosion will cause underpressured gas accumulations to become overpressured, not the converse (Katahara and Corrigan, 2002). Thus underpressured basin-center gas accumulations dictate that gas displaced water without becoming overpressured with respect to hydrostatic, that there was relatively little subsequent erosion, and that hydrostatic pore waters contact the gas zone only at its top.

*Some implications and consequences:* The porosity-permeability relationship of sandstone and shale (Fig. 17) can be combined with predictions of how sandstone and shale porosity changes with depth (App. 2) to produce permeability-depth curves for hydrostatic and overpressured basins (Fig. 19). The predicted sandstone permeability allows us to assess

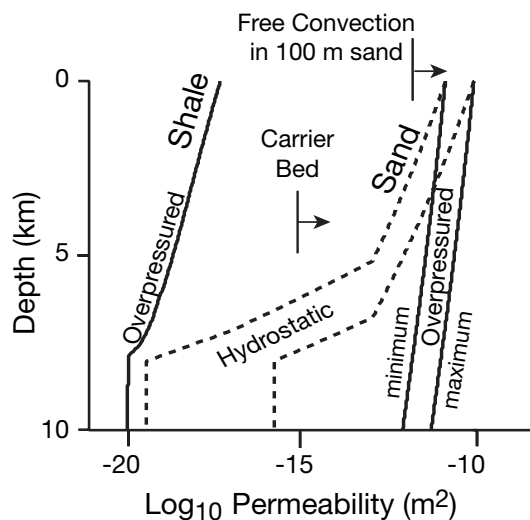


FIG. 19. Permeability of sand and shale under 1.1 hydrostatic and 0.85 lithostatic (overpressured) conditions as a function of depth. Curves were obtained by combining both sides (e.g. the min and max) of the sand band and the dynamic shale permeability at 0.5 lithostatic in Figure 17 with the porosity-depth curves in Appendix 2, Figure A5. The 1-md cutoff for carrier sand permeability and the sand permeability that allows free convection in a 100-m-thick sand (App. 1, Table A1.4) are indicated as vertical line segments with arrows pointing to the right.

the role of carrier beds in petroleum migration. Carrier beds are the petroleum equivalent of aquifers. The fine pores of shales overlying sandstone layers resist hydrocarbon entry until the capillary entry pressure is exceeded (see Berg, 1975; Schowalter, 1979, discussion of Fig. 14). If the sandstones are regionally extensive and more permeable than  $10^{-15} \text{ m}^2$  (England et al., 1987), the hydrocarbons may find it easier to migrate laterally than vertically and can do so over large distances (10s to 100s km). Figure 19 suggests that clean regional sandstones shallower than ~7 to 8 km in hydrostatically pressured basins could be effective carrier beds. Sands in overpressured basins can be effective carrier beds to much greater depths!

The contrasting thermal conductivity of sandstone and shale can force convection of pore fluids in folded sandstone. This convection will precipitate quartz at the top of the layer where the circulation is upward and dissolve quartz at the base of the layer where pore-water circulation is downward. The time required for the porosity to fill completely as the result of quartz precipitation in upflow locations can be calculated (Table A1.8). Figure 20 plots this filling time for a 100-m-thick sandstone bed with permeability equal to those on the edges of the sandstone band in Figure 17 that is folded with an amplitude to wavelength ratio of 0.01 in overpressured and hydrostatically pressured basins. At shallow depths folded quartz arenite sandstones could modify their porosity significantly in a few 10s to 100s of m.y. Convection in arkose or litharenite sandstones could modify their porosity in an

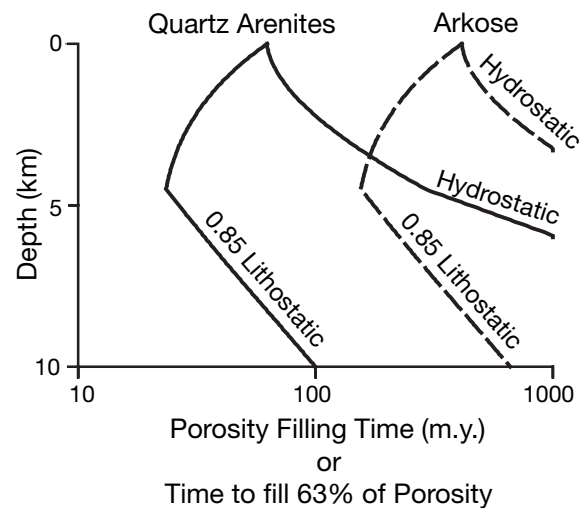


FIG. 20. Time to fill pores with silica in folded coarse quartz arenite and fine arkose sandstones (left and right boundary of sandstone band in Fig. 17). Curves are calculated from formulas and parameters in Appendix 1, Table A1.8 for a folded sand bed 100 m thick with an amplitude to wavelength ratio of 0.01. Curves are presented for both hydrostatic and 0.85 lithostatic pore pressures and for coarse quartz arenite (left boundary of sand band in Fig. 17) and fine arkose (right boundary of sand band) sandstones. Filling time decreases with depth because water viscosity decreases by a factor of five between the surface and ~4-km depth, and this outweighs the decrease in sandstone permeability with depth. The kink in the curves results from holding the viscosity constant at  $2 \times 10^{-4} \text{ Pa}\cdot\text{s}$  below this depth. Sand permeability depends on porosity as shown in Figure 17, and porosity changes with depth as shown in Appendix 2, Figure A5. The rate of alteration is proportional to the geothermal gradient squared. Overpressured basins with high-temperature gradients will be those best able to modify the porosity of their sands by convectively dissolving and precipitating silica.

overpressured basin. Folded sandstones in basins with a high geothermal gradient could alter their porosity even more quickly because the rate of alteration is proportional to the thermal gradient squared.

Figure 21 shows how flow across a basin through a basal aquifer will affect the temperature of the aquifer. At the recharge (left) end, the aquifer first slopes down 5 km over a lateral distance of 500 km, is horizontal for 100 km, and slopes up to the surface over the next 500 km. As the flow rate through the aquifer increases, the temperature at a 1-km depth at the discharge end increases and then declines as the whole basin is cooled by the water inflow. The maximum increase in temperature is 67°C, about 80°C less than the unperturbed, no-flow temperature at the basin center (150°C). This temperature occurs at  $N_{PEe} = 0.9$ , which is equivalent to a pore-water flux of 34 m/yr in a 30-m-thick aquifer with one percent margin slope and a rock thermal conductivity of 1.5 W/m·°K and water heat capacity of 4186 J/m<sup>2</sup>·°K. Flow rates this high are unlikely. This flow system is limited by rainfall, which is at most 10 m/yr in rainforests. Rainfall could be focused into an exposed aquifer, but the J aquifer of the Great Artesian basin in Australia suggests that such focusing will be minimal. The J aquifer is exposed in the Great Dividing Range where the rainfall reaches 0.6 m/yr (Halbermehl, 1980) and is ideally situated to intercept and concentrate rainfall. The ground-water flux through the aquifer is <0.25 m<sup>3</sup>/m<sup>2</sup>·yr (Bentley et al., 1986), about half the rainfall in the

recharge area, however. Thus, it appears that under circumstances found today, the temperature is not perturbed as much as indicated by MVT deposits.

Faults and fractures can concentrate flow and facilitate the discharge of warm fluids. Forster and Smith (1989) show that infiltration in a 12-km-wide intermountain basin can produce warm springs along valley faults if their transmissivity is  $>10^{-12}$  m<sup>3</sup> and the host permeability is  $\sim 10^{-16}$  m<sup>2</sup>. Deloule and Turcotte (1989) calculate the temperature and silica deposition of fluids propelled vertically upward by a lithostatic pressure gradient through 1- to 10-mm cracks that terminate at the surface or the floor of a cavern. They show that larger cracks are effective at allowing base metal-rich solutions to vent to potential sites of ore deposition, whereas small cracks precipitate and become plugged with base metal sulfides and quartz before metals can be discharged. Their models provide a potential explanation for both deposits and trace metal occurrences in MVT districts.

Quantification allows us to test conceptual models of natural systems and to use observations of them to determine critical properties such as permeability. The most useful tools are sometimes the simplest. A set we have found useful is presented and discussed in Appendix 1.

### Analysis of Some Ore Systems

#### Mississippi Valley-type deposits

Mississippi Valley-type lead-zinc deposits are perhaps the most modeled type of basin-related ore deposits. Recent work has sharpened, but not resolved, questions regarding almost all aspects of their formation. Excellent reviews by Sverjensky (1986), Anderson and Macqueen (1988), Leach and Sangster (1993), Spirakis (1995), and Leach et al. (2005) provide additional background for the discussion that follows.

We discuss these deposits at considerable length because the physical and chemical constraints on them are particularly strong yet their formation mechanism is still not understood. Under the perceived constraints it is difficult to identify even a single mechanism that could produce them, and consequently we stand to learn a great deal about the dynamics of continental-scale brine flow. The main constraint on the mineralization flow systems is that the shallow deposit sites were briefly heated by at least several tens of degrees Celsius during ore deposition. Without this heating constraint, the deposits could be explained as the natural consequence of slow expulsion by compaction, as originally suggested (Noble, 1963; Jackson and Beales, 1967), or by cross-basin topography-driven flow or basin tilting, as suggested by later workers. The heating requires rapid brine discharge (Cathles and Smith, 1983; Bethke, 1985), and the brevity of heating requires that the flow occurred in short pulses. The problem is how to produce these pulses of rapid brine expulsion. The currently favored hypotheses of topography-driven brine flow and episodic expulsion from overpressured basins no longer appear viable, as we discuss below. Other aspects of MVT deposits are unresolved, such as why some are dominated by lead and others zinc, and why they are associated with gas-filled basins at least in North America. We offer solutions to some of these problems, but our main point is that important aspects of these deposits remain to be understood.

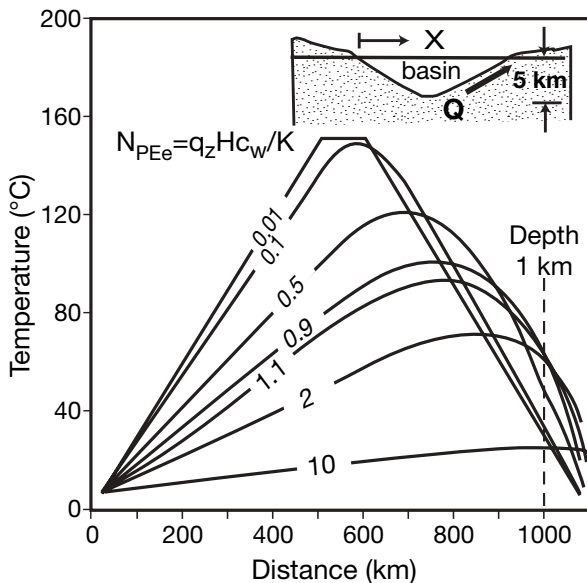


FIG. 21. Changes in temperature caused by fluid flow through a thin basal aquifer. The aquifer geometry is sketched in the insert (sides slope to 5-km depth over 500 km; central flat portion is 100 km wide). A Peclet number equivalent,  $N_{PEe}$ , controls how temperature is perturbed by flow. In this expression,  $H$  is the thickness of the aquifer and  $q_z$  is the vertical fluid mass flux in the basin margins,  $c_w$  is the heat capacity of water, and  $K$  the thermal conductivity of all units. For  $N_{PEe} = 0.9$ , the temperature at 1-km depth on the discharge margin is elevated the most (37°C) above the no-flow temperature of 30°C. For  $P = 0.9$ ,  $H = 30$  m,  $c_w = 4,186$  J/kg·°K, and  $K = 1.5$  W/m·°K, the vertical Darcy mass flux,  $q_z$ , equals 340 kg m<sup>-2</sup> yr<sup>-1</sup> and  $Q$  is the total discharge from the aquifer in m<sup>2</sup> m<sup>-1</sup> yr<sup>-1</sup>. The mass flux that will most perturb the temperature at 1-km depth on the discharge margin is 34,000 kg m<sup>-2</sup> yr<sup>-1</sup>, which is equivalent to a Darcy (superficial) volume flux of 34 m/yr. Further discussion can be found in Cathles (1987).

**Brines:** It is agreed that MVT metals were transported by basinal brines of high salinity and low Br/Cl ratios, indicating that they were formed by the evaporation of seawater with perhaps a substantial contribution from the dissolution of halite (Chi and Savard, 1997; Viets et al., 1997). A recent analysis of published basinal brine compositions (Hanor, 1997) shows that basinal brines are in chemical equilibrium with a set of buffer minerals in the sediments and that the natural ratio of Zn to Pb is  $\sim 5/1$ . A combination of factors (decrease in the rock-buffered pH, increase in the  $\text{Cl}^-$  activity coefficient, increase in the dominance of higher order chloride complexes such as  $\text{ZnCl}_4^{2-}$ ) causes the solubility of Zn (and Pb) to increase abruptly by five orders of magnitude in a step function fashion at a chlorinity of  $\sim 10^5$  mg/L (equivalent to  $\sim 170,000$  mg/L total dissolved solids; Fig. 22). This strong increase in metal solubility allows dissolution to achieve high concentrations of metals in saline brines. For chlorinities  $>10^5$  mg/L, it is possible that reduced sulfur can be transported together with high concentrations of base metals, and that ore sulfides could be precipitated by a slight decrease in chlorinity (Hanor, 1997). Simultaneous transport of sulfur, in reduced or oxidized form, and base metals seems to be required by the coherent sphalerite banding that is observed over  $\sim 10$ s of kilometers (Fig. 2), and the coherent variation of lead and sulfur isotope ratios that is observed in MVT galena (Sverjensky et al., 1979; Hart et al., 1981; Crocetti and Holland, 1989).

The volume of brine in potential source basins is large enough to account for the associated MVT mineralization. From Figure 1 it can be seen, for example, that the Arkoma basin today contains  $\sim 3 \times 10^5$  km<sup>3</sup> of sediment (a volume  $100 \times 300 \times 10$  km deep) and, at 10 percent average porosity,

$\sim 30,000$  km<sup>3</sup> of pore space. The pore space in the basin today is residual from  $\sim 135,000$  km<sup>3</sup> of pore space that was compacted as the sediments accumulated (e.g.,  $135,000 \text{ km}^3 = 30,000 \text{ km}^3 \times (0.55-0.10)/0.10$ , where the initial sediment porosity is 0.55 and 0.10 is the assumed limit of compaction). An equal volume of brine would almost certainly have been expelled from the deformed accretionary prism to the south (Fig. 5). The Southeast Missouri and Upper Mississippi Valley districts contain  $\sim 57$  Mt of combined lead and zinc metal (Table 1). If the brines in the Arkoma basin contained 100 mg/L Pb + Zn, the amount of metal in the ore deposits of these districts could be dissolved in 570 km<sup>3</sup> of brine. Thus, even if noneconomic mineralization is equivalent to ten times the mass of metal contained in the ore deposits and the average metal content of the brine was 10 mg/L, the potential volume of expelled brine can easily account for the amount of metal in and around the deposits.

Noble gas and halogen analyses of fluid inclusions suggest that three different brines were involved in the MVT-related midcontinent metal transport: (1) an I-rich, shale-sourced Illinois-Kentucky brine, (2) a Br- and Pb-rich Viburnum Trend brine associated with the Lamotte Sandstone aquifer, and (3) a Tri-State brine that is seen in inclusions throughout the Ozark region, including those in the Viburnum Trend main-stage dolomite (Kendrick et al., 2002a). Trace element zonation suggests that the brines flowed, perhaps at different times, into the Viburnum Trend from both the south (Arkoma basin) and the north (Illinois basin; Shelton et al., 1992).

**Metals:** Sulfur isotope studies indicate that sulfur in the deposits came from seawater sulfate, although possibly by dissolution of a sulfate mineral such as anhydrite (e.g., Crocetti and Holland, 1989). The relative proportions of Pb, Zn, or F in different districts are curious (Table 1). For instance, the Appalachian deposits contain zinc and very little lead. The Viburnum Trend and Old Lead Belt ores have very high Pb/Zn ratios for MVT deposits and are noteworthy as the largest known deposits of lead in the Earth's crust (Gustafson and Williams, 1981). In the Viburnum Trend and Old Lead Belt, almost all of the lead was deposited in the main-stage ores as octahedral galena, which is less radiogenic and more enriched in <sup>34</sup>S relative to <sup>32</sup>S than the minor amounts of lead deposited in the later cubic galena stage in these and other MVT deposits in the midcontinent. Goldhaber et al. (1995) suggested that the main-stage lead was leached from the hematitic pigments of the Lamotte Sandstone aquifer. While hematite was being leached, the reduced sulfur activity was very low, and the brines were able to carry high concentrations of Pb and produce the Viburnum Trend and Old Lead Belt lead deposits. When the hematite pigment was leached (Fig. 23), the brines became more reduced, resulting in more reduced sulfur and less lead in solution, and the lead that was transported was sourced from the more radiogenic felsic basement. This is a good story, but if oxidized sandstones favor lead-rich MVT deposits, it seems odd that the Upper Mississippi Valley district, whose brines were also transported by the hematitic Lamotte-Mount Simon Sandstone aquifer (Fig. 4), hosts so little lead (Table 1).

Fluorite is the main ore mineral in the southern Illinois fluorite district. Trace amounts of fluorine in the St. Peter Sandstone decrease northward across the Illinois basin (Fig. 24),

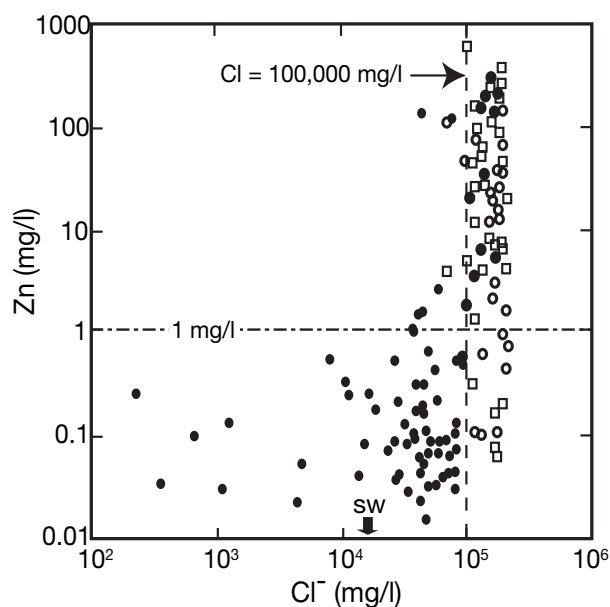


FIG. 22. Total zinc concentration in brines from the Gulf of Mexico basin as a function of chloride concentration. Solid dots are solutions from southern and offshore Louisiana, circles are solutions from southwest Arkansas, and the squares are solutions from central Mississippi. Zinc solubility increases in almost a step function at a chlorinity of  $10^5$  mg/L. Seawater contains 0.005 mg/L Zn and has a chlorinity of 19,180 mg/L, as indicated by the arrow on the abscissa labeled sw. Modified from Hanor (1997).

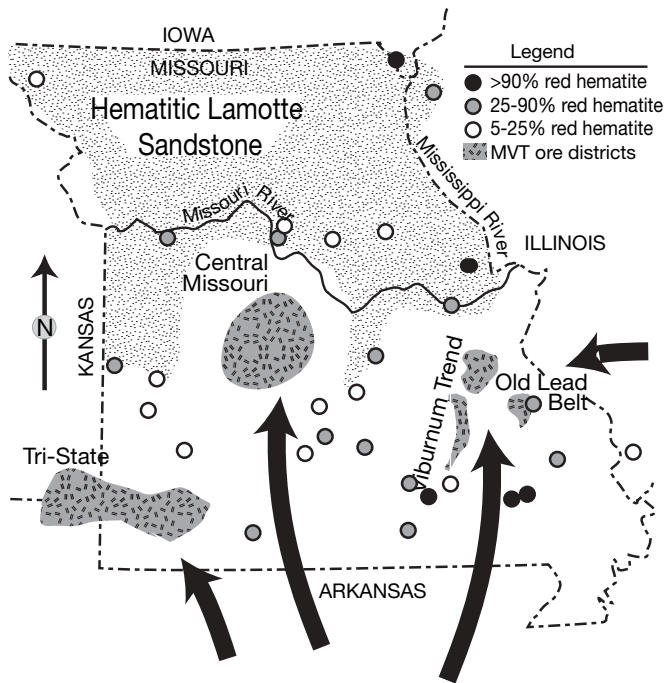


FIG. 23. Light stippled and filled circles show where red hematitic cement occurs in the Lamotte Sandstone. In white areas, the hematite has been leached by migrating basinal brines. Likely flow directions for the brines, based on the absence of hematite cement, are shown by arrows. Ore districts and showings are labeled. Modified from Goldhaber et al. (1995).

suggesting that the brines moved north from the fluorite district toward the Upper Mississippi Valley district. The fluorine could have been supplied by the rhyolite basement (Richardson et al., 1988), the Hicks Dome and associated intrusions in southern Illinois (Plumlee et al., 1995), or shale. Iodine-rich, shale-sourced brines are responsible for fluorite mineralization in the South Pennine ore field in England, where low  $^3\text{He}/^4\text{He}$  ratios in fluorite inclusions rule out a mantle helium contribution (e.g., a magmatic source) for the F, and high concentrations of radiogenic  $^4\text{He}$ , unless introduced later, require that the brines were retained in the shales for ~50 m.y. before being expelled into carbonate aquifers to precipitate fluorite (Kendrick et al., 2002b).

*Temperature of ore deposition:* Sangster et al. (1994) examined the critical issue of the temperature at which MVT ores were deposited. Combining fluid inclusion homogenization temperatures in sphalerite and the conodont color alteration (CAI) index in adjacent strata in 14 MVT districts, these authors found that, excepting sites that were eroded before mineralization, the MVT districts were all hotter than expected for their depth of burial at the time of mineralization. MVT districts that lie above their associated basal aquifers (Upper Mississippi Valley and Polaris) are more thermally mature than their surroundings (have higher CAI index conodonts). MVT districts located in their basal flow aquifers (Pine Point, Newfoundland Zinc, Central Missouri, northern Arkansas, and Tri-State) have the same thermal maturity as their surroundings (no CAI contrast). However, the homogenization temperatures of ore mineral inclusions (upper quartile and maximum) indicate that all districts were anomalously

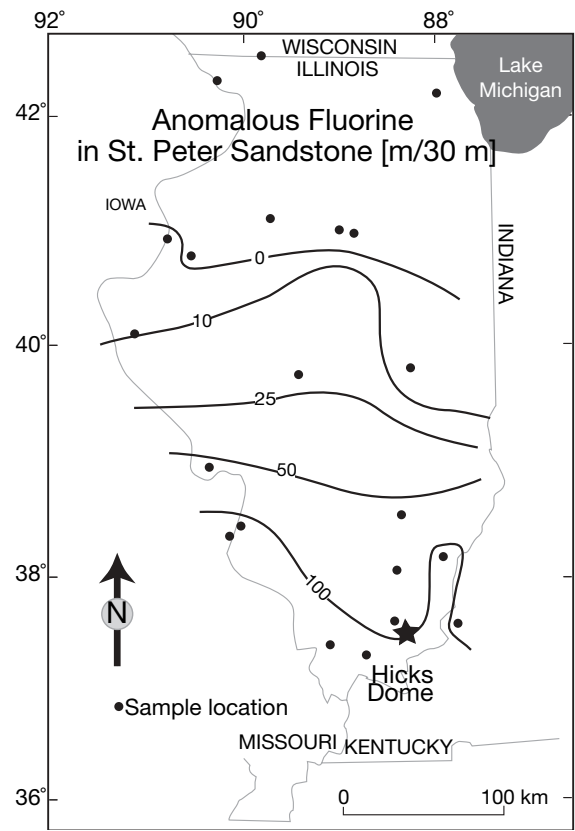


FIG. 24. Contours of anomalous fluorine concentration from the base of the St. Peter Sandstone to the top of the Maquoketa Formation measured in meters of core with excess fluorine per 30 m of core. Star indicates the location of the Hicks Dome. From Rowan and Goldhaber (1995).

hot for their burial depths at the time of mineralization (4<sup>th</sup> column, Table 2). Furthermore, in most cases, the deposits could have remained at ore deposition temperatures for at most a few 100,000 yrs without maturing conodonts more than observed (6<sup>th</sup> column, Table 2). This is particularly well documented in the Upper Mississippi Valley district where zinc diffusion halos (Lavery and Barnes, 1971), the maturity of organic matter (Rowan and Goldhaber, 1995), and conodont maturity (Table 2) all indicate that the total heating time could not have been longer than ~200,000 yrs.

*Temperature and salinity constraints:* During ore deposition the metal-depositing fluids were both hot relative to the temperature expected at the shallow depths of formation (Anderson and Macqueen, 1988; Sangster et al., 1994) and hypersaline. This is a problem for cross-basin topography-driven flow models because topography-driven flow tends to cool a basin as it warms its discharge side (Cathles, 1987; Fig. 21) and tends to flush brines from the basin before the margins are warmed. Deming and Nunn (1991) point out that many topography-driven flow models (e.g., Bethke, 1986; Bethke and Marshak, 1990) require unrealistically high heat flows (~100 mW/m<sup>2</sup> or more) to match the observed mineralization temperatures, and that basins permeable enough to warm their discharge margins are cooled more than seems reasonable in their recharge zones. For example, the recharge end of the Ouachita-Arkoma flow system may have been strongly

TABLE 2. Temperature and Maturity Relationships in Selected MVT Districts (from Sangster et al., 1994)

MVT ore district	Burial depth at mineralization (km)	Fluid inclusion homogenization <sup>1</sup> (T <sub>75%</sub> -T <sub>100%</sub> ) (°C)	Temperature gradient for T <sub>surf</sub> = 15°C (°C/km)	CAI index	Maximum duration <sup>2</sup>	
					T <sub>75%</sub> , CAI <sub>min-max</sub> (yrs)	T <sub>100%</sub> , CAI <sub>max</sub> (yrs)
Pine Point	1.5	85–95	43–50	1–1.5	12,500–177,000	106,000
C. Missouri	0.8	100–110	100–110	1.5–2	40,200–794,000	290,000
N. Arkansas	0.46	120–130	220–240	1.5–2	6,640–112,000	45,000
Tri-State	0.25	110–120	360–400	1.5–2	16,000–290,000	112,000
UMV <sup>3</sup>	1.5	130–150	60–74	1	280	70

<sup>1</sup> Fluid inclusion homogenization temperatures are given at the 75<sup>th</sup> percentile and maximum values

<sup>2</sup> The maximum time duration that conodonts could be at these temperatures and have the range of alteration indices (CAI) observed are calculated from third and fifth columns using the conodont maturation kinetics in Epstein et al. (1977)

<sup>3</sup> UMV = Upper Mississippi Valley district

heated rather than cooled. Low-salinity inclusion fluids in barite with homogenization temperatures of ~300°C have been found in organic-rich seams in Cambrian shale on the shores of Lake Ouachita, Arkansas (Shelton et al., 1992).

Salt in MVT brines originates from a mixture of evaporated seawater and dissolved halite (Chi and Savard, 1997; Viets et al., 1997). In a topography-driven flow system, recharging fresh water will quickly flush salinity from the basin unless halite dissolution occurs. The boundary between fresh and salt water will move through the aquifer at the true velocity of the water (i.e., the water flux divided by the aquifer porosity), which for a porosity of 20 percent is five times the water flux. If the aquifers contained 20 wt percent salt that dissolved with the incursion of meteoric water, the halite dissolution front would move through the aquifer at 0.6 times the water flux (App. 1, Table A1.9). Bethke (1986), Garven et al. (1993), and Arnold et al. (1996) find a horizontal water flux of ~10 m/yr in the Cambrian aquifers of the Illinois basin is needed to perturb temperatures as observed in the Upper Mississippi Valley district. The methods in figure 4 of Cathles (1987) yield a similar estimate. At a flux of 10 m/yr, meteoric water will flush brine from a 1,000-km-long aquifer with 20 percent porosity in 20,000 yrs. Considering dispersion, the discharging brine will decrease to 50 percent of its initial salinity at 20,000 yrs, to 25 percent in 40,000 yrs, and so on. Dissolution of 20 wt percent halite in the aquifer system would take ~170,000 yrs (10<sup>6</sup>-m-long aquifer divided by halite dissolution velocity, which is 0.6 times the darcy velocity of 10 m/yr). Considering that topography-driven flow will continue for at least tens of millions of years after it is established, the presence of halite in Cambrian aquifers will not help the salinity-flushing problem much. Furthermore, brines are still in the aquifers today (Cathles, 1993). Brines could have been reintroduced after mineralization (Appold and Garven, 1999) and/or introduced continuously as cross-basin topography-driven flow was taking place as suggested by Rowan and de Marsily (2001). The latter is necessary if gravity drives the brine flow because thermal fronts move ~2.5 times more slowly than salinity fronts (App. 1, Table A1.9), and it is therefore difficult to elevate the temperature in MVT districts before salinity is strongly diminished.

*Duration of heating:* The short duration of heating poses additional difficulties. It is very difficult to limit the duration

of marginal heating in realistic topography-driven flow models. Models in which basin recharge areas are elevated from the start of the simulation produce heat pulses of limited duration at their discharge margins. In a model of flow across the Arkoma basin, for example, Garven et al. (1993, their fig. 15) show that temperatures at deposit depths near the Ozark dome increase from 60° to 125°C for a few tens of thousands of years and then decrease to ~90°C. For longer sections, the duration of heating is longer (Garven et al., 1993; Appold and Garven, 1999). However, Deming and Nunn (1991) showed that no thermal pulse occurs at the discharge side of a basin that is tilted slowly, as must occur geologically. In all of these models, salinity is greatly reduced before the margin temperature is raised.

Rowan et al. (2002) suggested that transient heating by the Hicks Dome and other intrusions could account for the short-duration heating. They show that if heat flow in the Hicks Dome area of southern Illinois is increased from 62.5 to 155 mW/m<sup>2</sup> for 2 m.y., the observed basin-wide coal maturity and the range of sphalerite homogenization temperatures in the Upper Mississippi Valley and Fluorite districts can be matched with reasonable erosion and other parameters. Temperatures at the Upper Mississippi Valley and the Fluorspar districts are elevated for only ~200 k.y. in their models.

*Fluid access:* Rowan et al. (2002) introduced warm brines at depth on the southern vertical boundary of their model and thus sidestepped the last topography-driven flow-modeling challenge: fluid access. The flow rates required to elevate basin-margin temperatures can only be achieved in models with vertical sediment permeability of >10<sup>-16</sup> m<sup>2</sup> (0.1 md; Deming and Nunn, 1991). At a porosity of 15 percent, this is the permeability expected for clean arkosic sandstone (Fig. 17), which is unrealistically high for the basins associated with MVT deposits. Even a single low-permeability stratum can decrease the average vertical permeability well below 10<sup>-16</sup> m<sup>2</sup>. The 60-m-thick Marquoketa Shale, for example, probably reduces the average permeability of the permeable units overlying the Mount Simon Sandstone in the Upper Mississippi Valley district from ~4 × 10<sup>-16</sup> to <0.1 × 10<sup>-16</sup> m<sup>2</sup> (calculated from data in Arnold et al., 1996). A single shale in the recharge areas would have similar impact. The average vertical permeability of the Western Canada Sedimentary Basin, which hosts the Pine Point MVT district, is 0.1 × 10<sup>-16</sup> m<sup>2</sup> (Adams et al., 2004).

Fluid access is also impeded by the fact that the interiors of the basins that are considered the potential brine sources for the North American MVT mineralization (the Appalachian, Arkoma, and Western Canada Sedimentary Basins) are gas saturated and underpressured. Gases can be underpressured only if they are not connected to adjacent hydrostatically pressured pore waters (see discussion above). Hence, flow across the underpressured parts of MVT-associated basins is impossible and has been impossible from the time these areas became gas filled and underpressured.

The underpressured nature of the MVT basins today also means that brines could not have been expelled from overpressured portions of these basins, at least since they filled with gas. As discussed above, an overpressured gas-filled basin cannot become underpressured if it is uplifted and eroded (Katahara and Corrigan, 2002). From the time they filled with gas, these basins could have episodically imbibed brine but could not expel it.

*Brine expulsion:* Assuming that the constraints discussed above are all valid, what process could expel brines rapidly enough to produce MVT deposits? Displacement of brine by gas generation has been suggested for the Cadjebut MVT deposit on the northeast margin of the Fitzroy trough, Canning basin, Australia. Sedimentation rates were very slow during ore deposition, which makes brine overpressuring unlikely. Separation of the ore district from distant uplands by intervening basement highs makes topography-driven flow unlikely, and the presence of extensional structures active just before mineralization eliminates seismic pumping. Metal deposition occurred simultaneously with hydrocarbon migration (30% of the sphalerites are stained purple with hydrocarbon-filled fluid inclusions), and a regional unconformity overlies the deposit. Eisenlohr et al. (1994) argued that the Cadjebut deposit formed when regressing seas moved the basin surface through the ocean thermocline, causing the sea floor, and quickly thereafter the basin sediments, to warm by as much as 16°C. This temperature increase could rapidly mature gas that would expel brine and form the deposits. Minor reverse faulting, subhorizontal veins filled with ore, and fragments within an ore matrix that provide evidence for brecciation suggest overpressured conditions at the time of mineralization. Whether the interior of the basin was under- or overpressured is thus uncertain, but brine displacement by gas is strongly suggested at Cadjebut.

We assess various possibilities for brine expulsion in Appendix 6 and conclude that gas generation could not expel brine from the Arkoma basin as rapidly or episodically as is required by the thermal constraints of the midcontinent MVT deposits. In fact this calculation shows that the thermal constraints are so restrictive that it is difficult to identify even a single viable hypothesis. We show in Appendix 6, however, that a rapid increase in sea level over the Arkoma basin, such as might occur as continental glaciers melt at the start of an interglacial, could compact the pore space in the gas-filled parts of the basin and displace enough brine to warm the flow paths from the Arkoma basin to all the associated MVT deposits. The brine is displaced rapidly enough to elevate ore-district temperatures and for short enough periods (~10,000 yrs), that a dozen or so pulses would not warm the deposit sites more than is allowed by maturity indicators (Table 2).

Furthermore, glacial sea-level fluctuations during the Permian could produce the midcontinent MVT mineralization over the time span indicated by paleomagnetic measurements (Fig. 2). As noted earlier, western Pennsylvania was deforming after 255 Ma. Thus, prism compression cannot be ruled out as a potential mechanism for episodic brine release.

Another possibility is rapid and episodic injection of brine into the Cambrian aquifers from the deforming Ouachita accretionary prism (Fig. 5). But this mechanism would only apply when the prism was deforming, from ~305 to 290 Ma (gray vertical bar, Fig. 2) and could not account for the deposits formed later.

*Other interesting aspects of MVT deposits:* MVT mineralization is associated with organic material, sulfide deposition, and dolomitization; commonly, anhydrite is replaced by carbonate minerals. Organic material reduces sulfate via biochemical and thermochemical sulfate reduction (Anderson and Garven, 1987). In saline brines with  $Mg^{+2}$  present, sulfate reduction consumes acid and causes white, sparry dolomite precipitation, unless sulfide precipitation also occurs (whereupon the sulfide precipitation generates acid and causes dolomite to dissolve). Reaction-path simulations of anhydrite reduction by methane show that dolomite is precipitated before the  $HS^-$  activity reaches the concentrations adequate to precipitate sphalerite. At conditions suitable for sphalerite precipitation, dolomite is dissolved slightly. After the zinc content of the solution is depleted, dolomite is again precipitated. The interplay between brine, sulfate minerals, organic material, and sulfides can be complex, and Anderson and Garven (1987) presented process diagrams for all the combinations that have been suggested in the literature (e.g., transporting sulfate and base metals in brine and reacting with organic carbon at the site of deposition, transporting base metals and organic carbon in brine and precipitating sulfides by interaction with sulfate at the deposit, etc.).

There is an interesting dichotomy in MVT districts between observations that indicate large-scale process coherency on one hand and small-scale chaos on the other. The uniformity of sphalerite (Fig. 2) and cathodoluminescent banding across 10s to 100s of kilometers, the regular changes in lead isotope composition (Fig. 25, Heyl et al., 1966), and coherent trends in sulfur and lead isotope composition with time in galena crystals are significant. If examined on a finer scale (Delouie et al., 1986), however, the coherent lead and sulfur zoning in galena crystals becomes chaotic and uncorrelated. There are other complications: (1) periods of sulfide dissolution are interspersed with deposition, (2) fluid inclusions in MVT districts have a very large range of homogenization temperatures, (3) vast quantities of brine have flowed through thermally anomalous deposit sites but there has been remarkably little silica deposition (Rowan and Leach, 1989; Leach et al., 1991), and (4) it is notable that the simple mineral associations in MVT deposits are thermodynamically incompatible (e.g., the minerals do not coexist at the same pressure and temperature; Barton, 1981).

Perhaps many of these conundrums should be expected (Cathles, 1993; Shelton et al., 1993). MVT districts were sites where hot brines occasionally discharged at high enough rates to temporarily warm the deposits and their surroundings. If, between these flow events, local meteoric waters flowed into



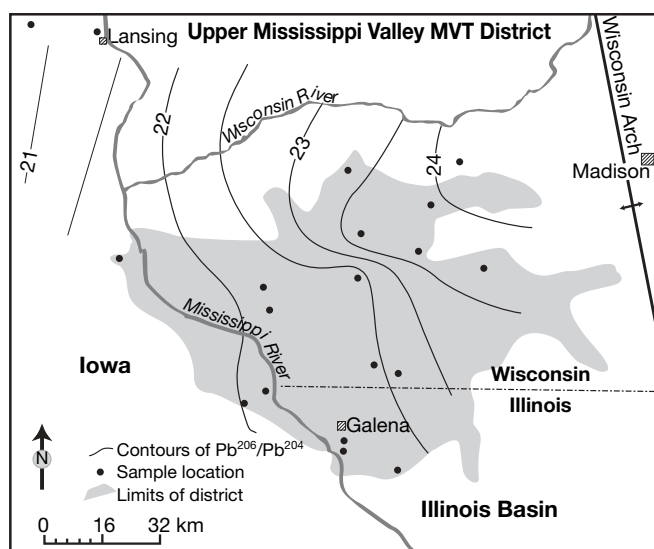


FIG. 25. Distribution of  $Pb^{206}/Pb^{204}$  in the Upper Mississippi Valley Zn-Pb district. Modified from Heyl et al. (1966).

the districts, driven by topography, as is occurring from the Ozarks into the Old Lead Belt and Viburnum Trend districts today (Cathles, 1993), then relationships in Appendix 1, Table A1.9 mean that saline fluid would be flushed by meteoric water before the sites were cooled; thus, high-temperature but low-salinity fluid could be trapped as inclusions. Similarly, low-temperature high-salinity inclusions could be trapped in the early stages of an expulsive pulse, because the high-salinity front would move through the district ahead of the thermal front. Minerals precipitated over a wide range of temperatures during repeated fluid pulses would be incompatible at any single pressure and temperature, explaining Barton's (1981) observation of thermodynamic incompatibility. Mixing during inflow and outflow could produce the observed small-scale chaotic isotopic fluctuations. Sulfide dissolution could occur during periods of inflow. During periods of major outflows of brine, however, brines from different aquifers could mix in differing proportions, producing coherent district-scale patterns and coherent and correlated isotopic variations in single galena crystals. Brines could be expelled from different basins at different times. Flow to the Ozark districts from the Illinois basin might have occurred at some times, while at other times flow was from the Arkoma basin. In other words, the complexities we observe might be just those that we would expect from local recharge phenomena, and the large-scale regularities might be just those expected from the regional periodic expulsion through all available aquifers of brines from the basins surrounding the MVT districts.

#### *Sedimentary-hosted stratiform base metal deposits*

Sedimentary-hosted stratiform and sedimentary rock-hosted stratiform Pb-Zn deposits contain over 50 percent of the world's reserves of lead and zinc (Goodfellow et al., 1993), and copper sedimentary-hosted stratiform and sedimentary rock-hosted stratiform deposits contribute 20 to 25 percent of

the world's production and reserves of copper (Kirkham, 1989). Sedimentary-hosted stratiform deposits form where brines discharge from basins, as do MVT deposits, but these systems have different and instructive features.

*Copper sedimentary rock-hosted stratiform deposits:* Sedimentary rock-hosted stratiform copper deposits such as White Pine (discussed above), the Kupferschiefer deposits in Germany and Poland, and the Zairian and Zambian Copperbelt (Selley et al., 2005) deposits occur over extensive areas where major thicknesses of permeable, coarse-grained, red-bed clastic sediments (Brown, 1992) are capped by organic- and pyrite-rich shales (Gustafson and Williams, 1981; Brown, 1992). Organic matter and pyrite in shale are oxidized when oxidized brine is forced through. Base metal sulfides replace preexisting sulfides, carbonates, and clastic rock fragments as the brines cross the redoxcline, a term Brown (1992) uses to describe the gradual or smeared-out nature of the redox front, separating the oxidized and as-yet unoxidized sediment.

The well-studied Lubin district in Poland is one of seven copper sedimentary rock-hosted stratiform districts in a 500-km east-west zone at the southern margin of the Zechstein basin, which covers 600,000 km<sup>2</sup> of Europe from Poland to England (Oszczpalski, 1989). The district is located at the edge of the small (130- × 200-km) Lubin extensional rift basin that is filled with oxidized terrestrial sediments and bimodal volcanic rocks (heavily albitized and hematized) of the Rotliegendes Formation.

The Lubin basin is one of many extensional basins that formed in the Early Permian when Late Carboniferous coal-bearing clastic Hercynian foreland basin sediments were uplifted, eroded, and extended in a basin-and-range topography. Sediments filled the basins in a semidesert setting of seasonal rivers and shallow playa lakes, and a peneplane developed. The region was covered by white dune sands (the Weissliegendes) immediately before a regional Late Permian transgression deposited up to 800 m of shallow marine Zechstein sediments in a series of carbonate-anhydrite-salt deposition cycles. The transgression reworked the top of the Weissliegendes into beach sands and then deposited a thin (~1-m) laminated, black, coaly shale known as the Kupferschiefer, in a coal swamp or lagoonal setting (Jowett et al., 1987).

After the Kupferschiefer was indurated, oxidized brines from the Rotliegendes Formation were forced up through it, especially above clastic sequences on the margins of the rift basin. Where the throughput was greatest, the Kupferschiefer and other basal strata at the base of the Zechstein were oxidized to Rote Faule, a mining term meaning red "fooling" (in the sense of being barren rock). Adjacent to the Rote Faule are areas of copper enrichment, surrounded by areas of lead and then zinc enrichment, and finally barren shale. Enrichment and zonation occurred as ore minerals replaced preexisting minerals and one another. Pyrite in the unaltered Kupferschiefer was replaced by sphalerite, which was in turn replaced by galena, and then by chalcopyrite. Replacement proceeded in this fashion through bornite, chalcocite, and finally hematite. The replacement mineral typically invaded the host mineral along an irregular front. Pyrite never replaced another sulfide, and hematite replaced all (Jowett et al., 1987).

Mineral replacement occurs over distances of less than 60 m vertically, but 50 to 100 km laterally. The metal ratio, thickness, and grade of the mineralized interval, and surface density of copper, lead, and zinc in kg/m<sup>2</sup> across all of Poland have been mapped using 50,000 samples from 774 drill holes (Oszczpalski and Rydzewski, 1997). These maps clearly show that copper-rich zones being mined at Lubin and the other districts contain little lead and zinc, but that lead and zinc are concentrated at the base of the Zechstein in adjacent areas in a fashion similar to copper. According to Renzsch et al. (1976), the ratios of potentially minable copper to lead to zinc across the whole area are 1/1.6/3.4, which is similar to the abundance ratios of these metals in the rift-basin volcanic rocks (1/1.6/4). The Lubin district contains >10<sup>9</sup> t of ore at >2 wt percent Cu (Gustafson and Williams, 1981). Based on the volcanic abundance ratios, potentially mineable copper, lead, and zinc in the Lubin district are ~200, 560, and 1,200 Mt, respectively.

Gold in the Lubin district occupies a particular oxidation slice of the redoxcline. The average precious metal contents of the Kupferschiefer ore in the Lubin-Sierszowice copper district are 30 ppb gold and 100 ppm silver, but much higher concentrations of gold (up to 95 ppm) occur on the oxidized side of the redox barrier below the copper mineralization. The gold was probably transported by thiosulfate complexes and precipitated at an earlier stage of reduction than copper (Piestrzynski et al., 2002). Sulfide mineralization in clean Weissliegendes sandstones probably resulted when migrating brines contacted trapped methane and were reduced (Jowett et al., 1987; Jowett, 1992). Methane generated from the Late Carboniferous coals is produced today in parts of the Weissliegendes.

The replacement nature of the metal sulfides implies that lead and zinc enrichment is located where relatively little brine passed through the Kupferschiefer. Where larger volumes of oxidized brine passed through, copper sulfides replace the lead and zinc sulfides to become the sole ore sulfides. The lateral metal zoning must reflect the relative amounts of brine that have moved vertically through the Zechstein sediments, rather than lateral migration. This is required by the permeability structure in this area. The presence of the very permeable Weissliegendes sandstones immediately below the Kupferschiefer makes it physically impossible to develop the horizontal pressure gradients that would be necessary to move fluids horizontally through the thin, impermeable Kupferschiefer shale in the quantities required to produce the zoning. The metal replacement is similar to that which occurs during secondary enrichment beneath porphyry copper leach caps (Anderson, 1982) and to the progressive enrichment of a fixed sulfur lattice with copper that occurs when copper diffuses into the reduced interiors of rock fragments in copper leach dumps (Dudas et al., 1975; Cathles, 1979).

About 20 percent of the sulfide ore in the Kupferschiefer at the Lubin mine occurs in veinlets that are concordant, discordant, and nearly perpendicular to bedding (Oszczpalski, 1989). The subhorizontal and vertical crosscutting veinlets form a conjugate set, with lateral dimensions of up to 0.3 and 0.6 m, respectively. These veinlets are 1 to 5 mm thick, have fibrous minerals perpendicular to the walls, vein-parallel host shards, trails of host shards crossing the vein, and mineral

zones mirrored on either side of the median line (Jowett, 1987; Jowett et al., 1987). The vertical veinlets are probably natural hydraulic fractures, and the horizontal veinlets likely formed when brines, at pressures close to lithologic, expanded weak laminations in the shale. Fluid-escape structures (sand flames), indicating fluid overpressures, have been noted in the White Pine deposit as described earlier. Thus, in contrast to the MVT deposits in the United States midcontinent, the mineralizing brines in copper-rich sedimentary-hosted stratiform deposits may have typically been overpressured and had pressures close to lithostatic at the sites of sulfide replacement and ore deposition.

Mass-balance calculations based on mineralization density maps of Oszczpalski and Rydzewski (1997) show that ~2,800 km<sup>3</sup> of brine could have been compactively expelled from half the local Lubin rift basin. This volume could have easily produced the observed volume of Rote Faule but to produce the known copper mineralization, the mineralizing fluid would have had to contain ~130 ppm copper, which is unrealistically high. This copper-transport estimate does not include the brine volume required to transport lead and zinc. Brines must have been contributed from a substantial portion of the entire Zechstein basin (Cathles et al., 1993). The evaporite-capped, regionally extensive and permeable Weissliegendes and Rotliegendes sandstones would have facilitated the required regional brine flows to the southern margin of the Zechstein basin.

*Convective sedimentary-hosted stratiform and sedimentary rock-hosted stratiform deposits:* The sedimentary rock-hosted stratiform deposits discussed above may have extracted metals (especially copper) from volcanic rocks (or volcanically derived sediments) but otherwise show no signs of influence from igneous processes. However, some sedimentary-hosted stratiform base metal deposits may form when igneous intrusions cause the convective circulation of brines, commonly where these brine discharge on the sea floor. Perhaps the clearest example is the sedimentary-hosted stratiform deposit forming today in the Red Sea, where un lithified metalliferous sediments are accumulating in the ~10-km-diameter Atlantis II deep (Shanks and Bischoff, 1977); 94 × 10<sup>6</sup> t of sediments with 2 wt percent zinc, 0.5 wt percent copper, 39 ppm silver, and 0.5 ppm gold have recently been deposited (Herzig and Hannington, 1995). The brines responsible for metal deposition have not been sampled directly but are thought to be normal seawater that acquired high salinity by evaporite dissolution and acquired heat (>330°C) and metals by interaction with basalt at the Red Sea spreading axis (Winckler et al., 2000). The fluids are saline enough to pond in a hot brine pool, which precipitates sulfides as it cools.

An example of a copper sedimentary rock-hosted stratiform deposit that was probably formed by intrusion-driven brine convection that did not discharge onto the sea floor is the Boleo deposit on the west side of the Gulf of California in Baha California Sur, Mexico. As described by Bailes et al. (2001), ore occurs in five clay-rich tuff layers a few meters thick that contain pyrite. The clay layers are fairly evenly interspersed in a ~150-m-thick clastic sub-basin. Syngenetic framboidal pyrite in the layers is replaced by chalcocite, bornite, chalcopyrite, and sphalerite. The layers are more copper rich at their base and zinc rich at their top, and there is a

general zoning from copper at the base to zinc at the top of the 150-m section. Ore deposition occurred over a period of a few million years in the late Miocene. These observations, together with the thin and immature nature of the sediment accumulations, and the common occurrence of convective systems in the Gulf of California (e.g., Guaymas basin, Cerro Prieto, Salton Sea), suggest that metal deposition occurred by convectively driven brine circulation. The rising brines were distributed laterally by conglomerate layers that underlie each clay-tuff layer. The brines could thus leak vertically through these layers in a reasonably uniform fashion, which would promote the efficient extraction of metals from the brines. The presence of chalcocite suggests that the temperature of ore formation was low ( $\sim 100^\circ\text{C}$ ).

*Exhalative Pb-Zn sedimentary-hosted stratiform deposits:* Sedimentary-hosted stratiform deposits that formed very near the sea floor have been called SEDEX (sedimentary exhalative) deposits (e.g., Large et al., 2005). The stacked stratiform ore lenses in sedimentary horizons of any lithology in these deposits suggest that metal precipitation was very close to, and perhaps above, the sediment-water interface (Sangster, 1990). The brines thus cooled rapidly, causing precipitation of very fine grained sulfides. Cooke et al. (2000) distinguished exhalative Pb-Zn sedimentary-hosted stratiform deposits that formed where  $\sim 150^\circ\text{C}$  brines with  $\Sigma\text{SO}_4^{2-} > \Sigma\text{H}_2\text{S}$  were reduced from those that precipitated where  $\sim 250^\circ\text{C}$  brines with  $\Sigma\text{SO}_4^{2-} < \Sigma\text{H}_2\text{S}$  were cooled. The former (e.g., McArthur River, Mt. Isa; like most MVT deposits) generally are larger, lack barite, gold (but see Kupferschiefer discussion above), and stringer feeder pipe ore. By contrast, the latter (e.g., Selwyn basin, Red Dog, Meggen, Ramelsberg, Sullivan) are smaller, have barite caps (except when the bottom waters were anoxic), have stringer feeder pipe ores, and are locally enriched in gold and tin. The causes for these differences are both chemical (barium and tin have very low solubility in oxidized solutions, and a reduction trap probably removes metals with greater efficiency than a mixing or cooling trap) and physical (hotter brines are less likely to form brine pools and thus are more likely to deposit syngenetic metals over a surface vent, e.g., stringer ore).

The exhalative Pb-Zn sedimentary-hosted stratiform deposits are almost always associated with major faults, and thermal or thermohaline convection facilitated by these faults may be a key to their formation (Large et al., 2002; Yang et al., 2004a, b). Russell (1978, 1986; Russell et al., 1981) have long suggested that fault-assisted convection could have been responsible for the Irish MVT deposits.

#### *Ore deposits of the hydrologic system*

Geochemically, timing can be everything. A good example is the window of opportunity that nature briefly opened for natural fission reactors. Before  $\text{O}_2$  levels in the atmosphere increased to the point that uranium could be leached from the crust (2.45–2.1 Ga), uranium ore deposits could not form. After 2 Ga, fissionable  $^{235}\text{U}$  had decayed below the fraction required for fission. In the brief window between 2.45 and 2 Ga, nature could form uranium deposits like those in the Athabasca basin that could ignite in spontaneous nuclear fires. This occurred in Gabon, Africa, as discussed by Gauthier-Lafaye and Weber (2003).

#### Summary and Suggestions for Future Work

The last 100 years have seen remarkable advances in understanding resources in the upper continental crust, but there remains a lot to be understood. The topic is challenging because the resources are the diverse products of sequences of interacting processes that can operate over very large scales of time and space. Observations suggest that the movements of basin brine produce trace Pb-Zn mineralization easily, but large deposits require exceptionally permeable and well-capped continental-scale aquifers. The Kupferschiefer sedimentary rock-hosted stratiform Cu-Pb-Zn mineralization in Germany and Poland requires the expulsion of overpressured brines from nearly the entire Zechstein basin to its southern margin. The MVT Pb-Zn deposits in North America are associated with underpressured, gas-filled basins. The brief thermally anomalous nature of their ore deposition requires pulses of rapid brine flow. The low permeability and partial gas fill of the recharge margins makes sufficiently rapid flows difficult to achieve by cross-basin, topography-driven flow, and there are other problems with this hypothesis. The underpressured gas makes expulsion (by compaction, hydrocarbon generation, or gravity flow) of brine unlikely. The constraints on MVT ore systems are so restrictive that it is difficult to identify even one viable brine-flow mechanism. A rapid increase in the sea level associated with melting of continental glaciers could compress the porosity of the gas-saturated parts of the Arkoma basin and displace brine rapidly enough to produce the associated MVT deposits. This mechanism could produce pulses of mineralization long after Arkoma sedimentation ceased, as observed. Expulsion of brine accompanying the main period of construction of the Ouachita accretionary prism, on the other hand, could produce MVT deposits only between  $\sim 305$  and 290 Ma and could not account for the late-forming deposits (i.e., Upper Mississippi Valley, Tri-State, and northern Arkansas). Deformation continued after the prism construction, however, and this might have propelled the mineralizing brines in some as-yet-unidentified fashion. The metal zoning in the Kupferschiefer results from the progressive replacement of ferrous iron by Zn, Pb, and Cu, followed by flushing of all metals except ferric iron, but convincing explanation for the changes in metal ratios in the midcontinent United States. MVT districts (i.e., why the Upper Mississippi Valley deposits are almost all zinc, whereas the Viburnum Trend and Old Lead Belt districts contain so much lead) seem to be lacking. Nor is it apparent why so little silica has been deposited.

The fluid drive for basin-related base metal deposits needs not always be one of expulsion. It is commonly convection driven by igneous intrusion (as in the Red Sea, Salton Sea, and Boleo mineralization). Deposition needs not always be by the reduction of oxidized brines or by cooling of the brines near the sea floor or in a brine pool. A general principle might be that base metal deposits are produced near where large volumes of basinal brines with chlorinity  $> 10^5$  mg/L (or hot brines of lower chlorinity) discharge, but many variations on the mechanism of brine propulsion and metal precipitation—reduction, replacement, cooling, mixing—are clearly possible.

What of the future? How can we deal effectively with the interdependencies, combination-lock complexity (in which a few independent variables combine in nearly an infinite number of ways), and diversity of mineral resources? Table 3 summarizes much of what we have discussed and suggests that one way may be to focus on conditions that enable, or are critical thresholds to, ore formation. For example, uranium roll-front deposits could not form before atmospheric oxygen increased to near-present concentrations, MVT, sedimentary rock-hosted stratiform and sedimentary-hosted stratiform deposits may require brines with  $\sim 10^5$  mg/L chlorinity (Fig. 22), metamorphic lode gold deposits require fluids with low chlorinity, porphyry deposits require a large volume of magma undergoing volatile exsolution, and VHMS deposits require a host with  $>10^{-16}$  m<sup>2</sup> permeability. MVT and expulsive sedimentary rock-hosted stratiform (and sedimentary-hosted stratiform if such exist) deposits are enabled by regional, continental-scale aquifers (the latter including red-bed sediments) capped by low permeability strata. MVT fluid-low systems may even require the passage of organic components through the gas-generation window to produce gas-filled basins. Increasing our confidence in a short list of enabling and threshold parameters seems one good way to better understand, explore for, and derive information from mineral deposits in the continental crust.

Attention to simple, sometimes even back of the envelope, physical and chemical principles or generalizations can also be very useful, and we hope the techniques described in Appendix 1 and the applications made in the text will encourage the broader use of this approach. Radiogenic noble gases should percolate through the crust at the rate they are generated, just as will gases such as CO<sub>2</sub> or nonaqueous fluids

such as petroleum that are generated slowly by other means. These gases can indicate subsurface processes that are related to mineralization and thus help to define exploration targets. The difficulty for a brine to flow laterally through a thin shale that is underlain by very permeable strata requires that the metal zoning in the Kupferschiefer is the result of progressive replacement by vertical brine flow. Integration of processes and parameters such as dynamic permeability is necessary, powerfully simplifying and productive of useful insights.

Global and critical temporal controls are possible. A worldwide drop in sea level can rapidly raise the temperature in basins covered by shallow seas and trigger gas generation and set the stage for, or cause, brine expulsion and MVT mineralization, as at Cadjebut. Changes in sea level over gas-filled basins could cause pulses of brine expulsion. Simultaneous MVT mineralization in geographically widely distributed basins could confirm both the global character of some sea-level drops and the hypothesis that MVT mineralization can be associated with gas-filled basins. If the pulsed formation of MVT deposits is associated with glacial melting, the search would be restricted to the intervals of geologic time with continental-scale glacial cycles. The global chemical and evolutionary changes noted in the introduction should be recorded in ore deposits. Connections could be subtle but important, particularly when biologic evolution is involved. For example, condensation of magmatic volatiles produced oxidized waters in volcanic arcs long before photosynthesis increased the level of atmospheric oxygen. Organisms that adapted to these environments might have developed a tolerance for oxidation poisoning that served them well when O<sub>2</sub> concentrations later increased in the atmosphere.

TABLE 3. Energy Source, Fluid Drive, Deposit Characteristics, Enabling and Threshold Factors for Deposit Formation

Energy source	Solar energy		Earth's internal energy				
	Uranium	MVT <sup>1</sup>	SHS and SRHS <sup>2</sup>	Metamorphic Au	VHMS <sup>3</sup>	Porphyry Cu	
Deposit type							
Drive			Expulsive	Convective			
Hydrologic	-----						
Expulsive		-----					
Convective			-----		-----		
Characteristics							
Temperature	~50°C	>80°C	~150°C	~250°C	>350°C	350°C	>450°C
Pressure	Hydrostatic	Hydrostatic	Lithostatic	Hydrostatic	Lithostatic	Hydrostatic	Lithostatic to hydrostatic
Salinity		-----Hypersaline-----		Low	Seawater	≥Moderate	
Enabling							
Organics	-----						
Red beds		-----					
Reg. aquifer	-----						
Imperm cap		-----					
Magma volatiles							
Threshold	Atm O <sub>2</sub>	-----High salinity-----	High-moderate salinity	Low salinity	-----Magma volume-----	>10 <sup>-16</sup> m <sup>2</sup>	

<sup>1</sup> MVT = Mississippi Valley-type Pb-Zn deposits

<sup>2</sup> SHS = sediment-hosted stratiform base metal deposits where metal was introduced into unconsolidated sediments; SRHS = sedimentary rock-hosted stratiform base metal deposits where metal was introduced after the sediments were at least partially lithified

<sup>3</sup> VHMS = volcanic-hosted massive sulfide deposits

What should be our grand challenge for the next 100 yrs? An appropriate challenge might be to construct quantitative models of regional-scale fluid-flow, rock formation, and chemical alteration in a way that also includes ore deposition on the district and deposit scale, and to test these models against ore deposit and alteration zoning data everywhere. This would force examination of the entire multiphase flow system and all its interactions and resource consequences. Having constructed and tested such models, we would better understand the various processes that produce resources in various environments (magmatic, sedimentary, surficial, etc.), and we would be better able to infer the scientific implications of resource data. Since resources are Nature's environmental experiments, the models would also apply to environmental questions and their related problems. Our strategy should be to construct models that can be run by anyone from a personal computer in a fashion similar to an Excel® spreadsheet. This will allow a large labor force of interested scientists to be engaged in testing the models, while at the same time more effectively exploring for and studying hydrocarbon and mineral resources and making derivative applications.

### Acknowledgments

Discussions with and material from colleagues have greatly assisted preparation of this manuscript. We would like to thank especially Dick Holland for providing a prepublication copy of his review of atmospheric chemistry, Phil Nelson for very helpful discussions on permeability and basin-center gas, Bill Thomas and Thomas Becker for discussions of the Ouachita system, and Alden Carpenter for discussion of CO<sub>2</sub> in the Gulf of Mexico. The first author thanks a lifetime of collaborators for teaching him about the geology and chemistry of ore deposits. Without them, the willingness of industry colleagues to show and explain their deposits, and the contributions of many students, this review would have not been possible. The research upon which this review is based was supported by many organizations. We thank particularly the Gas Research Institute, the Department of Energy, Kennecott Copper Corporation, Chevron, Texaco, the corporate sponsors of the Global Basins Research Network, the Canadian Association of Mining Industry Research Organization, the National Science Foundation, and the Petroleum Research Fund. Finally we thank the organizers of the 100<sup>th</sup> Anniversary volume, especially Jeff Hedenquist, for encouraging preparation of this manuscript, and Steve Ingebritsen, Jeremy Richards, and Jeff Hedenquist for very helpful reviews and editorial suggestions.

### REFERENCES

- Adams, J.J., Rostron, B.J., and Mendoza, C.A., 2004, Coupled fluid flow, heat flow, solute transport and erosion in the Alberta basin: Implications for the Athabasca oil sands: *Canadian Journal of Earth Sciences*, v. 41, p. 1077–1095.
- Adams, S.S., 1991, Evolution of genetic concepts for principle types of sandstone uranium deposits in the United States: *ECONOMIC GEOLOGY MONOGRAPH* 8, p. 225–248.
- Alexander, L.L., and Flemings, P.B., 1995, Geologic evolution of a Pliocene-Pleistocene salt-withdrawal mini-basin; Eugene Island Block 330, offshore Louisiana: *American Association of Petroleum Geologists Bulletin*, v. 79, p. 1737–1756.
- Allan, J., and Creaney, S., 1991, Oil families of the Western Canada Basin: *Bulletin of Canadian Petroleum Geology*, v. 39, p. 107–122.
- Al-Shaieb, Z., Puckette, J.O., Abdalla, A.A., and Ely, P.B., 1994, Megacompartiment complex in the Anadarko basin: A completely sealed overpressured phenomenon: *American Association of Petroleum Geologists Memoir* 61, p. 55–68.
- Anderson, G.M., and Garven, G., 1987, Sulfate-sulfide-carbonate associations in Mississippi Valley-type lead-zinc deposits: *ECONOMIC GEOLOGY*, v. 82, p. 482–488.
- Anderson, G.M., and Macqueen, R.W., 1988, Mississippi Valley-type lead-zinc deposits, in Roberts, R.G., and Sheahan, P.A., eds., *Ore deposit models*: *Geoscience Canada Reprint Series* 3, p. 79–90.
- Anderson, J.A., 1982, Characteristics of leached capping and techniques of appraisal, in Titley, S.R., ed., *Advances in geology of porphyry copper deposits; southwestern North America*: Tucson, AZ, University Arizona Press, p. 275–295.
- Appold, M.S., and Garven, G., 1999, The hydrology of ore formation in the Southeast Missouri district: Numerical models of topography-driven fluid flow during the Ouachita orogeny: *ECONOMIC GEOLOGY*, v. 94, p. 913–935.
- Arbenz, J.K., 1989, The Ouachita system: *Geological Society of America, Geology of North America, Volume A*, p. 371–396.
- Arnold, B.W., Bahr, J.M., and Fantucci, R., 1996, Paleohydrogeology of the Upper Mississippi Valley zinc-lead district: *Society of Economic Geologists Special Publication* 4, p. 378–389.
- Bailes, R.J., Christoffersen, J.E., Escandon, V.F., and Peatfield, G.R., 2001, Sediment-hosted deposits of the Boleo copper-cobalt-zinc district, Baja California Sur, Mexico: *Society of Economic Geologists Special Publication* 8, p. 291–306.
- Ballentine, C.J., and Burnard, P.G., 2002, Production, release and transport of noble gases in the continental crust: *Reviews in Mineralogy and Geochemistry*, v. 47, p. 481–538.
- Banner, J.L., Wasserburg, G.J., Dobson, P.F., Carpenter, A.B., and Moore, C.H., 1989, Isotopic and trace element constraints on the origin and evolution of saline groundwaters from central Missouri: *Geochimica et Cosmochimica Acta*, v. 53, p. 383–398.
- Barnes, H.L., Adams, S.S., and Rose, A.W., 1981, Ores formed by diagenetic and metamorphic processes: *Mineral resources: Genetic understanding for practical applications*: Washington, DC, National Academic Press, p. 73–81.
- Barton, P.B., Jr., 1981, Physical-chemical conditions of ore deposition: *Physics and Chemistry of the Earth*, v. 13-14, p. 509–528.
- Bayley, R.W., and Muehlberger, W.R., 1968, Basement rock map of the United States exclusive of Alaska and Hawaii: Washington, DC, U.S. Geological Society. 1:2,500,000 scale.
- Bear, J., 1972, *Dynamics of fluids in porous media*: New York, NY, Dover, 764 p.
- Beard, D.C., and Weyl, P.K., 1973, Influence of texture on porosity and permeability of unconsolidated sand: *American Association of Petroleum Geologists Bulletin*, v. 57, p. 349–369.
- Bentley, H.W., Phillips, F.M., Davis, S.N., Habermehl, M.A., Airey, P.L., Calif, G.E., Elmore, D., Gove, H.E., and Torgersen, T., 1986, Chlorine 36 dating of very old groundwater: 1. The Great Artesian basin, Australia: *Water Resources Research*, v. 22, p. 1991–2001.
- Berg, R.B., 1975, Capillary pressures in stratigraphic traps: *American Association of Petroleum Geologists Bulletin*, v. 59, p. 939–956.
- Berner, R.A., 2001, Modeling atmospheric O<sub>2</sub> over Phanerozoic time: *Geochimica et Cosmochimica Acta*, v. 65, p. 685–694.
- Bethke, C.M., 1985, A numerical model of compaction-driven groundwater flow and heat transfer and its application to the paleohydrology of intracratonic sedimentary basins: *Journal of Geophysical Research*, v. 90, p. 6817–6828.
- 1986, Hydrologic constraints on genesis of the Upper Mississippi Valley mineral district from Illinois basin brines: *ECONOMIC GEOLOGY*, v. 81, p. 233–249.
- Bethke, C.M., and Marshak, S., 1990, Brine migrations across North America—the plate tectonics of groundwater: *Annual Review of Earth and Planetary Sciences*, v. 18, p. 287–315.
- Bloch, S., Lander, R.H., and Bonnell, L., 2002, Anomalously high porosity and permeability in deeply buried sandstone reservoirs: Origin and predictability: *American Association of Petroleum Geologists Bulletin*, v. 86, p. 301–328.
- Bloom, A.L., 1998, *Geomorphology: Upper Saddle River*, Prentice Hall, 482 p.
- Bornhorst, T.J., 1995, Relationship between native copper deposits and tectonic development of the North American midcontinent rift system: *International Conference on Basement Tectonics*, 10<sup>th</sup>, Duluth, Minnesota, August 1992, *Proceedings*, p. 19–23.

- Bradley, D.C. and Leach, D.L., 2003, Tectonic controls of Mississippi Valley-type lead-zinc mineralization in orogenic forelands: *Mineralium Deposita*, v. 38, p. 652–667.
- Brown, A.C., 1992, Sediment-hosted stratiform copper deposits: *Geoscience Canada*, v. 19, p. 125–141.
- Byrnes, A.P., 2003, Aspects of permeability, capillary pressure, and relative permeability properties and distribution in low-permeability rocks important to evaluation, damage, and stimulation: Rocky Mountain Association of Geologists-Petroleum Technology Transfer Council (RMAG/PTTC) Fall Symposium, 2003, p. 1–12.
- Candella, P.A., and Holland, H.D., 1986, A mass transfer model for porphyry copper and molybdenum in mafic hydrothermal systems: The origin of porphyry-type ore deposits: *ECONOMIC GEOLOGY*, v. 81, p. 1–19.
- Carr, P., and Cathles, L.M., in press, Two-dimensional modeling studies of mafic sills with reference to the Bell River Complex: *ECONOMIC GEOLOGY*.
- Carruthers, D.J., 2003, Modeling of secondary petroleum migration using invasion percolation techniques: American Association of Petroleum Geologists Datapages Discovery Series 7, p. 21–37.
- Carruthers, D., and Ringrose, P., 1998, Secondary oil migration; oil-rock contact volumes, flow behaviour and rates: *Geological Society Special Publication* 144, p. 205–220.
- Cathles, L.M., 1979, Predictive capabilities of a finite difference model of copper leaching in low grade industrial sulfide waste dumps: *Mathematical Geology*, v. 11, p. 175–191.
- 1983, An analysis of the hydrothermal system responsible for massive sulfide deposition in the Hokuroku basin of Japan: *ECONOMIC GEOLOGY MONOGRAPH* 5, p. 439–487.
- 1987, A simple analytical method for calculating temperature perturbations in a basin caused by the flow of water through thin, shallow-dipping aquifers: *Applied Geochemistry*, v. 2, p. 649–655.
- 1993, A discussion of flow mechanisms responsible for alteration and mineralization in the Cambrian aquifers of the Ouachita-Arkoma basin-Ozark system: American Association of Petroleum Geologists Studies in Geology 36, p. 99–112.
- 1997, Thermal aspects of ore formation, in Barnes, H.L., ed., *Geochemistry of hydrothermal ore deposits*: New York, NY, Wiley, p. 192–227.
- 2002, Seal control of hydrocarbon migration and its physical and chemical consequences: Chicago, IL, Gas Research Institute, v. 2, p. 1–51.
- Cathles, L.M., and Losh, S.L., 2002, Seal control of hydrocarbon migration and its physical and chemical consequences: Chicago, IL, Gas Research Institute, v. 5, p. 1–63.
- Cathles, L.M., and Schoell, M., 1998, A model of inorganic CO<sub>2</sub> generation, migration, and titration in sedimentary basins [abs.]: *Geological Society of America Abstracts with Programs*, v. 30, p. 312.
- Cathles, L.M., and Smith, A.T., 1983, Thermal constraints on the formation of Mississippi Valley-type lead-zinc deposits and their implications for episodic basin dewatering and deposit genesis: *ECONOMIC GEOLOGY*, v. 78, p. 983–1002.
- Cathles, L.M., Schoell, M., and Simon, R., 1990, A kinetic model of CO<sub>2</sub> generation and mineral and isotopic alteration during steam flooding: *SPE Reservoir Engineering*, v. 5, p. 524–530.
- Cathles, L.M., Oszczepalski, S., and Jowett, E.C., 1993, Mass balance evaluation of the late diagenetic hypothesis for Kupferschiefer Cu mineralization in the Lubin basin of southwestern Poland: *ECONOMIC GEOLOGY*, v. 88, p. 948–956.
- Chen, D.F., and Cathles, L.M., III, 2003, A kinetic model for the pattern and amounts of hydrates precipitated from a gas stream: Application to the Bush Hill vent site, Green Canyon Block 185, Gulf of Mexico: *Journal of Geophysical Research*, v. 108, p. B1–B10.
- Chi, G., and Savard, M.M., 1997, Sources of basinal and Mississippi Valley-type mineralizing brines: Mixing of evaporated seawater and halite-dissolution brine: *Chemical Geology*, v. 143, p. 121–125.
- Cioppa, M.T., Al Aasm, I.S., Symons, D.T.A., and Gillen, K.P., 2003, Dating penecontemporaneous dolomitization in carbonate reservoirs: paleomagnetic, petrographic, and geochemical constraints: American Association of Petroleum Geologists Bulletin, v. 87, p. 71–88.
- Clendenin, C.W., and Duane, M.J., 1990, Focused fluid flow and Ozark Mississippi Valley-type deposits: *Geology*, v. 18, p. 116–119.
- Collinson, C., Sargent, M.L., and Jennings, J.R., 1988, Illinois basin region, in Sloss, L.L., ed., *Sedimentary cover, North American craton*: Denver, CO, Geological Society of America, p. 383–426.
- Cook, T.D., and Bally, A.W., 1975, *Stratigraphic Atlas of North and Central America*: Princeton, New Jersey, Princeton University Press, 272 p.
- Cooke, D.R., Bull, S.W., Large, R.R., and McGoldrick, P.J., 2000, The importance of oxidized brines for the formation of Australian Proterozoic stratiform sediment-hosted Pb-Zn (SEDEX) deposits: *ECONOMIC GEOLOGY*, v. 95, p. 1–17.
- Coveney, R.M., Jr., and Goebel, E.D., 1983, New fluid-inclusion homogenization temperatures for sphalerite from minor occurrences in the mid-continent area, in Kisvarsanyi, G., Grant, S.K., Pratt, W.P., and Koenig, J.W., eds., *International conference on Mississippi Valley-type lead-zinc deposits*, p. 234–242.
- Creaney, S., and Allan, J., 1990, Hydrocarbon generation and migration in the Western Canada Sedimentary Basin: *Geological Society Special Publication* 50, p. 189–202.
- Crocetti, C.A., and Holland, H.D., 1989, Sulfur-lead isotope systematics and the composition of fluid inclusions in galena from the Viburnum Trend, Missouri: *ECONOMIC GEOLOGY*, v. 84, p. 2196–2216.
- Cross, M.M., Manning, D.A.C., Bottrell, S.H., and Worden, R.H., 2004, Thermochemical sulphate reduction (TSR); experimental determination of reaction kinetics and implications of the observed reaction rates for petroleum reservoirs: *Organic Geochemistry*, v. 35, p. 393–404.
- Davis, T.B., 1984, Subsurface pressure profiles in gas saturated basins: American Association of Petroleum Geologists Memoir 38, p. 189–203.
- Deloule, E., and Turcotte, D.L., 1989, The flow of hot brines in cracks and the formation of ore deposits: *ECONOMIC GEOLOGY*, v. 84, p. 2217–2225.
- Deloule, E., Allegre, C.J., and Doe, B.R., 1986, Lead and sulfur isotope microstratigraphy in galena crystals from Mississippi Valley-type deposits: *ECONOMIC GEOLOGY*, v. 81, p. 1307–1321.
- Deming, D., and Nunn, J.A., 1991, Numerical simulations of brine migration by topographically driven recharge: *Journal of Geophysical Research*, v. 96, p. 2485–2499.
- Deroo, G., Powell, T.G., Tissot, B., and McCrossan, R.G., 1977, The origin and migration of petroleum in the Western Canadian sedimentary basin, Alberta: A geochemical and thermal maturation study: Ottawa, ON, Canada, Geological Survey of Canada, 136 p.
- de Witt, W., Jr., 1986, Devonian gas-bearing shales in the Appalachian basin: American Association of Petroleum Geologists Studies in Geology 24, p. 1–8.
- Dudas, F.O., Cathles, L.M., and Stephens, J.D., 1975, Rate controlling reactions in dump leaching: Rimming phenomena in leached waste: Lexington, Massachusetts, Kennecott Copper Corporation, Unpublished Ledgemont Laboratory Technical Report JTR 5, 50 p.
- Eisenlohr, B.N., Tompkins, L.A., Cathles, L.M., Barley, M.E., and Groves, D.I., 1994, Mississippi Valley-type deposits: Products of brine expulsion by eustatically induced hydrocarbon generation? An example from northwestern Australia: *Geology*, v. 22, p. 315–318.
- Eldridge, G.H., 1901, The asphalt and bituminous rock deposits of the United States: U.S. Geological Survey Annual Report, v. 22 pt. 1, p. 209–452.
- Elmore, R.D., 2001, A review of palaeomagnetic data on the timing and origin of multiple fluid-flow events in the Arbuckle Mountains, southern Oklahoma: *Petroleum Geoscience*, v. 7, p. 223–229.
- England, W.A., Mackenzie, A.S., Mann, D.M., and Quigley, T.M., 1987, The movement and entrapment of petroleum fluids in the subsurface: *Journal of the Geological Society of London*, v. 144, pt 2, p. 327–347.
- Epstein, A.G., Epstein, J.B., and Harris, L.D., 1977, Conodont color alteration—an index to organic metamorphism: U.S. Geological Survey Professional Paper, p. 1–27.
- Eugster, H.P., 1985, Oil shales, evaporites and ore deposits: *Geochimica et Cosmochimica Acta*, v. 49, p. 619–635.
- Fisher, A.G., 1975, Origin and growth of basins, in Fisher, A.G., and Judson, S., eds., *Petroleum and global tectonics*. Princeton, NJ, Princeton University Press, p. 47–79.
- Fisher, A.T., Zwart, G., Shipley, T., and Ogawa, Y., 1996, Relation between permeability and effective stress along a plate-boundary fault, Barbados accretionary complex: *Geology*, v. 24, p. 307–310.
- Forster, C.B., and Smith, L., 1989, The influence of groundwater flow on thermal regimes in mountainous terrain: A model study: *Journal of Geophysical Research*, v. 94, sec. B, p. B9439–B9451.
- Fournier, R.O., 1999, Hydrothermal processes related to movement of fluid from plastic into brittle rock in the magmatic-epithermal environment: *ECONOMIC GEOLOGY*, v. 94, p. 1193–1211.
- Franca, A.B., Araujo, L.M., Maynard, J.B., and Potter, P.E., 2003, Secondary porosity formed by deep meteoric leaching, Botucatu eolianite, southern South America: American Association of Petroleum Geologists Bulletin, v. 87, p. 1073–1082.

- Freeze, A., and Cherry, J.A., 1979, *Groundwater*: Englewood Cliffs, New Jersey, Prentice-Hall, 604 p.
- Garven, G., Ge, S., Person, M.A., and Sverjensky, D.A., 1993, Genesis of stratabound ore deposits in the midcontinent basins of North America. 1. The role of regional groundwater flow: *American Journal of Science*, v. 293, p. 497–568.
- Gauthier-Lafaye, F., and Weber, F., 2003, Natural nuclear fission reactors: Time constraints for occurrence, and their relation to uranium and manganese deposits and to the evolution of the atmosphere: *Precambrian Research*, v. 120, p. 81–100.
- Gerlach, T.M., Westrich, H.R., and Symonds, R.B., 1996, Preeruption vapor in magma of the climactic Mount Pinatubo eruption: Source of giant stratospheric sulfur dioxide cloud, *in* Newhall, C.G., and Punongbayan, R.S., eds., *Fire and mud: Eruptions and lahars of Mount Pinatubo*, Philippines: Quezon City, Philippines, Philippine Institute of Volcanology and Seismology, p. 415–433.
- Germanovich, L.N., and Lowell, R.P., 1992, Percolation theory, thermoclasticity, and discrete hydrothermal venting in the Earth's crust: *Science*, v. 255, p. 2564–2565.
- Goldhaber, M.B., Reynolds, R.L., and Rye, R.O., 1978, Origin at a south Texas roll-type uranium deposit: II. Sulfide petrology and sulfur isotope studies: *ECONOMIC GEOLOGY*, v. 73, p. 1690–1705.
- Goldhaber, M.B., Church, S.E., Doe, B.R., Aleinikoff, J.N., Brannon, J.C., Podosek, F.A., Mosier, E.L., Taylor, C.D., and Gent, C.A., 1995, Lead and sulfur isotope investigation of Paleozoic sedimentary rocks from the southern midcontinent of the United States: Implications for paleohydrology and ore genesis of the Southeast Missouri lead belt: *ECONOMIC GEOLOGY*, v. 90, p. 1875–1910.
- Goodfellow, W.D., Lydon, J.W., and Turner, R.J.W., 1993, Geology and genesis of stratiform sediment-hosted (SEDEX) zinc-lead-silver sulphide deposits: *Geological Association of Canada Special Paper 40*, p. 201–251.
- Gussow, W.C., 1995, Time of migration of oil and gas in Alberta, Canada: *AAPG Bulletin*, p. 547–574.
- Gustafson, L.B., and Williams, N., 1981, Sediment-hosted stratiform deposits of copper, lead, and zinc: *ECONOMIC GEOLOGY 75TH ANNIVERSARY VOLUME*, p. 139–178.
- Hagni, R.D., 1976, Tri-State ore deposits: The character of their host rocks and their genesis, *in* Wolf, K.H., ed., *Handbook of strata-bound and stratiform ore deposits: II. Regional studies and specific deposits*: New York, NY, Elsevier, v. 6, p. 457–494.
- Halbermehl, M.A., 1980, The Great Artesian basin, Australia: *BMR Journal of Australian Geology and Geophysics*, v. 5, p. 9–38.
- Hallager, W.S., Ulrich, M.R., Kyle, J.R., Price, P.E., and Gose, W.A., 1990, Evidence for episodic basin dewatering in salt-dome cap rocks: *Geology*, v. 18, p. 716–719.
- Hanor, J.S., 1987, Kilometre-scale thermohaline overturn of pore waters in the Louisiana Gulf Coast: *Nature*, v. 327, p. 501–503.
- 1997, Controls on the solubilization of lead and zinc in basinal brines: *Society of Economic Geologists Special Publication 4*, p. 483–500.
- Hart, S.R., Shimizu, N., and Sverjensky, D.A., 1981, Lead isotope zoning in galena: An ion microprobe study of a galena crystal from the Buick mine, Southeast Missouri: *ECONOMIC GEOLOGY*, v. 76, p. 1873–1878.
- Hattori, K., 1996, Occurrence and origin of sulfide and sulfate in the 1991 Mount Pinatubo eruption products, *in* Newhall, C.G., and Punongbayan, R.S., eds., *Fire and mud: Eruptions and lahars of Mount Pinatubo*, Philippines: Quezon City, Philippines, Philippine Institute of Volcanology and Seismology, p. 807–824.
- Hattori, K.H., and Keith, J.D., 2001, Contribution of mafic melt to porphyry copper mineralization: Evidence from Mount Pinatubo, Philippines, and Bingham Canyon, Utah, USA: *Mineralium Deposita*, v. 36, p. 799–806.
- Head, I.M., Jones, D.M., and Larter, S.R., 2003, Biological activity in the deep subsurface and the origin of heavy oil: *Nature*, v. 426, p. 344–352.
- Herzig, P.M., and Hannington, M.D., 1995, Polymetallic massive sulfides at the modern seafloor: A review: *Ore Geology Reviews*, v. 10, p. 95–115.
- Heyl, A.V., and West, W.S., 1982, Outlying mineral occurrences related to the Upper Mississippi Valley mineral district, Wisconsin, Iowa, Illinois, and Minnesota: *ECONOMIC GEOLOGY*, v. 77, p. 1803–1817.
- Heyl, A.V., Delevaux, M.H., Zartman, R.E., and Brock, M.R., 1966, Isotopic study of galenas from the upper Mississippi Valley, the Illinois-Kentucky, and some Appalachian Valley mineral districts: *ECONOMIC GEOLOGY*, v. 61, p. 933–961.
- Hoeve, J., Sibbald, T.I.I., Ramaekers, P., and Lewry, J.F., 1980, Athabasca basin unconformity-type uranium deposits: A special class of sandstone-type deposits?: Uranium in the Pine Creek Geosyncline, Vienna, 1980, International Atomic Energy Agency, Proceedings Series, p. 575–594.
- Holland, H.D., 2003, The geologic history of seawater, *in* Elderfield, H., ed., *The oceans and marine geochemistry*: New York, NY, Elsevier, *Treatise on Geochemistry 6*, p. 583–625.
- Horita, J., Zimmermann, H., and Holland, H.D., 2002, Chemical evolution of seawater during the Phanerozoic: Implications from the record of marine evaporites, *in* Candela, P.A., ed., A special issue dedicated to Heinrich D. Holland: Oxford, UK, Pergamon: *Geochimica et Cosmochimica*, v. 66, p. 3733–3756.
- Houseknecht, D.W., and McGilvery, T.A., 1990, Red Oak field, *in* Beaumont, E.A., and Foster, N.H., eds., *Structural traps. II. Traps associated with tectonic faulting*: *Treatise of Petroleum Geology Atlas of Oil and Gas Fields A-017*, p. 201–225.
- Hunt, J.M., 1990, Generation and migration of petroleum from abnormally pressured fluid compartments: *American Association of Petroleum Geologists Bulletin*, v. 74, p. 1–12.
- Ingebritsen, S.E., and Sanford, W.E., 1998, *Groundwater in geologic processes*: Cambridge, UK, Cambridge University Press, 341 p.
- Jackson, S.A., and Beales, F.W., 1967, An aspect of sedimentary basin evolution: the concentration of Mississippi Valley type ores during late stages of diagenesis: *Bulletin of Canadian Petroleum Geology*, v. 15, p. 383–433.
- Jowett, E.C., 1987, Formation of sulfide-calcite veinlets in the Kupferschiefer Cu-Ag deposits in Poland by natural hydrofracturing during basin subsidence: *Journal of Geology*, v. 95, p. 513–526.
- 1992, Role of organics and methane in sulfide ore formation, exemplified by Kupferschiefer Cu-Ag deposits, Poland: *Chemical Geology*, v. 99, p. 51–63.
- Jowett, E.C., Ryzewski, A., and Jowett, R.J., 1987, The Kupferschiefer Cu-Ag ore deposits in Poland: A re-appraisal of the evidence of their origin and presentation of a new genetic model: *Canadian Journal of Earth Sciences*, v. 24, p. 2016–2037.
- Katahara, K.W., and Corrigan, J.D., 2002, Effect of gas on poroelastic response to burial or erosion: *American Association of Petroleum Geologists Memoir 76*, p. 73–78.
- Kendrick, M.A., Burgess, R., Leach, D., and Patrick, R.A.D., 2002a, Hydrothermal fluid origins in Mississippi Valley-type ore districts: Combined noble gas (He, Ar, Kr) and halogen (Cl, Br, I) analysis of fluid inclusions from the Illinois-Kentucky fluorspar district, Viburnum Trend and Tri-State districts, midcontinent United States: *ECONOMIC GEOLOGY*, v. 97, p. 453–469.
- Kendrick, M.A., Burgess, R., Patrick, R.A.D., Turner, G., and Leach, D., 2002b, Hydrothermal fluid origins in a fluorite-rich Mississippi Valley-type district: Combined noble gas (He, Ar, Kr) and halogen (Cl, Br, I) analysis of fluid inclusions from the South Pennine ore field, United Kingdom: *ECONOMIC GEOLOGY*, v. 97, p. 435–451.
- Kirkham, R.V., 1989, Distribution, settings, and genesis of sediment-hosted stratiform copper deposits: *Geological Association of Canada Special Paper 36*, p. 3–38.
- Knauth, L.P., 1998, Salinity history of the Earth's early ocean: *Nature*, v. 395, p. 554–555.
- Krause, F.F., Deutsch, K.B., Joiner, S.D., Barclay, J.E., Hall, R.L., and Hills, L.V., 1994, Cretaceous Cardium Formation of the Western Canada Sedimentary Basin, *in* Mossop Grant, D., and Shetsen, I., eds., *Geological Atlas of the Western Canada Sedimentary basin*: Calgary, AB, Canadian Society of Petroleum Geologists, p. 374–385.
- Kyle, J.R., 1980, Controls of lead-zinc mineralization, Pine Point district, Northwest Territories: *Mining Engineering*, v. 32, p. 1617–1626.
- Large, R.R., Bull, S., Selley, D., Yang, J., Cooke, D., Garven, G., and McGoldrick, P., 2002, Controls on the formation of giant stratiform sediment-hosted Zn-Pb-Ag deposits: With particular reference to the north Australian Proterozoic: Hobart, University of Tasmania, CODES Special Publication 4, p. 107–150.
- Large, R.R., Bull, S., Derrick, G., and Giles, D., 2005, Stratiform and stratabound Zn-Pb-Ag and Cu deposits of the Proterozoic sedimentary basins of northern Australia: *ECONOMIC GEOLOGY 100TH ANNIVERSARY VOLUME*, p. 000–000.
- Lavery, N.G., and Barnes, H.L., 1971, Zinc dispersion in the Wisconsin zinc-lead district: *ECONOMIC GEOLOGY*, v. 66, p. 226–242.
- Law, B.E., 2002, Basin-centered gas systems: *American Association of Petroleum Geologists Bulletin*, v. 86, p. 1891–1919.

- Law, B.E., and Spencer, C.W., 1998, Abnormal pressure in hydrocarbon environments: American Association of Petroleum Geologists Memoir 70, p. 1–11.
- Leach, D.L., Sangster, D. Large, R.R., Kelley, K.D., Gutzmer, J., Garven, G., Page, T., Walters, S., and Allen, C., 2005, Sediment-hosted lead-zinc deposits: A global perspective: *ECONOMIC GEOLOGY* 100<sup>TH</sup> ANNIVERSARY VOLUME, p. 000–000.
- Leach, D.L., and Rowan, E.L., 1986, Genetic link between Ouachita fold belt tectonism and the Mississippi Valley-type lead-zinc deposits of the Ozarks: *Geology*, v. 14, p. 931–935.
- Leach, D.L., and Sangster, D.F., 1993, Mississippi Valley-type lead-zinc deposits: Geological Association of Canada Special Paper 40, p. 289–314.
- Leach, D.L., Plumlee, G.S., Hofstra, A.H., Rowan, E.L., and Viets, J.G., 1991, Origin of late dolomite cement by CO<sub>2</sub>-saturated deep basin brines: Evidence from the Ozark region, central United States: *Geology*, v. 19, p. 348–351.
- Leach, D.L., Bradley, D., Lewchuk, M.T., Symons, D.T.A., de Marsily, G., and Brannon, J., 2001, Mississippi Valley-type lead-zinc deposits through geological time: Implications from recent age-dating research: *Mineralium Deposita*, v. 36, p. 711–740.
- Lenormand, R., Touboul, E., and Zarcone, C., 1988, Numerical models and experiments on immiscible displacements in porous media: *Journal of Fluid Mechanics*, v. 189, p. 165–187.
- Lister, C.R.B., 1974, On the penetration of water into hot rock: *Geophysical Journal of the Royal Astronomical Society*, v. 39, p. 465–509.
- Long, K.R., DeYoung, J.H., Jr., and Ludington, S.D., 1998, Database of significant deposits of gold, silver, copper, lead, and zinc in the United States. Part B, Database of significance deposits: U.S. Geological Survey Open-File Report 98-0206-A, B.
- Losh, S., Walter, L., Meulbroek, P., Martini, A., Cathles, L., and Whelan, J., 2002, Reservoir fluids and their migration into the South Eugene Island Block 330 reservoirs, offshore Louisiana: American Association of Petroleum Geologists Bulletin, v. 86, p. 1463–1488.
- Luo, X., Zhang, F., Miao, S., Wang, W., Huang, Y., Zhou, B., Loggia, D., and Vasseur, G., 2004, Experimental verification of oil saturation and losses during secondary migration: *Journal of Petroleum Geology*, v. 27, p. 241–251.
- Machel, H.G., 1987, Saddle dolomite as a by-product of chemical compaction and thermochemical sulfate reduction: *Geology*, v. 15, p. 936–940.
- 1989, Relationships between sulphate reduction and oxidation of organic compounds to carbonate diagenesis, hydrocarbon accumulations, salt domes and metal sulphide deposits: *Carbonates and Evaporites*, v. 4, p. 137–151.
- 2004, Concepts and models of dolomitization—a critical reappraisal, in Braithwaite, C.J.R., Rizzi, G., and Darke, G., eds., *The geometry and petrogenesis of dolomite hydrocarbon reservoirs*: Geological Society, London, Special Publication v. 235, p. 7–63.
- Marmont, S., 1988, Unconformity-type uranium deposits, in Roberts, R.G., and Sheahan, P.A., eds., *Ore deposit models*: Ottawa, Ontario, Geological Association of Canada, p. 103–115.
- Masters, C.D., Root, D.H., and Attanasi, E.D., 1991, Resource constraints in petroleum production potential: *Science*, v. 253, p. 146–152.
- Masters, J.A., 1984, Lower Cretaceous oil and gas in western Canada: American Association of Petroleum Geologists Memoir 38, p. 1–33.
- Mauk, J.L., Kelly, W.C., van der Pluijm, P.B., and Seabor, R.W., 1992, Relations between deformation and sediment-hosted copper mineralization: Evidence from the White Pine part of the Midcontinent rift system: *Geology*, v. 20, p. 427–430.
- Maxwell, J.C., 1962, Origin of slaty and fracture cleavage in the Delaware Water Gap area, New Jersey and Pennsylvania, in Engle, A.E., James, H.L., and Leonard, B.F., eds., *Petrologic studies—a volume in honor of A F Buddington*: Geological Society of America, p. 281–311.
- McBride, B.C., 1998, The evolution of allochthonous salt along a megaregional profile across the northern Gulf of Mexico basin: American Association of Petroleum Geologists Bulletin, v. 82, p. 1037–1054.
- McCabe, C., and Elmore, R.D., 1989, The occurrence and origin of late Paleozoic remagnetization in the sedimentary rocks of North America: *Reviews of Geophysics*, v. 27, p. 471–494.
- McKibben, M.A., and Hardie, L.A., 1997, Ore-forming brines in active continental rifts, in Barnes, H.L., ed., *Geochemistry of hydrothermal ore deposits*: New York, NY, John Wiley and Sons, p. 877–935.
- McLimans, R.K., Barnes, H.L., and Ohmoto, H., 1980, Sphalerite stratigraphy of the Upper Mississippi Valley zinc-lead district, Southwest Wisconsin: *ECONOMIC GEOLOGY*, v. 75, p. 351–361.
- Meckel, L.D., Jr., Smith, D.G., and Wells, L.A., 1992, Ouachita foredeep basins: Regional paleogeography and habitat of hydrocarbons: American Association of Petroleum Geologists Memoir 55, p. 427–444.
- Milkov, A.V., and Sassen, R., 2001, Estimate of gas hydrate resource, northwestern Gulf of Mexico continental slope: *Marine Geology*, v. 179, p. 71–83.
- Moore, J.C., and Vrolijk, P., 1992, Fluids in accretionary prisms: *Reviews of Geophysics*, v. 30, p. 113–135.
- Mossop, G.D., and Shetsen, I., 1994, Geological atlas of the Western Canada Sedimentary Basin: Calgary, AB, Canadian Society of Petroleum Geologists, 517 p.
- Muffler, L.J.P., and White, D.E., 1968, Origin of CO<sub>2</sub> in the Salton Sea geothermal system, southeastern California, U.S.A: *International Geological Congress*, 23d, Prague, 1968, Proceedings, v. 17, p. 185–194.
- Muskat, M., 1937, *The flow of homogeneous fluids through porous media*: New York, NY, McGraw Hill, 737 p.
- Nelson, P.H., 1994, Permeability-porosity relationships in sedimentary rocks: *The Log Analyst*, v. 35, p. 38–62.
- Nelson, P.H., 2000, Evolution of permeability-porosity trends in sandstones [abs.]: Society of Professional Well Log Analysts Annual Logging Symposium, 41<sup>st</sup>, Houston, TX, 2000, 14 p.
- Neuzil, C.E., 1994, How permeable are clays and shales?: *Water Resources Research*, v. 30, p. 145–150.
- Noble, E.A., 1963, Formation of ore deposits by water of compaction: *ECONOMIC GEOLOGY*, v. 58, p. 1145–1156.
- Orr, W.L., 1977, Geologic and geochemical controls on the distribution of hydrogen sulfide in natural gas, in Campos, R., and Goni, J., eds., *Advances in organic geochemistry*: Madrid, Spain, John Wiley and Sons, p. 571–597.
- Ortoleva, P.J., 1994, Basin compartmentation: Definitions and mechanisms: American Association of Petroleum Geologists Memoir 61, p. 39–51.
- Oszczpalski, S., 1989, Kupferschiefer in southwestern Poland: Sedimentary environments, metal zoning, and ore controls: Geological Association of Canada Special Paper 36, p. 571–600.
- Oszczpalski, S., and Ryzdzewski, A., 1997, Metallogenic atlas of the Zechstein copper-bearing series in Poland: Warsaw, Poland, Zaklad Produkcji Poligraficznej, 32 p.
- Paull, C.K., and Dillon, W.P., 2001, *Natural gas hydrates: Occurrence, distribution and detection*: Washington, DC, American Geophysical Union, 315 p.
- Piestrzynski, A., Pieczonka, J., and Gluszek, A., 2002, Redbed-type gold mineralisation, Kupferschiefer, south-west Poland: *Mineralium Deposita*, v. 37, p. 512–528.
- Plant, J.A., Simpson, P.R., Smith, B., and Windley, B.F., 1999, Uranium ore deposits: Products of the radioactive Earth: *Reviews in Mineralogy*, v. 38, p. 255–319.
- Plumlee, G.S., Goldhaber, M.B., and Rowan, E.L., 1995, The potential role of magmatic gases in the genesis of Illinois-Kentucky fluorspar deposits: Implications from chemical reaction path modeling: *ECONOMIC GEOLOGY*, v. 90, p. 999–1011.
- Popov, M.A., Nuccio, V.F., Dyman, T.S., Gognat, T.A., Johnson, R.C., Schmoker, J.W., Wilson, M.S., and Bartherger, C., 2001, Basin-centered gas systems of the United States: U.S. Geological Survey Open-File Report 01-135, CD-ROM.
- Price, R. A., 1986, The southeastern Canadian Cordillera: Thrust faulting, tectonic wedging, and delamination of the lithosphere: *Journal of Structural Geology*, v. 8, p. 239–254.
- Rentzch, J., Schirmer, B., Rollig, G., and Tischendorf, G., 1976, On the metal source of non-ferrous mineralizations in the Zechstein basement (Kupferschiefer-type), in Fedak, J., ed., *The current metallogenic problems of central Europe*: Warsaw, Poland, Instytut Geologiczny, p. 171–188.
- Revil, A., and Cathles, L.M., III, 1999, Permeability of shaly sands: *Water Resources Research*, v. 35, p. 651–662.
- Reynolds, R.L., and Goldhaber, M.B., 1978, Origin of a south Texas roll-type uranium deposit: I. Alteration of iron-titanium oxide minerals: *ECONOMIC GEOLOGY*, v. 73, p. 1677–1689.
- 1983, Iron disulfide minerals and the genesis of roll-type uranium deposits: *ECONOMIC GEOLOGY*, v. 78, p. 105–120.
- Richardson, C.K., Rye, R.O., and Wasserman, M.D., 1988, The chemical and thermal evolution of the fluids in the Cave-in-Rock fluorspar district,



- Illinois: Stable isotope systematics at the Deardorff mine: *ECONOMIC GEOLOGY*, v. 83, p. 765–783.
- Riediger, C., Grasby, S., and Kalkreuth, W., 2002, Rocky Mountain geology: hydrocarbon source rocks and coal: Canadian Society of Coal Science and Organic Petrology, August 31–September 4, 2004, Field Trip Guidebook 4, p. 82.
- Roberts, H.H., and Carney, R.S., 1997, Evidence of episodic fluid, gas, and sediment venting on the northern Gulf of Mexico continental slope: *ECONOMIC GEOLOGY*, v. 92, p. 863–879.
- Rowan, E.L., and de Marsily, G., 2001, Infiltration of late Palaeozoic evaporative brines in the Reelfoot rift: a possible salt source for Illinois basin formation waters and MVT mineralizing fluids: *Petroleum Geoscience*, v. 7, p. 269–279.
- Rowan, E.L., and Goldhaber, M.B., 1995, Duration of mineralization and fluid-flow history of the Upper Mississippi Valley zinc-lead district: *Geology*, v. 23, p. 609–612.
- Rowan, E.L., and Leach, D.L., 1989, Constraints from fluid inclusions on sulfide precipitation mechanisms and ore fluid migration in the Virburnum Trend lead district, Missouri: *ECONOMIC GEOLOGY*, v. 84, p. 1948–1965.
- Rowan, E.L., Goldhaber, M.B., and Hatch, J.R., 2002, Regional fluid flow as a factor in the thermal history of the Illinois basin: Constraints from fluid inclusions and the maturity of Pennsylvanian coals: American Association of Petroleum Geologists Bulletin, v. 86, p. 257–277.
- Russell, M.J., 1978, Downward-excavating hydrothermal cells and Irish-type ore deposits: Importance of an underlying thick Caledonian prism: Institution of Mining and Metallurgy Transactions, v. 87, sec. B, p. B168–B170.
- 1986, Extension and convection; a genetic model for the Irish Carboniferous base metal and barite deposits, in Andrew, C.J., Crowe, R.W.A., Finlay, S., Pennell, W.M., and Pyne, J.F., eds., *Geology and genesis of mineral deposits in Ireland: Dublin, Ireland, Irish Association of Economic Geologists*, p. 545–554.
- Russell, M.J., Solomon, M., and Walshe, J.L., 1981, The genesis of sediment-hosted, exhalative zinc + lead deposits: *Mineralium Deposita*, v. 16, p. 113–127.
- Ryder, R.T., and Zagorski, W.A., 2003, Nature, origin, and production characteristics of the Lower Silurian regional oil and gas accumulation, central Appalachian basin, United States: American Association of Petroleum Geologists Bulletin, v. 87, p. 847–872.
- Sangster, D.F., 1990, Mississippi Valley-type and sedex lead-zinc deposits: A comparative examination: Transactions of the Institution of Mining and Metallurgy, v. 99, sec. B, p. B21–B42.
- Sangster, D.F., Nowlan, G.S., and McCracken, A.D., 1994, Thermal comparison of Mississippi Valley-type lead-zinc deposits and their host rocks using fluid inclusion and conodont color alteration index data: *ECONOMIC GEOLOGY*, v. 89, p. 493–514.
- Schwalter, T.T., 1979, Mechanics of secondary hydrocarbon migration and entrapment: American Association of Petroleum Geologists Bulletin, v. 63, p. 723–760.
- Screaton, E.J., Fisher, A.T., Carson, B., and Becker, K., 1997, Barbados Ridge hydrogeologic tests: Implications for fluid migration along an active decollement: *Geology*, v. 25, p. 239–242.
- Selley, D., Broughton, D., Scott, R., Bull, S., McGoldrick, P., and Hitzman, M., 2005, Geology and mineralization of the Zambian copperbelt: *ECONOMIC GEOLOGY 100<sup>TH</sup> ANNIVERSARY VOLUME*, p. 000–000.
- Shanks, W.C., III, and Bischoff, J.L., 1977, Ore transport and deposition in the Red Sea geothermal system: A geochemical model: *Geochimica et Cosmochimica Acta*, v. 41, p. 1507–1519.
- Shelton, K.L., Bauer, R.M., and Gregg, J.M., 1992, Fluid-inclusion studies of regionally extensive epigenetic dolomites, Bonnetterre Dolomite (Cambrian), southeast Missouri: Evidence of multiple fluids during dolomitization and lead-zinc mineralization: *Geological Society of America Bulletin*, v. 104, p. 675–683.
- 1993, Fluid-inclusion studies of regionally extensive epigenetic dolomites, Bonnetterre Dolomite (Cambrian), southeast Missouri: Evidence of multiple fluids during dolomitization and lead-zinc mineralization: Reply: *Geological Society of America Bulletin*, v. 105, p. 972–978.
- Shosa, J.D., and Cathles, L.M., 2001, Experimental investigation of capillary blockage of two phase flow in layered porous media: Petroleum systems of deep-water basins: Bob F. Perkins Conference—GCSSEPM Foundation Annual Research Conference, 21<sup>st</sup>, Global and Gulf of Mexico Experience, Houston, Texas, December 2–5, 2001, Gulf Coast Society of Economic Paleontologists and Mineralogists, p. 725–739.
- Smith, W.H.F., and Sandwell, D.T., 1997, Global sea floor topography—from satellite altimetry and ship depth soundings: *Science*, v. 277, p. 1956–1962.
- Spirakis, C.S., 1995, Problems with applying topography-driven flow to genesis of the Upper Mississippi Valley zinc-lead district and to fluid flow in the Illinois basin: U.S. Geological Survey Bulletin, v. 2094C, p. 1–12.
- Stamatakos, J., Hirt, A.M., and Lowrie, W., 1996, The age and timing of folding in the Central Appalachians from paleomagnetic results: *Geological Society of America Bulletin*, v. 108, p. 815–829.
- Studlick, J.R.J., Shew, R.D., Basye, G.L., and Ray, J.R., 1990, A giant carbon dioxide accumulation in the Norphlet Formation, Pisgah anticline, Mississippi, in Barwis, J.H., McPherson, J.G., and Studlick, J.R.J., eds., *Sandstone petroleum reservoirs: New York, NY, Springer-Verlag*, p. 181–203.
- Surdam, R.C., 1997, Seals, traps, and the petroleum system: Tulsa, OK, American Association of Petroleum Geologists, 317 p.
- Sverjensky, D.A., 1981, The origin of a Mississippi Valley-type deposit in the Viburnum Trend, Southeast Missouri: *ECONOMIC GEOLOGY*, v. 76, p. 1848–1872.
- 1986, Genesis of Mississippi Valley-type lead zinc deposits: Annual Reviews of Earth and Planetary Science, v. 14, p. 177–199.
- Sverjensky, D.A., Rye, D.M., and Doe, B.R., 1979, The lead and sulfur isotopic compositions of galena from a Mississippi Valley-type deposit in the New Lead Belt, Southeast Missouri: *ECONOMIC GEOLOGY*, v. 74, p. 149–153.
- Swenson, J.B., and Person, M.A., 2000, The role of basin-scale transgression and sediment compaction in stratiform copper mineralization: Implications from White Pine, Michigan, USA: *Journal of Geochemical Exploration*, v. 69–70, p. 239–243.
- Symons, D.T.A., and Stratakos, K.K., 2002, Paleomagnetic dating of Alleghanian orogenesis and mineralisation in the Mascot-Jefferson City zinc district of East Tennessee, USA: *Tectonophysics*, v. 348, p. 51–72.
- Symons, D.T.A., Enkin, R.J., and Cioppa, M.T., 1999, Paleomagnetism in the Western Canada Sedimentary Basin: Dating and fluid flow and deformation events: *Bulletin of Canadian Petroleum Geology*, v. 47, p. 534–547.
- Tieh, T.T., and Ledger, E.R., 1987, Sphalerite in sandstone and limestones of the Gulf Coast and North Texas: *ECONOMIC GEOLOGY*, v. 82, p. 1064–1069.
- Tokunaga, T., Mogi, K., Matsubara, O., Tosaka, H., and Kojima, K., 2000, Buoyancy and interfacial force effects on two-phase displacement patterns: An experimental study: American Association of Petroleum Geologists Bulletin, v. 84, p. 65–74.
- Torgersen, T., 1989, Terrestrial helium degassing fluxes and the atmospheric helium budget: Implications with respect to the degassing processes of continental crust: *Chemical Geology*, v. 79, p. 1–14.
- Torgersen, T., and Clarke, W.B., 1985, Helium accumulation in groundwater. I. An evaluation of sources and the continental flux of crustal (super 4) He in the Great Artesian basin, Australia: *Geochimica et Cosmochimica Acta*, v. 49, p. 1211–1218.
- U.S. Geological Survey, World Energy Assessment Team (W.E.A.T.), 2000, U.S. Geological Survey World Petroleum Assessment 2000: Description and results: Digital Data Series 60.
- Ulrich, M.R., Kyle, J.R., and Price, P.E., 1984, Metallic sulfide deposits in the Winnfield salt dome, Louisiana: Evidence for episodic introduction of metalliferous brines during cap rock formation: *Gulf Coast Association of Geological Societies Transactions* 34, p. 435–442.
- Viets, J.G., Hofstra, A.H., and Emsbo, P., 1997, Solute compositions of fluid inclusions in sphalerite from North American and European Mississippi Valley-type ore deposits: Ore fluids derived from evaporated seawater: *Society of Economic Geologists Special Publication* 4, p. 465–482.
- Wallace, P.J., 2003, From mantle to atmosphere: Magma degassing, explosive eruptions, and volcanic volatile budgets, in De Vivo, B., and Bodnar, R.J., eds., *Melt inclusions in volcanic systems: Methods, applications and problems: Amsterdam, Elsevier*, p. 105–127.
- White, W.S., 1971, A paleohydrologic model for mineralization of the White Pine copper deposit, northern Michigan: *ECONOMIC GEOLOGY*, v. 66, p. 1–13.
- Wilkinson, D., 1986, Percolation effects in immiscible displacement: *Physical Review A*, v. 34, p. 1380–1391.
- Willett, S.D., Issler, D.R., Beaumont, C., Donelick, R.A., and Girst, A.M., 1997, Inverse modeling of annealing of fission tracks in apatite. 2: Application to the thermal history of the Peace River Arch region, Western Canada Sedimentary Basin: *American Journal of Science*, p. 970–1011.

- Winckler, G., Kipfer, R., Aeschbach, H.W., Botz, R., Schmidt, M., Schuller, S., and Bayer, R., 2000, Sub sea floor boiling of Red Sea brines: New indication from noble gas data: *Geochimica et Cosmochimica Acta*, v. 64, p. 1567–1575.
- Yang, J., Bull, S., and Large, R., 2004a, Numerical investigation of salinity in controlling ore-forming fluid transport in sedimentary basins: Example of the HYC deposit, northern Australia: *Mineralium Deposita*, v. 39, p. 622–631.
- Yang, J., Large, R.R., and Bull, S.W., 2004b, Factors controlling free thermal convection in faults in sedimentary basins: Implications for the formation of zinc-lead mineral deposits: *Geofluids*, v. 4, p. 237–247.

Supplement to

# Fluid Flow and Petroleum and Mineral Resources in the Upper (<20-km) Continental Crust

LAWRENCE M. CATHLES, III AND JENNIFER J. ADAMS

## APPENDIX 1

### Estimation Methods

#### Table of useful flow relationships

Quantification allows us to test conceptual models of natural systems and to use observations of natural systems to determine important characteristics, such as the rate of fluid flow through them and their bulk (e.g., effective) permeability.

A number of useful methods for estimating rates of fluid flow or estimating how much flow has taken place are summarized in Table A1, with references to sources of extended discussion. The table summarizes the following:

A1.1 = a method for estimating the rate of vertical flow near an intrusion margin using the insight from Elder (1966) that cold surrounding waters will compress a hot upwelling zone laterally and increase the vertical flux until the pressure gradient in the hot zone equals that in its cold water surroundings;

A1.2 = a heat balance method for estimating the mass of pore water that can be convectively circulated by an igneous intrusion of known mass;

A1.3 = equations (derived below) specifying the time required for an intrusion to cool by convection or conduction;

A1.4 = the critical Raleigh numbers at which free convection will begin in closed or open layers heated from below, the spacing of upwelling plumes, and the critical Raleigh number

for permeability decreasing exponentially with depth and for a fracture in an impermeable host;

A1.5 = the increase in heat flow that will be caused by this convection;

A1.6 = the rate of convection in a folded sand that is caused by the unequal thermal conductivities of sandstone and shale;

A1.7 = the rate of quartz dissolution and precipitation caused by this circulation expressed as the change in sand porosity;

A1.8 = the time required for parts of the folded sand to plug solid with silica;

A1.9 = the rate at which solute, thermal, or chemical fronts will move through a porous media relative to the flux (e.g., Darcy or superficial velocity) of pore water;

A1.10 = the alteration rate of a rock caused by the flow of pore water that is in local chemical equilibrium with the host;

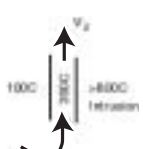
A1.11 = the alteration produced by the movement of a thermal front;

A1.12 = the mass of a chemical component transported across a surface per unit area of that surface;

A1.13 = the Peclet number, which describes how vertical fluid flow modifies temperature or chemical gradients near the earth's surface; and

A1.14 = a formula that estimates the rate and depth of fluid flow from uplands to the stream in a drainage basin.

TABLE A1. Simple Physical and Chemical Porous Media Flow Equations

Case	Equation	Parameters	Reference
1. Vertical fluid flux near an intrusion	$V_z = \frac{k\Delta\rho g}{\mu_w} = \frac{k\rho_o g\alpha\Delta T}{\mu_w}$ 	Coeff thermal expansn $\alpha [^\circ K^{-1}] = 10^{-3}$ Water density 4°C $\rho_o [kg/m^3] = 1000$ Water viscosity $\mu_w [Pa \cdot s] = 2 \times 10^{-4}$ Permeability (1 md) $k [m^2] = 10^{-15} = 1md$ Acceleration gravity $g [m/s^2] = 9.8$ Vertical fluid flux $V_z [m/s] = 0.4m/yr$	Cathles (1977, 1981, 1997)
2. Mass of 350°C water, Q, needed to cool intrusion of mass $M_{intr}$	$\frac{Q}{M_{intr}} = \frac{c_m(T_{1200C} - T_{100C}) + L}{c_w(T_{350C} - T_{100C})} = 1.28$ <p>same for both mafic and felsic intrusions</p>	Heat capacity rock $c_m = 841J/kg$ Heat capacity water $c_w = 4196J/kg \cdot K$ Latent heat crystallization $L = 420J/kg \cdot K$	Norton and Cathles (1979)

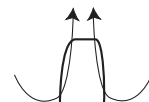


TABLE A1. (Cont.)

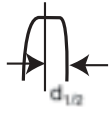

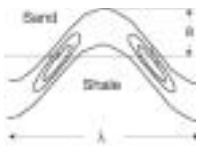
Case	Equation	Parameters	Reference																					
3. Time to cool an intrusion of half-width $d_{1/2}$	$t_{cond}^{25\%} [k.y.] = 170 d_{1/2}^2 [km]$ $t_{conv} [k.y.] = 17 \frac{d_{1/2} [km]}{k}$ $k_{crit} [md] = \frac{0.1}{d_{1/2} [km]}$	t to cool by conduction to $t_{cond}^{25\%}$ $\Delta T = 25$ percent $t_{conv}$ t to cool by convection in k.y. $k_{crit}$ k[md] where cond = conv cooling $d_{1/2}$ Half width of intrusion in km $\bar{k}$ Permeability of host in md	Appendix 1 Figure A2 																					
4. Critical Rayleigh number, $R_c$ , and permeability at which pore water in a layer of thickness H will convect	$R = \frac{j_{conv} = (k\rho_o g\alpha\Delta T/\mu_w)\rho_o c_w \Delta T}{j_{cond} = K\Delta T/H} = \frac{k\alpha\rho_o g c_w G_T H^2}{vK}$ $R_c = \left\{ \begin{array}{l} 27.1 \text{ free flow} \\ 4\pi^2 \text{ no flow (also all below)} \\ 4\pi^2 \text{ } k \rightarrow \bar{k} \text{ exp. } l > H \\ 14.4 \text{ } H^2 \rightarrow l^2 \text{ exp. } l < H \\ 16.4 \text{ } H^2 \rightarrow WH \text{ fault} \end{array} \right\}$ <p>Critical permeabilities (<math>^{\circ}</math> = free flow)</p> <table border="1"> <thead> <tr> <th>H[m]</th> <th>k[m<sup>2</sup>]</th> <th>k[md]</th> </tr> </thead> <tbody> <tr> <td>30</td> <td><math>25 \times 10^{-12}</math></td> <td>25 000</td> </tr> <tr> <td>100</td> <td><math>2.2 \times 10^{-12}</math></td> <td>2200</td> </tr> <tr> <td>1000</td> <td><math>2.2 \times 10^{-14}</math></td> <td>22</td> </tr> <tr> <td>5000<math>^{\circ}</math></td> <td><math>9 \times 10^{-16}</math></td> <td>0.9</td> </tr> <tr> <td>5000<math>^{\circ}</math></td> <td><math>9 \times 10^{-16}</math></td> <td>0.6</td> </tr> <tr> <td>10,000<math>^{\circ}</math></td> <td><math>1.5 \times 10^{-17}</math></td> <td>0.15</td> </tr> </tbody> </table>	H[m]	k[m <sup>2</sup> ]	k[md]	30	$25 \times 10^{-12}$	25 000	100	$2.2 \times 10^{-12}$	2200	1000	$2.2 \times 10^{-14}$	22	5000 $^{\circ}$	$9 \times 10^{-16}$	0.9	5000 $^{\circ}$	$9 \times 10^{-16}$	0.6	10,000 $^{\circ}$	$1.5 \times 10^{-17}$	0.15	Vert conv heat flow $j_{conv}$ Vert cond heat flow $j_{cond}$ $T_{bot} - T_{top}$ $\Delta T [^{\circ}K]$ Layer thickness $H [m] = 100$ Geothermal grad $G_T [^{\circ}K/m] = 0.02$ Kinematic viscosity $\nu [m^2/s] = 2 \times 10^{-7}$ Thermal cond $K [W/m^{\circ}K] = 2.4$ Exponentially decreasing perm. $k = k_o \exp(-z/l)$ Average perm $\bar{k} = k_o \frac{l}{H} (1 - \exp(-H/l))$ Fault width $W [m]$ Critical fault transmissivity $10^{12} m^3$ , for $H = 10 km$	Lapwood (1948)  Exponential decrease in permeability (Mal'kovskii and Pek, 1999) Convection in fault (Mal'kovskii and Pek, 1997)
H[m]	k[m <sup>2</sup> ]	k[md]																						
30	$25 \times 10^{-12}$	25 000																						
100	$2.2 \times 10^{-12}$	2200																						
1000	$2.2 \times 10^{-14}$	22																						
5000 $^{\circ}$	$9 \times 10^{-16}$	0.9																						
5000 $^{\circ}$	$9 \times 10^{-16}$	0.6																						
10,000 $^{\circ}$	$1.5 \times 10^{-17}$	0.15																						
5. Total conductive heat flux	$Nu = \frac{R}{R_c}$	Rayleigh number from above $R$ Critical Rayleigh number from above $R_c$ Nusselt number $Nu$	Palm et al. (1972)																					
6. Maximum vertical flow rate in folded sand layer encased in shale	$V_z = \frac{k}{\mu_w} \rho_o g \alpha \frac{K_{sh} G_T H}{K_{sd}} \left( \frac{K_{sd}}{K_{sh}} - 1 \right) \left( \frac{2\pi a}{\lambda} \right)^2$ 	Amplitude of fold $a [m]$ Wavelength of fold $\lambda [m]$ Geothermal gradient $G_T = J_{HF} / K_{sh}$ Heat flux $J_{HF} [W/m^2]$ Thermal conductivity shale $K_{sh} [W/m \cdot ^{\circ}K] = 1.31$ Thermal conductivity sdst $K_{sd} [W/m \cdot ^{\circ}K] = 2.44$	Wood and Hewett (1982), Davis et al. (1985), Cathles (1997)																					
7. Rate of change of porosity in folded sand layer	$\frac{\partial \phi}{\partial t} = \frac{V_z G_T}{\rho_{SiO_2}} \frac{\partial C_{SiO_2}}{\partial T}$	Change in $C_{SiO_2}$ with temperature $\frac{\partial C_{SiO_2}}{\partial T} [^{\circ}K^{-1}] = 5 \times 10^{-6}$ Density of silica $\rho_{SiO_2} [kg/m^3] = 2700$	Wood and Hewett (1982), Davis et al. (1985), Cathles (1997)																					
8. Time for initial sand layer porosity to plug with silica	$\tau = \frac{\phi_o}{\partial \phi / \partial t}$	Preattered sand porosity $\phi_o = 0.55$ Filling time $\tau [s]$ If $V$ declines with $\phi$ $\phi = \phi_o \exp(-t/\tau)$	Wood and Hewett (1982) Figure 20																					

TABLE A1. (Cont.)

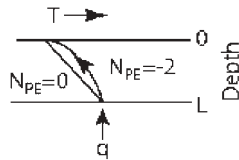
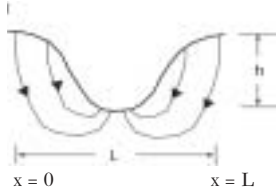
Case	Equation	Parameters	Reference
9. Velocity of a thermo-chemical front	Front type	$\frac{\text{fluid storage}}{\text{porous media storage}}$	Darcy flux of pore water $V [m/s]$
			True velocity of front $v_f [m/s]$
	Pore water	$\frac{\rho}{\phi\rho} = 5$ for $\phi = 0.2$	Wt % salt in the sediment $C_{salt}$
	Temperature	$\frac{\rho c_w}{\rho_m c_m} = 2$	Concentr. dissol. O <sub>2</sub> at 1 atm $C_{O_2} = 8.6 ppm$
	Dissolution 20 wt % salt	$\frac{\rho C_{salt}^{sat}}{\rho_m G_{salt}} = 0.6$	Pyrite grade (mass fraction) $G_{py}$
	Oxidation 1 wt % pyrite	$\frac{\rho C_{O_2}}{\rho_m G_{py} R_{O_2 py}} = 3.2 \times 10^{-4}$	g O <sub>2</sub> to leach 1 g pyrite $R_{O_2 py} = 1.07$
		Saturated brine salinity [g/g] $C_{salt}^{sat} = 0.26$	
		Density of sediment [kg/m <sup>3</sup> ] $\rho_m = 2200$	
		Assume 1 mole O <sub>2</sub> leaches 2.7 moles pyrite	
	$v_f = \frac{\text{fluid storage}}{\text{porous media storage}} V$		
10. Rate of change of mass (or mole) fraction of i in sediment	$\dot{X}_{ir} = \frac{1}{\rho_m} \left( \frac{\partial C_i}{\partial T} \rho \vec{V} \cdot \vec{\nabla} T + \frac{\partial C_i}{\partial C_{Cl}} \rho \vec{V} \cdot \vec{\nabla} C_{Cl} \right) + \frac{\partial C_i}{\partial P} \rho \vec{V} \cdot \vec{\nabla} P$	Mass fraction i $C_i [kg_i / kg_{pore\ fluid}]$	Local equilibrium: Cathles (1983), Henley et al. (1984), Hanor (1997)
		Mass fraction Cl $C_{Cl} [kg_{Cl} / kg_{pore\ fluid}]$	
		Rate change of rock mass fraction $\dot{X}_{ir} [kg_i / kg_{rock}]$	
11. $\Delta$ mass (or mole) fraction $i$ across thermal front	$\Delta X_{ir} = \frac{\rho}{2\rho_m} (C_i^{350^\circ C} - C_i^{100^\circ C})$ constant pressure and salinity	$\Delta$ mass fraction $i$ across front $\Delta X_{ir} [kg_i / kg_{rock}]$	Cathles (1997)
		Fluid/media density $\frac{\rho_f}{\rho_m} = 0.4$	
		$\Delta$ SiO <sub>2</sub> concentration $C_{SiO_2}^{350^\circ C} - C_{SiO_2}^{100^\circ C} = 2 \times 10^{-6}$	
		$\Delta$ rock mass fraction $\Delta X_{SiO_2 r} = 0.04 wt\%$	
12. Mass of solution component $i$ vented across surface per m <sup>2</sup> of surface	$\sigma_i = \int_i C_i V \rho \partial t$	Surface density of $i$ $\sigma_i [kg_i / m^2]$	
13. Peclet number	$N_{PE} = \frac{j_{conv} = qc_w \Delta T}{i_{cond} = K \Delta T / L} = \frac{qc_w L}{K}$  Conductive profile significantly nonlinear if magnitude of $N_{PE}$ is greater than 1	Peclet Number $N_{PE}$	Bredehoeft and Papadopoulos (1965)
		Vertical interval analyzed $L [m]$	Figure A3  Figure 21 shows flow perturbations of $T$ along basal aquifer in terms of a dimensionless number similar to $N_{PE}$  See Deloule and Turcotte (1989) for silica deposition in crack
			

TABLE A1. (Cont.)

Case	Equation	Parameters	Reference
14. Infiltration rate	Solution of Laplace's equation, $\nabla^2 h = 0$ for water table elevation $h = h_0 \cos 2\pi x / L$ , where $h_0$ is the initial height of the water table and $x$ is the horizontal distance from the origin	Vertical darcy flux Infiltration rate	2/3 flow occurs above depth of $\sim 0.2 L$  See Forster and Smith (1989) for flow in faulted intermountain basin
	$V_z = -\frac{2\pi\rho_o gh}{\mu L} \cos \frac{2\pi x}{L} \exp \frac{-2\pi z}{L}$ $I = -V_z(x=0, z=0) = \frac{2\pi\rho_o ghk}{\mu_w L}$		
	For $L = 10$ km, $h = 200$ m, $l = 0.1$ m/yr, $k = 5 \times 10^{-16}$ m <sup>2</sup>		

One of the most frequently used and best ways to constrain fluid movements near the surface employs a simple solution to the conduction-advection equation published by (Bredehoeft and Papadopoulos, 1965). Figure A1 shows that the progressive modification of the linear conduction and/or diffusion gradient by fluid flow is characterized by the dimensionless Peclet number,  $N_{PE}$ , defined in Table A1.13. Measured temperatures or concentrations from a drill hole or series of drill holes plotted as a function of depth on this diagram (where any reasonable value for  $L$  is assumed) determine the  $N_{PE}$  by the contour they lie along. The vertical mass flux,  $q$ , can be calculated from this  $N_{PE}$  because all the parameters in it are usually fairly well known except the vertical pore mass flux. Bickle and McKenzie (1987) provide interesting extensions of this approach.

The movement of thermal, chemical, or combined thermochemical fronts can be described in a simple fashion if a Lagrangian coordinate system is chosen that moves with the front (see Cathles, 1997). Although the fronts spread due to diffusion and dispersion, the midpoint temperature or concentration moves with a velocity equal to the product of superficial (Darcy) velocity (fluid flux,  $V$ ) and the ratio of the storage capacity of the fluid to that of the porous media. The velocities of various fronts are given in Table A1.9. Meteoric water moving through a porous media will displace connate brine at five times the seepage velocity if the porosity is 20 percent, but if there is 20 wt percent salt in the sediment the salinity front will move at 0.4 times the seepage velocity,  $V$ , for example. Extended discussion can be found in Lake et al. (2002).

At temperatures greater than  $\sim 70^\circ\text{C}$ , inorganic solution species are in equilibrium with rock minerals (Cathles, 1983; Henley et al., 1984; Hanor, 1997). Pore fluids circulated through pressure, temperature, or salinity gradients alter the host inorganically as shown in Table A1.10. The special case of alteration caused by the passage of a thermal front separating  $350^\circ\text{C}$  upstream pore water from  $100^\circ\text{C}$  pore water downstream is given in Table A1.11. The mass fraction of silica in the sediment will increase by 0.04 wt percent with the passage of this front. Because the contrasts of other dissolved

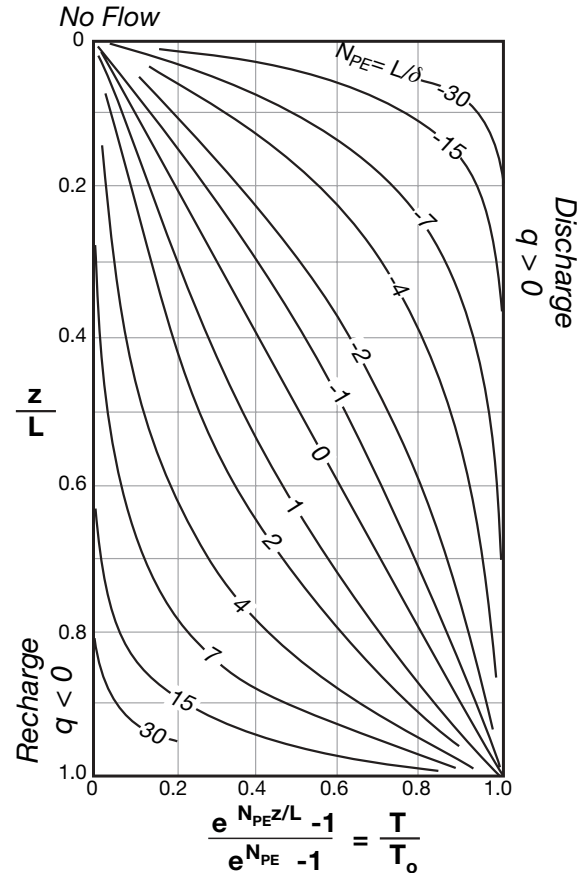


FIG. A1. Effect of vertical fluid flow on temperature (or solute concentration) that would otherwise increase linearly with depth. Shape of curve changes with the Peclet number (Table A1.13).  $T_o$  is the temperature ( $C_o$  is the concentration of a nonreactive solute) at depth  $L$  relative to the surface values. Peclet number is positive for fluid inflow (recharge), negative for outflow (discharge). The depth at which the temperature (or concentration) reaches  $1/e$  of its ultimate value,  $\delta$ , is defined at the top of the figure. Modified from Bredehoeft and Papadopoulos (1965).

elements are generally small compared to silicon, this illustrates that the movement of pore fluids in the subsurface will not produce useful element concentrations unless the thermal front is somehow anchored in space, as it might be at a boiling horizon or at the sea floor. The surface mass of minerals per unit area in plan, which could be deposited at such an interface, is quantified in Table A1.12. The most critical parameter in this expression is the solubility of the metal on the high temperature side of the front. Measured metal concentrations in several relevant ore-forming fluids are given in Table A2.

### Time required to cool a tabular intrusion

A simple back-of-the-envelope model for the time to cool a tabular intrusion was deduced from numerical experiments by Cathles (1981), assuming that the permeability of the host and intrusion was the same and independent of temperature, and assuming a total intrusion heat content of 500 J/g. Here we extend this treatment for the case where permeability is a function of temperature, and the heat content of the intrusion,  $H_{tot}$ , is 1,430 J/g. This heat content is realistic for both felsic and mafic intrusions (Norton and Cathles, 1979, table 12.1). As in the previous treatment the results are compared to the time to cool an infinite dike.

In this method, vertical inflow is determined by estimating the rate at which pore water can be circulated through the host by buoyancy in a 350°C flow zone adjacent to an intrusion. The cooling time is that required for the circulating fluids to extract the initial heat content of the intrusion, assuming they are warmed from 100° to 350°C and then discharged to the ocean.

The time to cool an infinite dike to 25 percent of its initial temperature contrast with its host is approximately  $5d_{1/2}^2/\kappa$  (Jaeger, 1968, fig. 1a), where  $d_{1/2}$  is the half width of the intrusion and  $\kappa$  is the thermal diffusivity of the intrusion and its host. Taking  $\kappa = 9.2 \times 10^{-7} \text{ m}^2/\text{s}$ , a 2-km-wide dike will take 170,000 years to achieve this degree of cooling.

The convection pattern near a tabular intrusion is shown in Figure A2. The buoyant pressure driving the circulation is  $\Delta\rho gh$ , where  $\rho$  is the density of the pore fluid,  $g$  the acceleration of

gravity, and  $h$  the height of the intrusion. Assuming that the inflow part of the circulation path, which offers resistance to flow, is  $2H$  long (we assume that there is little resistance in the cracking front portion of the flow path), the recharge mass flux is  $q = \frac{k}{\nu} \frac{\Delta\rho gh}{2H}$ , and the total recharge over the time it takes the intrusion to cool,  $t_{conv}$ , is  $Q = 2Hqt_{conv}$ . Here  $\nu$  is the kinematic viscosity of the pore fluid and  $\Delta\rho$  is the difference in density between the ambient pore fluid and the pore fluid in the hot (350°C) upwelling cracking front flow channel adjacent to the hot portion of the intrusion.

Of course  $Q$  is also the mass of hydrothermal water discharged to the ocean at the other end of the flow loop, and the heat discharged is therefore  $Qc_w(T_{350^\circ\text{C}} - T_{100^\circ\text{C}})$ , where  $c_w$  is the heat capacity of water in J/g. The mass of the intrusion per unit width perpendicular to the section,  $M_{intr} = 2\rho_{intr}d_{1/2}h$ , and if the heat content of the intrusion relative to its cooled state at the time of intrusion is  $H_{tot}$ , the time required to convectively cool can be found by setting this initial heat content of the intrusion equal to that carried off by the convective circulation:

$$H_{tot}(2\rho_{intr}d_{1/2}h) = 2H \left( \frac{k}{\nu} \frac{\Delta\rho gh}{2H} \right) c_w (T_{350^\circ\text{C}} - T_{100^\circ\text{C}}) t_{conv}.$$

Substitution of suitable parameter values leads directly to the equations in Table A1.3.

Figure A3 plots the time interval required for an intrusion of width  $2d_{1/2}$  to cool by conduction or convection for various host permeabilities.

### Inferring crustal permeability

Host permeability can be estimated by noting that, if the Rayleigh number of the upper 5 km of the upper crust exceeded the critical Rayleigh number by a factor of two, heat flow measured at the surface would vary by at least a factor of two over lateral distances equal to twice the thickness of the upper crust (Table A1.4). Because this is not observed, the permeability of the upper 5 km of the continental crust must be generally less than  $\sim 0.5 \times 10^{-15} \text{ m}^2$ , and the permeability of the upper 10 km of the continental crust (above the

TABLE A2. Metal Concentrations Measured in Several Common Fluid Types

Fluid	T (°C)	Cl	SO <sub>4</sub>	H <sub>2</sub> S	Zn	Pb	Cu	Ag	Au
		ppm (° = ppb)							
Salton Sea <sup>1</sup>	330	157,500	53	10	507	102	7	1.4 <sup>2°</sup>	
Oil field brine <sup>3</sup>	102	198,000	64	<0.09	243	70			
Guaymas basin, site 2 <sup>4</sup>	291	20,850			0.1	0.06	<0.01		
Broadlands wells 2 and 11 <sup>5</sup>	260	1,200	7	72	0.6 <sup>°</sup>	0.8 <sup>°</sup>	0.6 <sup>°</sup>	0.5 <sup>°</sup>	0.04 <sup>°</sup>
Seawater <sup>4</sup>	15	19,355	2,745	<1	<1	<1	<1		

<sup>1</sup> Well S2-14, data from McKibben and Hardie (1997)

<sup>2</sup> White (1968)

<sup>3</sup> Pennsylvania, W.M.H. Geiger no. 2 well; data cited in Goodfellow et al. (1993)

<sup>4</sup> Goodfellow et al. (1993)

<sup>5</sup> Broadlands geothermal area, New Zealand; data from tables A1b and A3 in Henley et al. (1986); wells 2 and 11 are adjacent and sampled interval has same temperature; Cl, SO<sub>4</sub>, and H<sub>2</sub>S data are from well 11; trace element data is from well 2

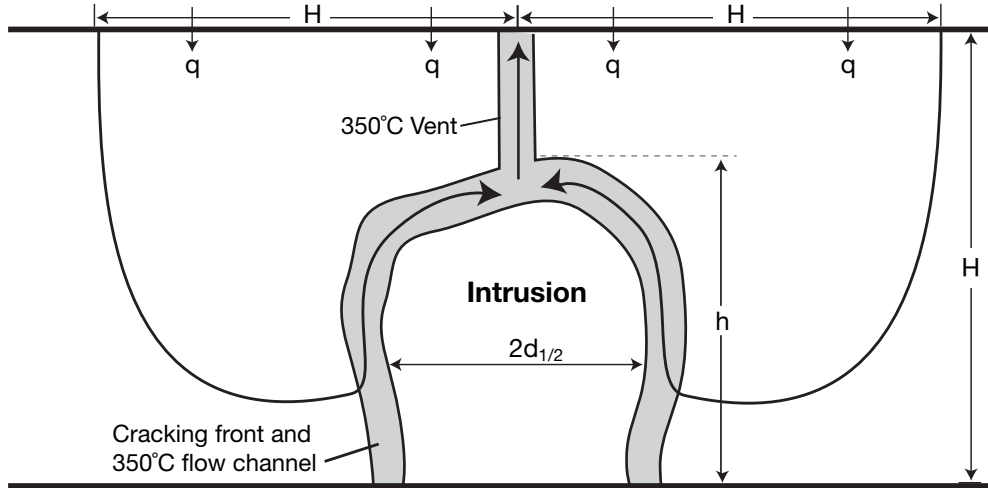


FIG. A2. Schematic of the pattern of convection around a tabular intrusion.

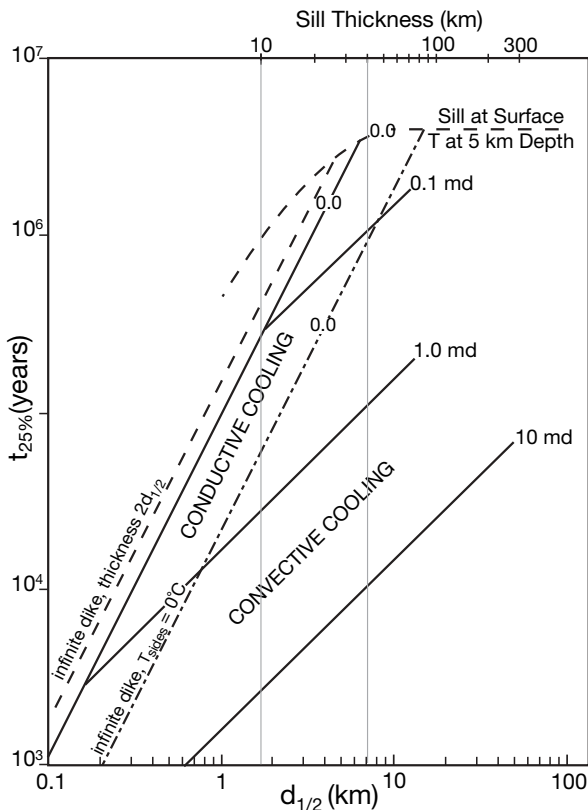


FIG. A3. Time required to cool an intrusion by either conduction or ground-water convection to 25 percent of its initial temperature contrast relative to ambient. The solid lines show cooling times for an intrusion of width  $2d_{1/2}$  as shown in Figure A1 and the insert in Table A1.3. The intrusion is dike-like (i.e., has infinite extent normal to the section). Conductive cooling lines have a slope of 2 on this log-log plot; convective cooling lines have a slope of unity. Dashed lines indicate that the conductive cooling of dikes and sills from Jaeger (1968). A sill 5 km thick with top at the surface provides an upper bound on cooling times.

amphibolite metamorphic zone) must be less than  $\sim 10^{-16} \text{ m}^2$ . The dynamic permeability in a metamorphic belt can be estimated, assuming local fluid/rock chemical equilibrium and reasonable temperature and pressure gradients, from the duration of metamorphism and the cumulative alteration. Manning and Ingebritsen (1999) and Ingebritsen and Manning (1999) use this approach, together with temperature profiles in the upper crust, to show that the dynamic permeability of the crust below  $\sim 10 \text{ km}$  during metamorphism is  $> 10^{-18} \text{ m}^2$  ( $1 \mu\text{d}$ ), and that the permeability of the shallower crust ranges from  $10^{-14}$  to  $10^{-17} \text{ m}^2$ .

The wide range in permeability in the upper 10 km of the crust suggests intrusions may cool either by conduction or convection. For example, the Dufault granodiorite in the Abitibi greenstone belt has a clear metamorphic halo and few associated massive sulfide deposits, and therefore cooled mainly by conduction. The adjacent Flavrian granodiorite has no metamorphic halo and many associated massive sulfide deposits, and cooled mainly by convection (see Goldie, 1979). The width ( $d_{1/2}$ ) of both intrusions is at least 2.5 km. Thus the permeability of the volcanics intruded by the Flavrian must have been  $> 0.5 \times 10^{-15} \text{ m}^2$ , whereas the permeability of the volcanics intruded by the Dufault must have been  $< 10^{-16} \text{ m}^2$  (Table A1.3). Here we have assumed the host permeability must be 10 times the critical for vigorous convective cooling.

#### Pattern of convection compared to expulsion

Models show thermal convection tends to sweep hot upwelling zones into narrow vents (Cathles, 1981), whereas fluids expelled from a basal aquifer will escape over a broad area (horsetail) as the aquifer approaches the surface (Cathles and Smith, 1983). Alteration halos will be useful guides to discovery of deposits in convecting systems but useless for finding deposits related to expulsive flow.



## APPENDIX 2

## Compaction in Overpressured Basins

Compaction of sand and shale is a linear function of effective stress (Palciuskas and Domenico, 1989; Revil and Cathles, 2001):

$$d\phi = -\phi_0\beta d\sigma_{eff},$$

where

$$d\sigma_{eff} = P - p, \quad (\text{A2.1})$$

and

$$dP = (\rho_g(1-\phi) + \rho_f\phi)g dz.$$

Here  $\phi$  is subsurface porosity,  $\phi_0$  is initial porosity at the surface,  $\beta$  is the rock compressibility,  $\sigma_{eff}$  effective stress,  $P$  lithostatic pressure,  $p$  pore fluid pressure,  $\rho_g$  the density of mineral grains,  $\rho_f$  the density of the pore fluid,  $g$  the acceleration of gravity, and  $z$  depth, all in mks units. The vertical axis is positive vertically down, making lithostatic pressure increase as  $z$  increases.

This set of equations is used below to determine compaction in the three zones shown in Figure A4. The shallowest zone, the hydrostatic zone, has hydrostatic pore fluid pressures. Below  $z_T^{top}$  the intrinsic permeability of the sediments is assumed to be zero and sediment loading thus causes fluid pressures to exceed hydrostatic at greater depths. Thus  $z_T^{top}$  is the depth to the top of the overpressured zone. Fluid pressure increases from hydrostatic to a fraction,  $F$ , of lithostatic in a transition zone. Porosity is constant and pore pressure increases parallel to lithostatic in this zone. In the lowermost zone, the pore pressure remains at  $F$  times lithostatic, which is the point at which the rock hydrofractures. Compaction occurs in the lowermost zone but more slowly than in the hydrostatic zone. The discussion below follows Revil and Cathles (2001).

Input parameters for the model are the depth to the top of the overpressured zone,  $z_T^{top}$ , fraction of lithostatic,  $F$ , the rock compressibility,  $\beta$ , and the initial porosity,  $\phi_0$ .

*Compaction at hydrostatic conditions*

Under hydrostatic conditions, indicated by subscript H, the following equations hold:

$$\begin{aligned} \text{(a)} \quad dP_H &= (\rho_g(1-\phi_H) + \rho_f\phi_H)g dz \\ \text{(b)} \quad dp_H &= \rho_f g dz \\ \text{(c)} \quad d\sigma_{eff} &= (1-\phi_H)(\rho_g - \rho_f)g dz \\ \text{(d)} \quad d\phi_H &= -\phi_0\beta(1-\phi_H)(\rho_g - \rho_f)g dz. \end{aligned} \quad (\text{A2.2})$$

The first three equations are the hydrostatic form of equation (A2.1), and the fourth results from substituting equation (A2.2.c) into the porosity equation (A2.1.a). Equation (A2.2.d) can be integrated to yield:

$$\phi_H = 1 - (1 - \phi_0)e^{(z/z_c)}, \quad (\text{A2.3})$$

where  $z_c$  is a characteristic depth that is used to simplify the following equations:

$$z_c = 1/\phi_0\beta g (\rho_g - \rho_f). \quad (\text{A2.4})$$

Substituting  $\phi_H$  into equation (A2.2.a) and integrating, and then integrating equation (A2.2.b) yields:

$$\begin{aligned} P_H &= \rho_g z + g z_c (\rho_g - \rho_f) (1 - \phi_0) \left( e^{(z/z_c)} - 1 \right) \\ p_H &= \rho_f g z. \end{aligned} \quad (\text{A2.5})$$

If compaction continues under hydrostatic conditions to  $\phi_{min}$ , the depth at which  $\phi_{min}$  is reached follows by substituting  $\phi_{min}$  into equation (A2.3) and is:

$$z_H^{\phi_{min}} = z_c \ln \frac{1 - \phi_{min}}{1 - \phi_0}. \quad (\text{A2.6})$$

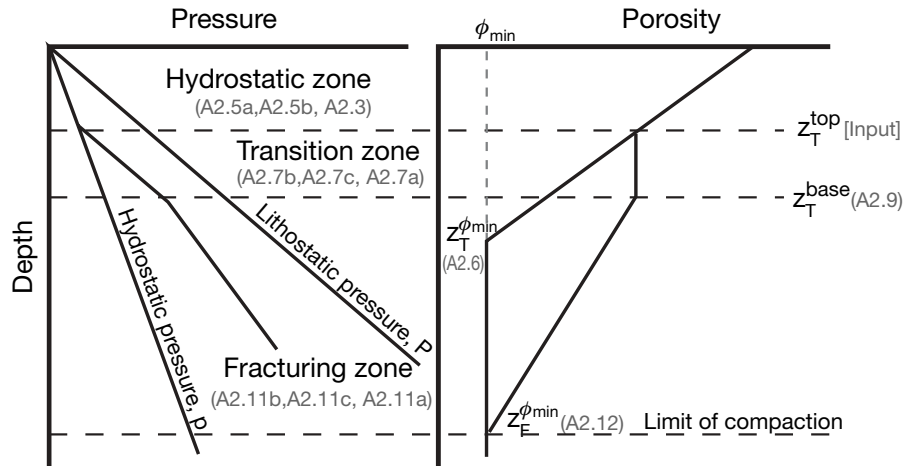


FIG. A4. Sketch of pressure and porosity relationships in a sediment package that becomes impermeable at and cannot develop pore pressures greater than a set fraction  $F$  of lithostatic. Equations to calculate each parameter are in gray type enclosed in parentheses. NB: For each zone, the equations to calculate the three values  $P$ ,  $p$ ,  $\phi$  are listed in this order in parentheses in the pressure-depth diagram.

Revil and Cathles (2001) show that the parameters that match shale compaction best in 40 wells in the offshore Louisiana Gulf of Mexico are  $\phi_o = 0.43$  and  $\beta = 3.3 \times 10^{-8} \text{ Pa}^{-1}$ .

#### Compaction from top of low permeability to base of transition zone

Suppose that the permeability becomes very low because of a change in lithology or capillary sealing at a depth,  $z_T^{top}$ . At this point, pore pressures will start to increase above hydrostatic, but until they reach a fraction  $F$  of lithostatic there is no compaction because the pore pressure will increase with the sediment load and the effective stress change will be zero. Porosity,  $\phi$ , thus remains constant at  $\phi_H(z_T^{top})$ . The equations in (A2.1) can be integrated easily over the transition zone:

$$\begin{aligned}\phi_T &= \phi_H(z_T^{top}) = \phi_H^{T-top} \\ P_T &= P_H(z_T^{top}) + (\rho_g(1 - \phi_H^{T-top}) + \rho\phi_H^{T-top})g(z - z_T^{top}) \quad (\text{A2.7}) \\ p_T &= \rho g z_T^{top} + (\rho_g(1 - \phi_H^{T-top}) + \rho\phi_H^{T-top})g(z - z_T^{top}).\end{aligned}$$

The sediments begin to fracture and leak when:

$$p_T = FP_T = p_T^{\max}. \quad (\text{A2.8})$$

Substituting into equation (A2.7), this condition is met at a depth  $z_T^{base}$ :

$$z_T^{base} = \frac{FP_H(z_T^{top}) - \rho g z_T^{top} + (1-F)((1 - \phi_H^{T-top}) + \rho\phi_H^{T-top})z_T^{top}g}{(1-F)((1 - \phi_H^{T-top}) + \rho\phi_H^{T-top})g}. \quad (\text{A2.9})$$

#### Compaction from the base of the transition zone to the limit of compaction

Equation (A2.1) in the fracturing zone (indicated by subscript  $F$ ) where pore fluid pressure is  $F$  times lithostatic are:

$$\begin{aligned}dP_F &= (\rho_g(1 - \phi_F) + \rho\phi_F)g dz \\ dp_F &= F dP_F \\ d\sigma_{\text{eff}} &= (1-F)(\rho_g - (\rho_g - \rho)\phi_F)g dz \quad (\text{A2.10}) \\ d\phi_F &= -\phi_o\beta d\sigma_{\text{eff}}\end{aligned}$$

The porosity equation can be integrated and substituted into the lithostatic and fluid pressure equations and integrated again as was done in the hydrostatic zone, with the result that:

$$\begin{aligned}\phi_F &= \frac{\rho_g}{\rho_g - \rho} - \left(\frac{\rho_g}{\rho_g - \rho} - \phi_T^{base}\right) \exp\left(\frac{z - z_T^{base}}{z'_c}\right) \\ P_F &= P_T^{base} + (\rho_g - \phi_T^{base}(\rho_g - \rho))z'_c g \left(e^{\frac{z - z_T^{base}}{z'_c}} - 1\right) \quad (\text{A2.11}) \\ p_F &= p_T^{base} + F(P_F - P_T^{base}).\end{aligned}$$

Here the characteristic depth of equation (A2.4) has been increased by a factor of  $(1-F)^{-1}$  such that:

$$z'_c = \frac{1}{\phi_o\beta} g(1-F)(\rho_g - \rho).$$

The depth at which  $\phi$  reaches  $\phi_{\min}$  is:

$$z_F^{\phi_{\min}} = z_T^{base} + z'_c \ln \left( \frac{\frac{\rho_g}{\rho_g - \rho} - \phi_{\min}}{\frac{\rho_g}{\rho_g - \rho} - \phi_T^{base}} \right). \quad (\text{A2.12})$$

#### Application

Figure A5a plots lithostatic pressure,  $P$ , as a function of depth for various depths to the base of the hydrostatic zone and top of the transition zone, which industry calls the TOOP (top of overpressure). Figure A5b shows how porosity varies with depth for these same cases and shows the excess porosity for each. If the overpressured pore fluids were bled off, the excess porosity would collapse. Excess porosity thus represents the fluid volume that could be expelled from the overpressured zones of a basin. Figure A5b shows, for example, that up to  $1,120 \text{ m}^3$  of brine per  $\text{m}^2$  of basin surface area could be vented from a basin overpressured at its surface. Less brine would be vented if the basin becomes overpressured below its depositional surface. For example, if the TOOP is 1,500 m below the sediment-water interface, sediments will compact along the hydrostatic curve (top curve) to 1,500-m depth, remain at the same porosity of  $\sim 0.2$ - to 5.5-km depth, and then compact more slowly with depth to the compaction limit of 5 percent. The excess porosity in this case is  $580 \text{ m}^3/\text{m}^2$ , so a  $100 \times 100 \text{ km}$  (plan) overpressured basin could expel  $5,800 \text{ km}^3$ .

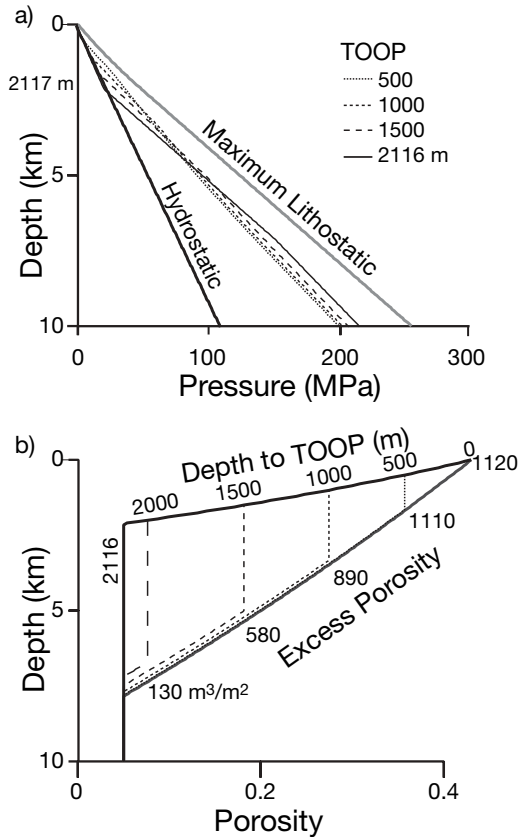


FIG. A5. (a). Pore pressure in a basin whose sediments become impermeable and overpressured between 0- and 2,117-m depth. TOOP = top of overpressure. Pore fluids increase along the hydrostatic curve to the TOOP depth, increase with the sediment load to 0.85 lithostatic pressure, and remain at 0.85 lithostatic thereafter. (b). The change in porosity with depth for the basin conditions described in (a). Excess porosity is porosity in excess of that which would exist under hydrostatic pore pressure conditions. This porosity would disappear, expelling an equal volume of brine, if the sediments below the TOOP were to become permeable.

## APPENDIX 3

## Fluid Fluxes in an Overpressured Basin Accumulating Sediments

Fluids are expelled from basins as the result of compaction, thermal expansion of pore waters with burial, and chemical reactions with positive volume change. The vertical fluxes associated with all these processes are related to the rate of sediment deposition. This appendix derives analytical expressions for all three fluxes.

*Compaction*

If the uncompacted (surface) sedimentation rate is  $S$  [m/s], conservation of solid mass requires that the vertical downward velocity of the solid grains be:

$$V_s(\phi) = S \frac{1 - \phi_o}{1 - \phi}. \quad (3.1)$$

Here  $V_s$  is the vertical flux of solid material (z-axis is positive vertically downward) in m/s,  $\phi$  is porosity, and  $\phi_o$  is the deposition porosity. Assuming the flow of fluid is zero at the base of the zone of compaction ( $\phi = \phi_{min}$ ), the vertical flux of the fluid due to compaction (e.g., porosity change) is:

$$V_C = -[\phi(z)V_s(\phi) - \phi_{min}V_s(\phi_{min})] \\ V_C = -\left(\phi \frac{1 - \phi_o}{1 - \phi} - \phi_{min} \frac{1 - \phi_o}{1 - \phi_{min}}\right)S. \quad (3.2)$$

Here  $V_C$  is the vertical flux of compactively expelled pore fluid (relative to the solid matrix) in  $m^3$  pore water/ $m^2$  area in a horizontal plane, and  $\phi_{min}$  is the minimum porosity. The compactive flux is  $V_C = (\phi_o - \phi_{min})S$  at the surface.

*Aquathermal expansion*

Assuming the flux is vertical, the vertical flux of pore water due to thermal expansion at depth  $z$  during burial is:

$$V_{AT} = \int_{H_{crust}}^z \phi(z) \alpha \bar{V}_s G_T dz. \quad (A3.3)$$

Here  $V_{AT}$  is the vertical pore water flux caused by thermal expansion (m/s),  $\phi(z)$  is the sediment or rock porosity as a function of depth,  $\alpha$  is the coefficient of thermal expansion in  $^{\circ}C^{-1}$ ,  $G_T$  is the geothermal gradient in  $^{\circ}C/m$ , and  $\bar{V}_s$  is the average subsidence of the solid matrix relative to the sediment-water interface (m/s). If we approximate the sediment flux as half the sedimentation rate:

$$\bar{V}_s = 0.5S \\ \phi(z) = \phi_o - \frac{\phi_o - \phi_{min}}{\tilde{z}_{\phi_{min}}} z, \text{ for } z \leq \tilde{z}_{\phi_{min}} \\ \phi(z) = \phi_{min}, \text{ for } z > \tilde{z}_{\phi_{min}} \quad (A3.4)$$

and integrate equation (A3.2) using these approximations, the aquathermal flux at  $z \leq \tilde{z}_{\phi_{min}}$  is:

$$V_{AT} = -0.5G_T \alpha S \left( \phi_{min} (H_{crust} - \tilde{z}_{\phi_{min}}) + \left( \phi_o (\tilde{z}_{\phi_{min}} - \tilde{z}_{\phi_{min}}) - \frac{\phi_o - \phi_{min}}{\tilde{z}_{\phi_{min}}} \left( \frac{\tilde{z}_{\phi_{min}}^2 - z^2}{2} \right) \right) \right) \quad (A3.5)$$

For  $z > \tilde{z}_{\phi_{min}}$ :

$$V_{AT} = -0.5G_T \alpha S \phi_{min} (H_{crust} - z) \quad (A3.6)$$

The first term inside the parentheses on the right hand side of equation (A3.5) is the aquathermal flux from the crust and sediments below the limit of compaction in the basin, assuming a constant porosity of  $\phi_{min}$  to the base of the crust. This flux is approximately one sixth the magnitude of the second term for  $\phi_{min} = 0.1$ . Thus, the assumption that the deep crust has a porosity of  $\phi_{min}$  impacts the shallow fluxes very little.

*Petroleum generation*

Assuming that generated petroleum represents new volume (i.e., the pores collapse on matured kerogen such that any reduction in its volume due to petroleum generation is cancelled by a slight extra compaction), the flux of pore brines caused by the generation of petroleum is estimated in two ways. First if the source layer is less than about a kilometer thick, assuming petroleum maturation occurs over a  $30^{\circ}C$  temperature interval and the geothermal gradient is  $20^{\circ}C/km$ , making the maturation interval 1,500 m, then:

$$V_{Gpet} = \frac{-G_K \rho_{sed} h}{1500 \rho_{pet}} \frac{1 - \phi_o}{1 - \phi(z_{source})} S, \text{ for } h < 1,000 \text{ m.} \quad (A3.7)$$

Here  $\rho_{sed}$  is the density of the source strata ( $kg/m^3$ ),  $h$  is the thickness of the source strata in m,  $\rho_{pet}$  is the density of the petroleum generated ( $kg/m^3$ ), and  $\phi(z_{source})$  is the porosity of the source strata, and  $G_K$  is the mass fraction of reactive kerogen in the source in kg reactive kerogen/kg solids.

If the source is thicker than  $\sim 1$  km, the petroleum flux is better estimated by:

$$V_{Gpet} = \frac{-G_K \rho_{sed}}{\rho_{pet}} \frac{1 - \phi_o}{1 - \phi(z_{source})} S. \quad (A3.8)$$

*Totals and estimates*

The total pore fluid flux,  $V_{tot}$ , is the sum of the partial fluxes caused by compaction, aquathermal pore fluid expansion, and petroleum maturation. There may be an additional metamorphic flux from the deeper portions of the crust that is not included in the first term on the right hand side of equation (A3.5) and we therefore explicitly include this possibility in the last term in the sum,  $V_{Metamorphic}$ .

$$V_{Tot} = V_C + V_{AT} + V_{Cpet} + V_{Metamorphic} \quad (A3.9)$$

The magnitude of the compactive flux is normally much greater than the aquathermal flux which is in turn much greater than the petroleum-driven pore fluid flux. Note we consider here that the generation of petroleum simply displaces pore water and thus the flux out of the basin is pore water not petroleum. In the next appendix, we calculate the migration rate of petroleum. Taking:

$$\begin{aligned} \rho_{sed} &= 2400 \text{ kg/m}^3 \\ \rho_{pet} &= 650 \text{ kg/m}^3 \\ \frac{1 - \phi_o}{1 - \phi(z_{source})} &= 0.5 \\ G_K &= 0.02 \\ h &= 100 \text{ m} \\ \phi_o &= 0.55 \\ \phi(z_{source}) &= 0.1 \\ \phi_{min} &= 0.1 \end{aligned}$$

we find the fluxes at the surface are as follows.

Type of flux	Magnitude	Percent of compactive flux	Comment
$V_C$	0.44S	100%	
$V_{AT}$	$6 \times 10^{-2}S$	14%	
$V_{Cpet}$	$2.5 \times 10^{-3}S$	0.6%	100 m and 2 wt percent kerogen
$V_{Cpet}$	$3.7 \times 10^{-2}S$	8.4%	1.5 km and 2 wt percent kerogen

The third flux will apply only while the organic-rich strata are passing through its maturation window. At other times it will be zero. The last flux will apply only if the entire basin contains 2 wt percent kerogen. The other fluxes apply in general.

## APPENDIX 4

## Dynamic Permeability of Actively Sedimenting Overpressured Basins

Assume that water occupies almost all the pore space in a sedimentary basin and that the sediments are impermeable and overpressured from the instant they are deposited (e.g.,  $z_t^{top} = 0$ , App. 2). We can rearrange equation (1) in the text to give the dynamic permeability of the basin sediments as a function of the fluxes defined in Appendix 3 and the pressure gradients defined in Appendix 2:

$$k_d = \frac{-\mu_w V_{Tot}}{\nabla_z p - \rho_w g}. \quad (\text{A4.1})$$

Here  $p$  is the fluid pressure defined in the various overpressured zones in the basin by equations (A2.7c and A2.11c, App. 2), and  $V_{Tot}$  is from equation (A3.9, App. 3).  $\nabla_z$  is the

gradient operator operating in the vertically downward direction only.  $k_d$  is the dynamic permeability, i.e., the permeability required for the known fluid fluxes to be produced by the known pore pressure gradient.

For hydrostatic conditions, the hydrostatic permeability,  $k_H$ , must be greater than:

$$k_H > \frac{\mu_w V_{Tot}}{0.1 \rho_w g}. \quad (\text{A4.2})$$

Here our criterion for hydrostatic conditions is that the water pressure gradient exceeds hydrostatic by less than 10 percent. For a total vertical fluid flux of  $V_{Tot}$ , this will be the case if equation (A4.2) holds.

## APPENDIX 5

## Migration Petroleum Saturation in Overpressured Basins

If petroleum occupies 100 percent of the pore space along a filament of migrating petroleum and we neglect the capillary term, equations (1) and (4a) in the text describe the rate at which it will migrate through an overpressured basin:

$$V_{Mpet} = \frac{-k_d}{\mu_{pet}} (\nabla_z p - \rho_{pet} g) = \frac{\mu_w V_{Tot}}{\mu_{pet}} \frac{\nabla_z p - \rho_{pet} g}{\nabla_z p - \rho g}. \quad (A5.1)$$

To obtain the second expression, we have substituted for  $k_d$  from equation (A4.1, App. 4). The ratio of petroleum generation to migration,  $V_{Cpet}$  to  $V_{Mpet}$ , under overpressured basin conditions is:

$$\frac{V_{Cpet}}{V_{Mpet}} = \frac{\mu_{pet}}{\mu_w} \left( \frac{\nabla_z p - \rho g}{\nabla_z p - \rho_{pet} g} \right) \frac{V_{Cpet}}{V_{Tot}} \quad (A5.2)$$

where  $V_{Cpet}$  is given by equations (A3.7 and A3.8, App. 3) and  $V_{Tot}$  is given by equation (A3.9, App. 3). All parameters are known and the ratio is independent of the sedimentation rate. The ratio of petroleum generation to migration can be thought of as the pore petroleum saturation necessary to migrate the petroleum as it is generated. If this ratio is small, petroleum migration will occur by invasion percolation.

Under hydrostatic conditions,

$$V_{Mpet} = \frac{k}{\mu_{pet}} (\rho - \rho_{pet}) g.$$

Substituting for  $k$  from equation (A4.2, App. 4) gives:

$$V_{Mpet} = \frac{10\mu_w V_{Tot}}{\mu_{pet} \rho} (\rho - \rho_{pet}). \quad (A5.3)$$

This is the minimum rate of migration of petroleum under hydrostatic conditions because  $k$  is the minimum required permeability for hydrostatic conditions to exist.

The maximum ratio of petroleum generation to migration under hydrostatic conditions is then:

$$\frac{V_{Cpet}}{V_{Mpet}} = \frac{0.1\mu_{pet}}{\mu_w} \left( \frac{\rho}{\rho - \rho_{pet}} \right) \frac{V_{Cpet}}{V_{Tot}}. \quad (A5.4)$$

This is the maximum ratio because  $k$  is the minimum needed for hydrostatic conditions and could be larger than this minimum. If it is larger,  $V_{Mpet}$  would be greater and the ratio smaller.

To complete expressions (A5.2) and (A5.3), we need to know the viscosity of water and petroleum in basins. An expression for the viscosity of water, valid from 0° to 150°C (Kaye and Laby, 1966) is:

$$\log \mu_w = -0.00259555 + 0.76353/T, \quad (A5.5)$$

where  $T$  is in °K and  $\mu_w$  is in Pa.s. The viscosity of petroleum is obtained from regressions suggested by Beggs and Robinson (1975) that give the viscosity of gas-saturated oil. Their regressions require temperature, the density of the oil, and the gas/oil ratio as input. We obtain the gas/oil ratio by regressing a plot of it against pore water pressure in England et al. (1987, Fig. 2). The expression we obtain for the gas/oil ratio is:

$$R_{g-o} = 0.05572 - 0.0032139p + 0.00021524p^2, \quad (A5.6)$$

where  $R_{g-o}$  is the gas/oil ratio in kg gas/kg oil, and  $p$  is pressure in MPa.

## APPENDIX 6

## Expulsion of Brine by Gas Zone Compaction

From the discussion in the text, the situation for the mid-continent United States MVT deposits that are associated with brine expulsion from the Arkoma basin can be summarized as follows:

1. The MVT deposits were thermally anomalous at the time of ore deposition (Table 2).
2. The sites were anomalously hot for less than ~100,000 yrs (Table 2).
3. Heating flow pathways requires expulsion of ~1,500 km<sup>3</sup> hot brine from the Arkoma basin (discussion below). This is more restrictive than the expulsion required to deposit the known base metal reserves of 57 Mt. This can be done with 570 km<sup>3</sup> of brine carrying 100 ppm base metal (see text).
4. Heating basin margins requires flow rates of ~0.2 km<sup>3</sup>/yr (discussion below).

Finding a physical process of brine migration that can satisfy these criteria is the main scientific challenge of MVT mineralization. Of course if the deposits were not thermally anomalous at the time of ore deposition the challenge would disappear. It would be far easier if the cumulative duration of heating were not so short. But assuming the above statements are true, what physical process could accommodate them? We argue below that many ideas do not appear to be viable, but compaction of a gas-saturated zone is a process that might work.

First consider criterion 3 above. Assuming flow in the Cambrian aquifers occurred through an area with east-west dimensions of 300 km at the Arkoma basin and tapering to 100 km east-west at the Upper Mississippi Valley (UMV) district (as illustrated in the insert in Fig. A6), the 750-km flow path between the Arkoma basin and the Upper Mississippi Valley district would have an area of 150,000 km<sup>2</sup>. If flow occurred through, on average a 100-m-thick vertical interval and through 20 percent of this corridor, considering that the heat capacity of brine is about twice that of rock, ~1,500 km<sup>3</sup> (= 0.2 × 0.1 × 150,000/2) of hot brine from the Arkoma basin will be needed to heat the brine flow pathways from the Arkoma basin to the Upper Mississippi Valley district.

Regarding criterion 4 above, Bethke (1986), Garven et al. (1993), and Arnold et al. (1996) find a brine flux of ~10 m/yr in the Cambrian aquifers of the Illinois basin is needed to perturb temperatures as observed in the Upper Mississippi Valley district. The methods in figure 4 in Cathles (1987) yield a similar estimate. Assuming that flow is through 20 percent of a 100-m-thick Cambrian aquifer, a flow rate of 10 m/yr will deliver brine to the 100-km-wide (east-west, see Figs. 25, A6) Upper Mississippi Valley district at the rate of ~0.02 km<sup>3</sup>/yr (= 0.2 × 10<sup>-2</sup> km/yr × 100 km × 0.1 km). Since the Upper Mississippi Valley has about 10 percent of the total MVT metal resources of the Arkoma basin (Table 1), the basin would need to expel brine at 10 times the rate required to form the Upper Mississippi Valley deposits in order to also form its other MVT deposits. The total expulsion rate is then ~0.2 km<sup>3</sup>/yr.

From Appendix 3, compaction from 20 to 10 percent porosity, aquathermal heating, and gas generation from a source bed thicker than 1 km with 2 wt percent kerogen could expel fluids at  $V_{tot} \sim 0.2 S$ . For a sedimentation rate  $S = 2$  km/m.y., brine expulsion from the 100- (N-S) by 300-km (E-W) Arkoma basin (see Fig. 1) will be  $1.2 \times 10^{-2}$  km<sup>3</sup>/yr (=  $0.2 \times 2 \times 10^{-6} \times 100 \times 300$ ). This is a very generous estimate of what might be expelled at times of high sediment accumulation in the Arkoma basin but is still 16 times smaller than the required expulsion rate of 0.2 km<sup>3</sup>/yr. In addition, much of the mineralization occurred (Fig. 2) when sedimentation in the Arkoma basin was very low. Also, if it were focused to achieve the required heating, this steady brine expulsion would heat the deposit sites for too long.

Maturation and aquathermal expulsion (which represents half the expulsion rate above, or 0.1 S) could be much faster if the basin were heated at the rate its surface might be heated by a fall in sea level. During glacial cycles, sea level falls by ~100 m over ~50,000 yrs. Tropical thermoclines can be very abrupt, with temperature changes of ~15°C occurring over an ~20-m depth. Thus the sediment-water interface could increase in temperature by 15°C over ~10,000 yrs, which is a heating rate of ~1,500°C/m.y. The change in surface temperature is rapidly transmitted through the basin (Eisenlohr et al., 1994). This rate is ~40 times the heating rate of ~30°C/m.y. expected for a sedimentation rate of 2 km/m.y., and thus the brine expulsion from a sea-level regression attending glaciation might expel brine from the Arkoma basin at the rate of ~0.24 km<sup>3</sup>/yr. The problem is that the thermal change is much less rapid after it has propagated into the subsurface to the 3- to 6-km depths where petroleum is generated. At these depths the heating rate expected is ~46° and 12°C/m.y., respectively, which is not much different from the heating rate at a sedimentation rate of 2 km/m.y. Thus, a sea-level change might help but probably cannot achieve the required expulsion rates.

As discussed in the text, cross-basin topography-driven flow is an attractive hypothesis but seems, on close inspection, not to be feasible for many reasons.

An entirely new way of expelling brine is possible if the Arkoma basin were gas filled at the time of mineralization. An increase in sea level (due to melting glacial ice, for example) will load a basin and increase the lithostatic pressure on all the sediments at the rate at which sea-level changes. Because, in a hydrostatically pressured active basin, pore fluid pressures increase quite quickly by the same amount as the sea-level rise, effective stress in water-saturated parts of the basin (lithostatic change-pore pressure change) will not change, and the sediments will not compact. However, pore pressures are low in the gas-saturated areas of a basin (see Fig. 9), and thus in these areas the effective stress will increase by the amount of sea-level rise, and the sediments will compact. Over the entire Arkoma basin, we show below that a 100-m rise in sea level could expel 2,100 km<sup>3</sup> of brine at a rate of ~0.21 km<sup>3</sup>/yr.

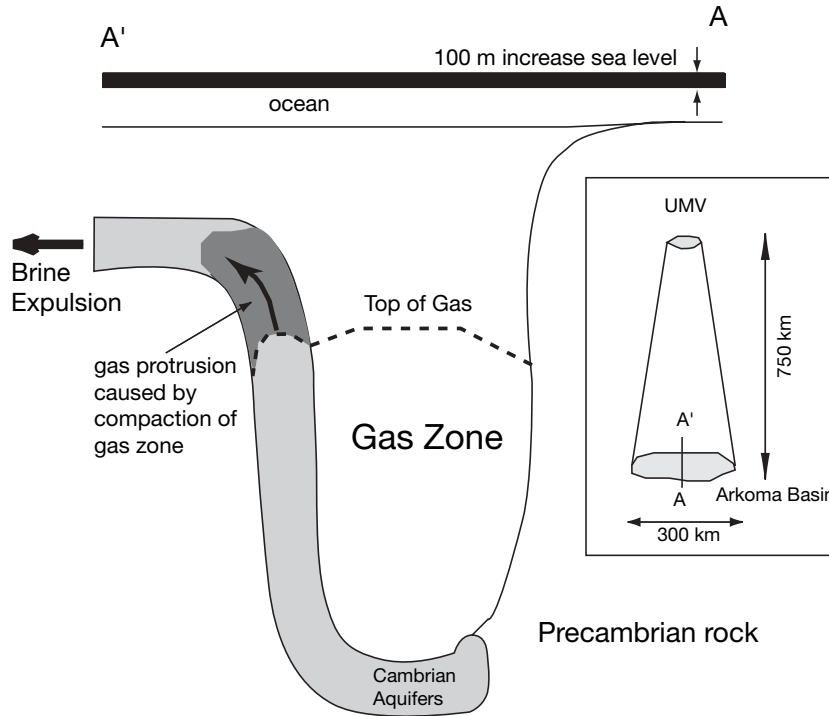


FIG. A6. Diagram illustrating how a rise in sea level could compress the gas-saturated zone in the Arkoma basin and cause the displacement of brine in the Cambrian aquifers. Insert shows the dimensions of the flow system connecting the Arkoma basin and Upper Mississippi Valley Pb-Zn district used in calculations.

This is enough to warm the brine flow pathways and warm the sites of ore deposition.

- A sea-level rise of 100 m will increase lithostatic pressure by  $10^6$  Pa.
- For a sediment compressibility of  $\phi_o\beta = 1.4 \times 10^{-8} \text{ Pa}^{-1}$ , this loading will produce a porosity change of 1.4 percent, using equation A2.1 (App. 2) in evaluating for the parameters in that appendix:

$$d\phi = -\phi_o\beta d\sigma_{eff} = 1.4 \times 10^{-8} \text{ Pa}^{-1} \times 10^6 \text{ Pa} = 1.4\%.$$

- A compaction of 1.4 percent applied over a 5-km-deep gas zone interval of the 100-km (N-S) by 300-km (E-W) Arkoma basin (see Fig. A6) yields a loss of pore space of  $2,100 \text{ km}^3$ . We assume this contraction of pore space in the gas-saturated zone will cause the gas zone to bulge out at depth, and displace brine.
- If sea level rises 100 m over 10,000 yrs during the Permian interglacials, as it did during the Pleistocene interglacials, the expulsion rate will be  $0.21 \text{ km}^3/\text{yr}$ .
- If this brine is channeled into the Cambrian aquifer system as illustrated in Figure A6, all the MVT deposits associated with the Arkoma basin could be produced by a number of such pulses.
- The system will recover during the icehouse portion of the glacial cycle. The gas-filled part of the basin will contract, brine will be pulled back over  $\sim 90,000$  yrs, to be rapidly expelled again during the melting portion of the next interglacial.

The above is only the outline of an argument. Many issues need eventually to be considered. For example, it is not certain the Arkoma basin was below sea level in the Permian. Flatlying, undeformed, marine, Permian sediments are known in northernmost Louisiana and southern Arkansas (Nicholas and Waddell, 1989), and Permian marine sediments are known in Kentucky (Kehn et al., 1982), but in general the Permian sediments are eroded. Thus it is possible, but by no means certain, that shallow seas covered the eastern half of the Arkoma basin in the Permian. The sediment compressibility may be different from that assumed, and the basin sediments may fully compact at depths shallower than the base of the Arkoma basin, which means that the volumes and rates suggested here could be off by a factor of two at least.

However, the argument and rough calculation shows that changes of water load in a gas-saturated basin could cause significant changes in pore volume, and the thermal constraints on MVT formation are so restrictive that this (or something similar involving the gas zone) is virtually the only viable hypothesis proposed to date. If this is the explanation for pulses of brine from MVT deposits, these deposits may tend to form mainly during glacial periods and in association with marine basins that are substantially gas filled. We say mainly because loading of the basin by means other than sea-level (lake-level changes, evaporite accumulation) change could load the basin rapidly enough and would not necessarily need a gas-filled basin, some MVT deposits may not have been thermal anomalies at the time of their formation and therefore may not require rapid fluid expulsion, and it may be possible to rapidly displace brine with rapid episodes of evaporation and new brine formation.



## APPENDIX REFERENCES

- Arnold, B.W., Bahr, J.M., and Fantucci, R., 1996, Paleohydrogeology of the Upper Mississippi Valley zinc-lead district: Society of Economic Geologists Special Publication 4, p. 378–389.
- Beggs, H.D., and Robinson, J.R., 1975, Estimating the viscosity of crude oil systems: *Journal of Petroleum Technology*, v. September, p. 1140–1141.
- Bethke, C.M., 1986, Hydrologic constraints on genesis of the Upper Mississippi Valley mineral district from Illinois basin brines: *ECONOMIC GEOLOGY*, v. 81, p. 233–249.
- Bickle, M.J., and McKenzie, D., 1987, The transport of heat and matter by fluids during metamorphism: *Contributions to Mineralogy and Petrology*, v. 95, p. 384–392.
- Bredehoeft, J.D., and Papadopoulos, I.S., 1965, Rates of vertical groundwater movement estimated from the Earth's thermal profile: *Water Resources Research*, v. 1, p. 325–328.
- Cathles, L.M., 1977, An analysis of the cooling of intrusives by ground-water convection which includes boiling: *ECONOMIC GEOLOGY*, v. 72, p. 804–826.
- 1981, Fluid flow and genesis of hydrothermal ore deposits: *ECONOMIC GEOLOGY 75TH ANNIVERSARY VOLUME*, p. 424–457.
- 1983, An analysis of the hydrothermal system responsible for massive sulfide deposition in the the Hokuroku basin of Japan: *ECONOMIC GEOLOGY MONOGRAPH 5*, p. 439–487.
- 1987, A simple analytical method for calculating temperature perturbations in a basin caused by the flow of water through thin, shallow-dipping aquifers: *Applied Geochemistry*, v. 2, p. 649–655.
- 1997, Thermal aspects of ore formation, in Barnes, H.L., ed., *Geochemistry of hydrothermal ore deposits*. New York, NY, Wiley, p. 192–227.
- Cathles, L.M., and Smith, A.T., 1983, Thermal constraints on the formation of Mississippi Valley-type lead-zinc deposits and their implications for episodic basin dewatering and deposit genesis: *ECONOMIC GEOLOGY*, v. 78, p. 983–1002.
- Davis, S.H., Rosenblat, S., Wood, J.R., and Hewett, T.A., 1985, Convective fluid flow and diagenetic patterns in domed sheets: *American Journal of Science*, v. 285, p. 207–223.
- Deloule, E., and Turcotte, D.L., 1989, The flow of hot brines in cracks and the formation of ore deposits: *ECONOMIC GEOLOGY*, v. 84, p. 2217–2225.
- Eisenlohr, B.N., Tompkins, L.A., Cathles, L.M., Barley, M.E., and Groves, D.I., 1994, Mississippi Valley-type deposits: Products of brine expulsion by eustatically induced hydrocarbon generation? An example from northwestern Australia: *Geology*, v. 22, p. 315–318.
- Elder, J.W., 1966, Heat and mass transfer in the Earth: Hydrothermal systems: New Zealand Department of Scientific and Industrial Research Bulletin, v. 169, p. 1–115.
- England, W.A., Mackenzie, A.S., Mann, D.M., and Quigley, T.M., 1987, The movement and entrapment of petroleum fluids in the subsurface: *Journal of the Geological Society of London*, v. 144, p. 327–347.
- Forster, C.B., and Smith, L., 1989, The influence of groundwater flow on thermal regimes in mountainous terrain: A model study: *Journal of Geophysical Research*, v. 94, sec. B, p. B9439–B9451.
- Garven, G., Ge, S., Person, M.A., and Sverjensky, D.A., 1993, Genesis of stratabound ore deposits in the midcontinent basins of North America. 1. The role of regional groundwater flow: *American Journal of Science*, v. 293, p. 497–568.
- Goldie, R., 1979, Metamorphism of the Flavrian and Powell plutons, Noranda area, Quebec: *Journal of Petrology*, v. 20, p. 227–238.
- Hanor, J.S., 1997, Controls on the solubilization of lead and zinc in basinal brines, in Sangster, D.F., ed., *Carbonate-hosted lead-zinc deposits*: Society of Economic Geologists Special Publication 4, p. 483–500.
- Henley, R.W., Truesdell, A.H., Barton, P.B., and Whitney, J.A., eds., 1984, *Fluid-mineral equilibria in hydrothermal systems*, Society of Economic Geologists, *Reviews in Economic Geology*, v. 1, 267 p.
- Henley, R.W., Hedenquist J.W., and Roberts P., eds., 1986, *Guide to the active epithermal (geothermal) systems and precious metal deposits of New Zealand*: Monograph Series on Mineral Deposits, v. 26, Gebruder Borntraeger, 222 p.
- Ingebritsen, S.E., and Manning, C.E., 1999, Geological implications of a permeability-depth curve for the continental crust: *Geology*, v. 27, p. 1107–1110.
- Jaeger, J.C., 1968, Cooling and solidification of igneous rocks, in Hess, H.H., and Poldervaart, A., eds., *Basalts—the Poldervaart treatise on rocks of basaltic composition*: New York, NY, Interscience Publishers, v. 2, p. 503–536.
- Kaye, G.W.C., and Laby, T.H., 1966, *Tables of physical and chemical constants*: New York, NY, John Wiley and Sons, 249 p.
- Kehn, T.M., Beard, J.G., and Williamson, A.D., 1982, Mauzy Formation, a new stratigraphic unit of Permian age in western Kentucky: *U.S. Geological Survey Bulletin 1529-H*, p. H73–H86.
- Lake, L.W., Bryant, S.L., and Araque-Martinez, A.N., 2002, *Geochemistry and fluid flow*: New York, NY, Elsevier, 226 p.
- Lapwood, E.R., 1948, Convection of a fluid in a porous media: *Proceedings of the Cambridge Philosophical Society*, v. 44, p. 508–521.
- Mal'kovskii, V.I., and Pek, A.A., 1997, Conditions for the development of thermal convection of a single phase fluid in a vertical fault: *Petrologiya*, v. 5, p. 428–434.
- 1999, Onset conditions of free thermal convection of a single-phase fluid in a horizontal porous layer with depth-dependent permeability: *Izvestiya (Physics of the Solid Earth)*, v. 35, p. 990–994.
- Manning, C.E., and Ingebritsen, S.E., 1999, Permeability of the continental crust: Implications of geothermal data and metamorphic systems: *Reviews of Geophysics*, v. 37, p. 127–150.
- McKibben, M.A., and Hardie, L.A., 1997, Ore-forming brines in active continental rifts, in Barnes, H.L., ed., *Geochemistry of hydrothermal ore deposits*. New York, NY, John Wiley and Sons, p. 877–935.
- Nicholas, R.L., and Waddell, D.E., 1989, The Ouachita system in the subsurface of Texas, Arkansas, and Louisiana: *Geological Society of America, Geology of North America*, v. F-2, p. 661–672.
- Norton, D., and Cathles, L.M., 1979, Thermal aspects of ore deposition, in Barnes, H.L., ed.: New York, NY, John Wiley and Sons, p. 611–631.
- Palciuskas, V.V., and Domenico, P.A., 1989, Fluid pressures in deforming porous rocks: *Water Resources Research*, v. 25, p. 203–213.
- Palm, E., Weber, J.E., and Kvernfold, O., 1972, On steady convection in a porous media: *Journal of Fluid Mechanics*, v. 54, p. 153–161.
- Revil, A., and Cathles, L.M., 2001, The porosity-depth pattern defined by 40 wells in Eugene Island South Addition, Block 330 area, and its relation to pore pressure, fluid leakage, and seal migration: *Petroleum Systems of Deep-Water Basins: Bob F. Perkins Conference—GCSSEPM Foundation Annual Research Conference, 21<sup>st</sup>, Global and Gulf of Mexico Experience*, Houston, Texas, December 2–5, 2001, Gulf Coast Society of Economic Paleontologists and Mineralogists, p. 687–712.
- White, D.E., 1968, Environments of generation of some base-metal ore deposits: *ECONOMIC GEOLOGY*, v. 63, p. 301–335.
- Wood, J.R., and Hewett, T.A., 1982, Fluid convection and mass transfer in porous sandstones: A theoretical model: *Geochimica et Cosmochimica Acta*, v. 46, p. 1707–1713.